Control of chromosome biorientation by a feedback loop involving the Ska complex and Aurora B kinase

Inauguraldissertation

zur

Erlangung der Würde eines Doktors der Philosophie

vorgelegt der

Philosophisch-Naturwissenschaftlichen Fakultät

der Universität Basel

von

Patrick Redli

aus Zürich, Schweiz

Basel, 2016

Genehmigt von der Philosophisch-Naturwissenschaftlichen Fakultät

auf Antrag von

Prof. Erich A. Nigg

Prof. Patrick Meraldi

Basel, den 23.02.2016

Prof. Jörg Schibler

- Dekan -

Summary

Proper chromosome attachment to opposite spindle poles (biorientation) and error-free chromosome segregation relies on the plasticity of kinetochore-microtubule attachments; these must remain flexible enough to allow the release of erroneously attached spindle microtubules, yet become sufficiently stable to harness forces for chromosome movements and silence the spindle assembly checkpoint. Aurora B kinase fosters chromosome biorientation by facilitating the dynamics of kinetochore-microtubule attachments through phosphorylation of kinetochore proteins that bind microtubules. Prominent among the substrates, whose microtubule and kinetochore binding is curtailed by Aurora B, is the Ska complex, a key factor for kinetochore-fiber stability. Here, we show that Ska is not only a substrate of Aurora B, but is also required, in turn, for Aurora B activity. Ska-deficient cells fail to biorient and display lagging chromosomes and micronuclei as a result of suppressed kinetochore-microtubule turnover. These defects coincide with diminished kinetochore localization of the Aurora B effectors MCAK and CENP-E, as well as reduced Aurora B substrate phosphorylation. We further show that Ska requires its microtubule binding capability to promote Aurora B activity in cells and directly stimulates Aurora B catalytic activity *in vitro*. Finally, we demonstrate that PP1 counters Aurora B activity to enable Ska kinetochore accumulation once biorientation is achieved, which allows Ska to exert its kinetochore-fiber stabilizing function. Together, we propose that the Ska complex enhances Aurora B activity to limit its own microtubule and kinetochore association and ensure that the dynamics and stability of kinetochore-microtubules fall within an optimal balance for chromosome biorientation and faithful chromosome segregation.

Introduction

The eukaryotic cell cycle and its control system

Cells are the basic structural and functional units of all living organisms and their ability to self-reproduce is indispensable for the development and continuity of life. In unicellular eukaryotes each cell division gives rise to a new organism. In multicellular species cell proliferation is crucial for embryogenesis and organismic growth during development, as well as for the constant renewal of most cells during adult tissue homeostasis. The elaborated series of events leading to somatic cell reproduction is known as the cell cycle.

The key steps during the cell cycle are the duplication of the chromosomes, which occurs in S phase, and their subsequent equal distribution to two nascent daughter cells, which occurs in M phase. Most cell cycles also contain two additional gap phases, G1 and G2, which separate the S and M phase. These regulatory transition periods provide cells time for growth and allow them to monitor whether the internal and external conditions are favorable to progress to the next cell cycle stage. During G1, if cells are deprived of appropriate growth signals or receive inhibitory signals from other cells, they may enter a prolonged resting state, known as G0 or quiescence state. When growth conditions become favorable again, cells may continue division by reentering G1 (Figure 1A) (Morgan, 2007).

To ensure that the key events of the cell cycle occur sequentially and are properly timed only once per cycle, higher eukaryotic cells have evolved an elaborated cell cycle control system. At the heart of this system are the Cyclin-

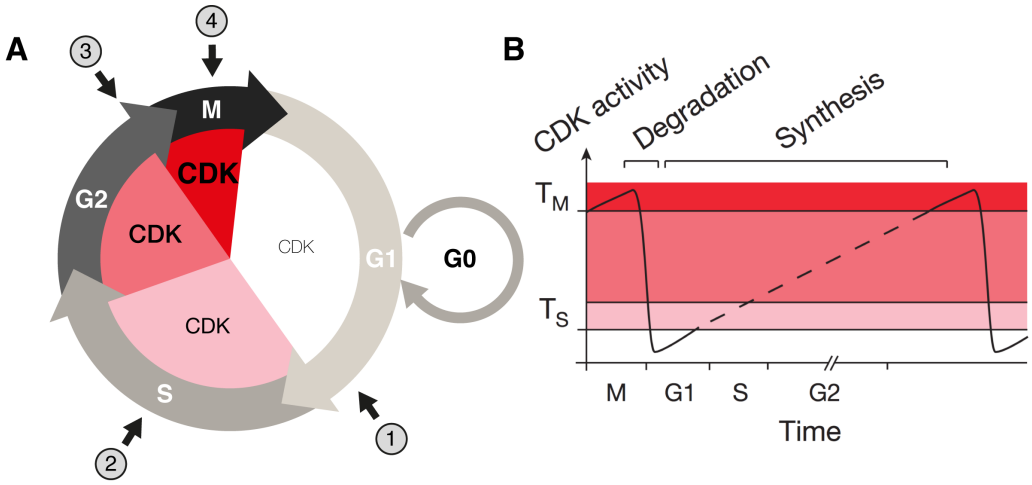

Figure 1. The eukaryotic cell cycle and its control system. *Left,* illustration of the different phases and CDK activity states during cell cycle progression (see text for detail). Black arrows and encircled numbers indicate the four cell cycle checkpoints (1: G1/S checkpoint; 2: intra-S phase checkpoint; 3: G2/M checkpoint; 4: spindle assembly checkpoint). *Right*, minimal threshold model of cell cycle control. Oscillation of CDK activity between two thresholds (T_s = S phase threshold; T_M = M phase threshold) drive the major cell cycle events. Illustration adapted from (Coudreuse and Nurse, 2010).

dependent kinases (CDKs), whose activity, substrate specificity, and subcellular localization depend on the binding to regulatory subunits, called Cyclins. According to the classical model of cell cycle control, oscillations in the levels of distinct Cyclins during the cell cycle lead to the timely formation and activation of specific Cyclin-CDK complexes that drive initiation of the various cell cycle events: D-type Cyclins and CDK4 or CDK6 regulate events in early G1 phase; Cyclin E-CDK2 triggers S phase initiation; Cyclin A-CDK2 and Cyclin A-CDK1 regulate the completion of S phase; and Cyclin B-CDK1 is responsible for entry into mitosis (Malumbres and Barbacid, 2005). However, the basic concept of this model that each cell cycle phase is driven by specific CDKs has been challenged by the results of knockout studies in mice showing that CDK4, CDK6, and CDK2 are all non-essential for the cell cycle of most cell types (Malumbres and Barbacid, 2009). Thus, a minimal threshold model of cell cycle control has been proposed, in which cell cycle transitions can be governed mainly through changes in the activity level of a single CDK – CDK1. Promiscuous

binding of CDK1 to Cyclins that accumulate in the course of the cell cycle by *de novo* synthesis is thought to promote a steady increase in CDK1 activity and to drive phase transitions at specific activity thresholds (Figure 1B). In addition, formation of distinct Cyclin-CDK1 complexes might confer specificity to the system by directing the kinase to different substrates and possibly changing its substrate specificity (Coudreuse and Nurse, 2010; Hochegger et al., 2008; Stern and Nurse, 1996).

Surveillance mechanisms, called checkpoints, which arrest the cell cycle at specific transition points when previous events are not completed successfully or the environmental conditions are not favorable, supplement the cell cycle control system of most cells. These include (i) the G1/S checkpoint (also know as restriction point in mammalian cells or start in yeast), which prevents cell cycle entry in mid to late G1 if cell growth is insufficient or DNA is damaged; (ii) the intra-S phase checkpoint that delays S phase progression in response to replication stress; (iii) the G2/M checkpoint that blocks entry into M phase if unreplicated or damaged DNA is sensed; and (iv) the M phase checkpoint, better known as spindle assembly checkpoint (SAC), which delays sister chromatid separation and completion of mitosis until the chromosomes are correctly attached to the mitotic spindle (Figure 1A) (Hartwell and Kastan, 1994; Morgan, 2007).

The events of mitosis

Certainly the most conspicuous and arguably the most beautiful event in the cell cycle is mitosis – the division of the nucleus. The latter notion is supported by drawings of Walther Flemming of his fixed and aniline dye stained preparations of dividing salamander cells, which provided the first cytological description of mitosis in animal cells in the late 1870s (Figure 2A) (Paweletz, 2001). Ever since this time, technological progress in imaging techniques has allowed to study mitosis in much more detail (Rieder and Khodjakov, 2003). Yet, classification of the mitotic stages based on the major morphological changes of chromosomes in the course of nuclear division endured. Thus, traditionally, mitosis is divided into five morphologically distinct phases: prophase, prometaphase, metaphase, anaphase, and telophase (Figure 2A–C).

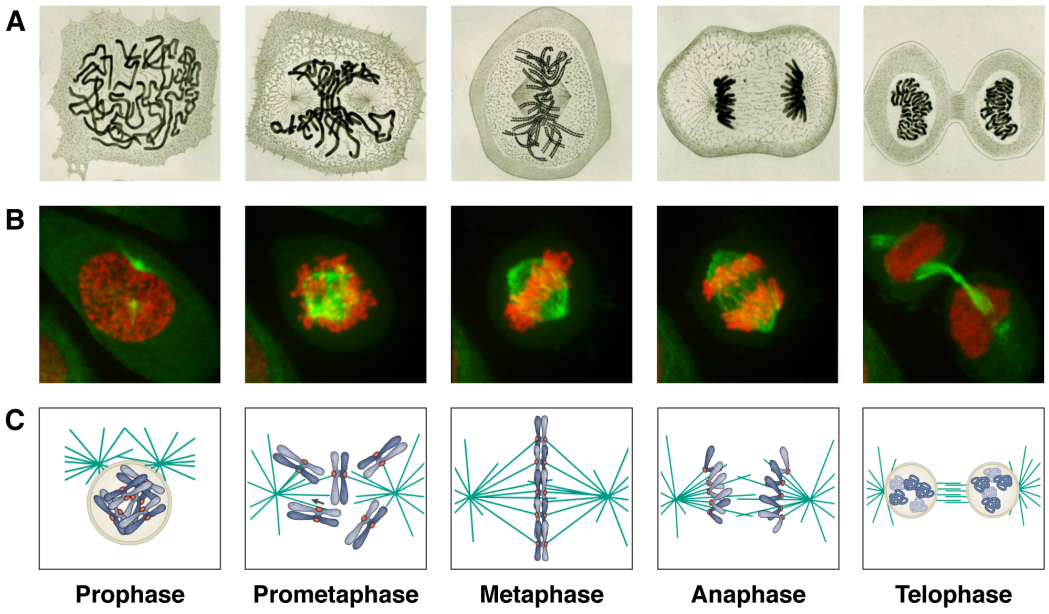

Figure 2. The phases of mitosis in vertebrate cells. (**A**) Drawings of mitosis in salamander cells found in Walther Flemming's book "Zellsubstanz, Kern und Zelltheilung" (Flemming, 1882)**.** Illustration adapted from (Rieder and Khodjakov, 2003).(**B**) State-of-the art live-cell microscopic view of mitosis in HeLa S3 cells stably expressing H2B-mCherry (red) and GFP-α-tubulin (green). Images are courtesy of Anna Santamaria. (**C**) Schematic depiction of the mitotic events. Illustration adapted from (Cheeseman and Desai, 2008).

In prophase, chromatin starts to condense to form well-defined chromosomes. By this time, the two centrosomes (organelles that serve as the main microtubule-organizing centers) that have been duplicated during S phase separate and migrate to opposite sides of the nucleus. There, a bipolar microtubule (MT)-based structure, known as the mitotic spindle, starts to assemble. The end of prophase and the beginning of prometaphase are marked by nuclear envelope breakdown (NEBD). Following NEBD, chromosomes start via kinetochores (KTs) (proteinaceous structures assembled at the centromeric regions of each sister chromatid) to interact both laterally and in an end-on fashion with spindle MTs. During this time, some chromosomes move polewards, while others move inward or glide to the spindle equator along MTs. Over time, along with the gradual MT capture from opposite spindle poles, chromosomes become positioned midway between the spindle poles during a process called congression. By metaphase, all chromosomes are aligned within an equatorial plate and are attached with their sister KTs to bundles of 20-25 spindle MTs oriented to opposite spindle poles, known as kinetochore-fibers (K-fibers) (McEwen et al., 1997). Once bioriented, sister chromatids separate and migrate toward opposite spindle poles during anaphase. This stage can be subdivided into anaphase A and B. In anaphase A, sister chromatids lose their cohesion, split apart, and move toward opposite poles, while in anaphase B, the spindle elongates and further increases the distance between the poles. Finally, during telophase, the chromosomes decondense and the nuclear envelope reforms to generate two separate nuclei. During the later stages of telophase and beginning of cytokinesis a cleavage furrow forms between them, which then ingresses and eventually gives rise to the midbody (or Flemming body). This structure participates

in the bisection of the cytoplasm and the generation of the two daughter cells during cytokinesis (Cheeseman and Desai, 2008; Maiato et al., 2004b; Walczak et al., 2010)

The kinetochore

The KT is a small, transiently assembled macromolecular complex consisting of more than 90 different proteins in metazoans (Ohta et al., 2010), which has at least five essential functions for accurate segregation of chromosomes during mitosis: (i) The KT establishes and maintains the attachment of chromosomes to dynamic spindle MTs plus-ends (ii) it controls KT-MT polymerization and depolymerization dynamics, (iii) it harnesses forces generated by KT-MT dynamics for chromosome movements, (iv) it monitors the attachment status and helps to correct improper MT attachments, and (v) it synchronizes the process of MT attachment with cell cycle progression by activating the SAC (Cheeseman and Desai, 2008; Cheeseman, 2014; Foley and Kapoor, 2013; Maiato, 2004; Santaguida and Musacchio, 2009; Walczak et al., 2010).

Kinetochore structure and molecular architecture

In electron microscopy (EM) studies of chemically fixed samples, the vertebrate KT appears as a trilaminar plate-like structure, with electron-dense inner and outer plates and an electron-translucent middle layer (Figure 3A and 3B) (Brinkley and Stubblefield, 1966; Jokelainen, 1967; Roos, 1973). A recent study suggest that this trilaminar structure may develop by rapid expansion from a compact cloud of fibrous material shortly after NEBD (Magidson et al., 2015). In addition, a fibrous corona, extending outward from the outer plate, has been described, which disappears upon MT attachment (Cassimeris et al., 1990). Likewise, the outer plate has been shown

to undergo significant alterations in shape upon the formation of end-on attachments, leading to its compaction from 400-500 nm to ~200 nm in diameter (Magidson et al., 2015), in line with the view that the KT is a highly adaptive and dynamic structure. The inner KT plate creates the interface with centromeric chromatin. The outer plate with a thickness of 50-75 nm forms the major interaction surface for binding of MT plus-ends, while the fibrous corona is thought to provide the surface for initial MT capture (Cheeseman and Desai, 2008; McEwen and Dong, 2010; Rieder and Salmon, 1998). In EM studies using modern high-pressure freezing instead of chemical fixation, however, such a three-layered organization is less distinct and the outer plate of the KT appears as a 50-75 nm thick mat of fibrous material (Figure 3C and 3D). This fibrous mat lacks a distinct middle layer and is directly connected with the electron-dense surface of the centromeric chromatin. Slender fibers, analogous to the corona region of unattached KTs from chemically fixed preparations, have been described to extend from this mat, forming a 100-150 nm wide ribosome exclusion zone (McEwen et al., 1998; McEwen and Dong, 2010). A more detailed electron tomography reconstruction of the outer KT region in high-pressure frozen preparations of PtK1 cells has revealed a network of long, crosslinked fibers that rearrange into an irregular network of short fibers upon MT attachment (Figure 3E–H). Based on this finding, it has been suggested that the outer KT region may function like a spider web that captures KT-MTs by entangling the MT plus-ends through multiple low-affinity connections to both the MT lattice and the MT tip (Dong et al., 2007; McEwen and Dong, 2010). In addition, work imaging thin sections of the KT at the interface with MTs has unveiled conserved fibril-like extensions from the KT, which contact the inner lumen-facing surface of intermediately curved protofilaments,

depicting a possible new mode of MT attachment and force-coupling (McIntosh et al., 2008; 2013). In essence, EM studies of the vertebrate KT structure over the last 50 years concur to indicate that the KT-MT attachment interface is of largely fibrous composition. This finding is consistent with biochemical and structural analyses showing that some of the key MT-binding components of the outer KT region are of elongated, rod-like or fibrous shape (O'Connell et al., 2012; Welburn and Cheeseman, 2008).

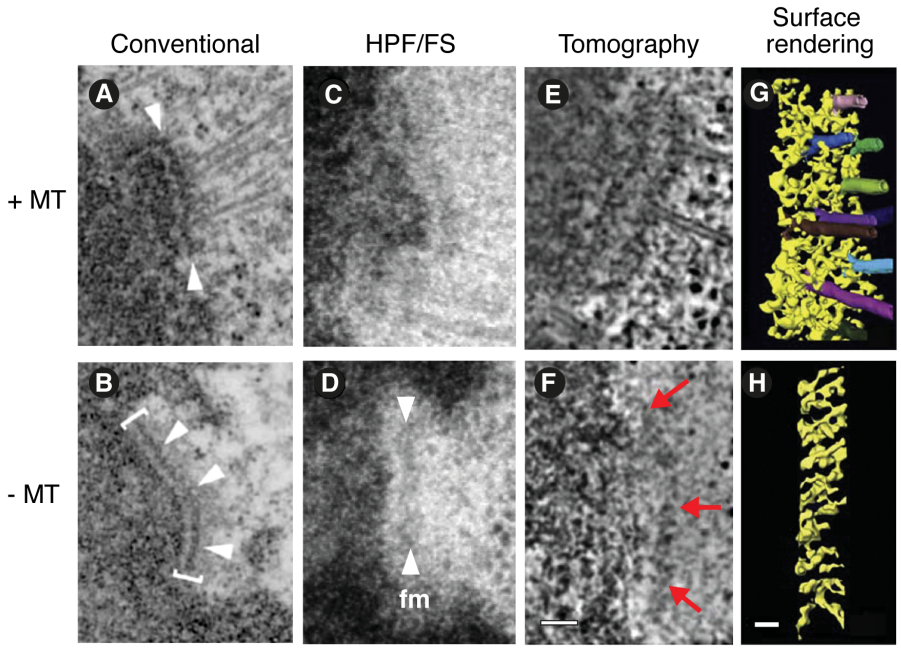

Figure 3. KT ultrastructure in PtK1 cells. (**A**,**B**) KT after convential chemical fixation in presence and absence of MTs. Brackets and arrowheads point at the electron-dense outer plate. Illustration adapted from (Maiato et al., 2006). (**C**–**F**) View of the KT after high-pressure freezing and freeze substitution (HPF/FS). White arrowheads indicate the fibrous mat (fm). Structural details revealed by electron tomography (**E**,**F**) and 3D rendering (**G**,**H**). Red arrows point at the KT outer layer. Illustration adapted from (O'Connell et al., 2012), original images reproduced from (Dong et al., 2007).

Complementing EM analyses of the KT structure, *in vivo* studies using super-resolution fluorescence microscopy with probes for many of the core KT proteins have generated nanometer-scale positional maps of individual proteins within the KT. These studies provide support for the notion of an overall layered domain organization of the KT, where KT protein complexes are arranged along the inner-outer KT axis (Figure 4A and 4B) (Suzuki et al., 2014; Wan et al., 2009; Varma et al., 2013). Furthermore, these studies have also documented structural alterations within the KT along the inner-outer KT axis, termed intra-KT stretch, in MT-attached KTs under tension *versus* KTs lacking tension (Wan et al., 2009). However, under physiological conditions such tension-dependent changes appear to be constrained to only ~10-20 nm, a finding that is inconsistent with models invoking spatial repositioning of outer KT components by intra-KT stretching as the key step in the phosphoregulation of KT-MT attachment stability and SAC activity (Krenn and Musacchio, 2015; Suzuki et al., 2014; Tauchman et al., 2015).

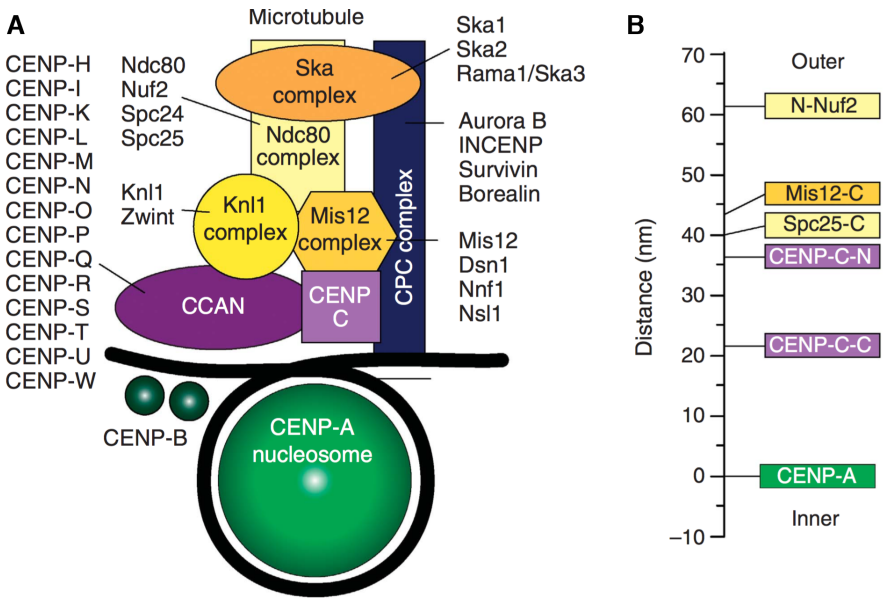

Figure 4. Protein architecture of the metazoan KT (**A**) Schematic of the metazoan KT. (**B**) Physical map of protein positions along the axis of the KT-MT attachment in metaphase in *D. melanogaster*. Illustration adapted from (Santaguida and Musacchio, 2009).

Kinetochore specification and assembly

The KT is built upon a defined region on chromosomes during the onset of mitosis, known as the centromere. In most eukaryotes, KT formation is restricted to a single chromosomal *locus* (termed monocentric). In contrast, some nematode, arthropod, and flowering plant species assemble the KT along the entire length of each chromosome (termed holocentric) (Figure 5A) (Melters et al., 2012). The main property of the centromere that specifies it as the site for KT assembly is the presence of the histone H3 variant CENP-A. A 15 residue sequence in the histone fold of CENP-A, known as the CENP-A targeting domain (CATD), distinguishes CENP-A from the canonical histone H3 and provides the basis for the establishment and propagation of centromere identity (Black et al., 2010; De Rop et al., 2012; Gascoigne and Cheeseman, 2011). In budding yeast, a single CENP-A (Cse4) containing nucleosome is deposited per chromosome at a sequence-specific DNA element of 125 base pairs in length, forming a point centromere. Invariably, KTs built upon point centromeres bind a single MT (Furuyama and Biggins, 2007; Yamagishi et al., 2014). In fission yeast and many animal and plant species, multiple CENP-A nucleosomes are typically found within much larger regions of DNA, which can encompass 40-100 kilobases in fission yeast up to several megabases in some animal and plant species. These so-called regional centromeres assemble KTs that can bind multiple MTs (Figure 5B) (Verdaasdonk and Bloom, 2011). In humans and other primates, centromere regions are enriched of thousands of tandem repeats of a 171 base pair sequence, termed α-1 satellite DNA. This sequence also contains a 17 base pair motif, known as CENP-B box, which is recognized by the centromere protein B (CENP-B) (Black et al., 2010; Masumoto et al., 1989; Ohzeki et al., 2002).

Although there is a clear correlation between the presence of repetitive α-satellite DNA and centromere location, α-satellite DNA is neither necessary nor sufficient to specify centromere identity. This is well exemplified by human cases in which a centromere was found relocated within an intact chromosome to form an inheritable neocentromere in a region that lacks α-satellite DNA (Amor et al., 2004). Instead, centromere identity is determined in most eukaryotes primarily epigenetically by CENP-A chromatin deposition and centromere-specific post-translational modifications of the canonical histones (McKinley and Cheeseman, 2015).

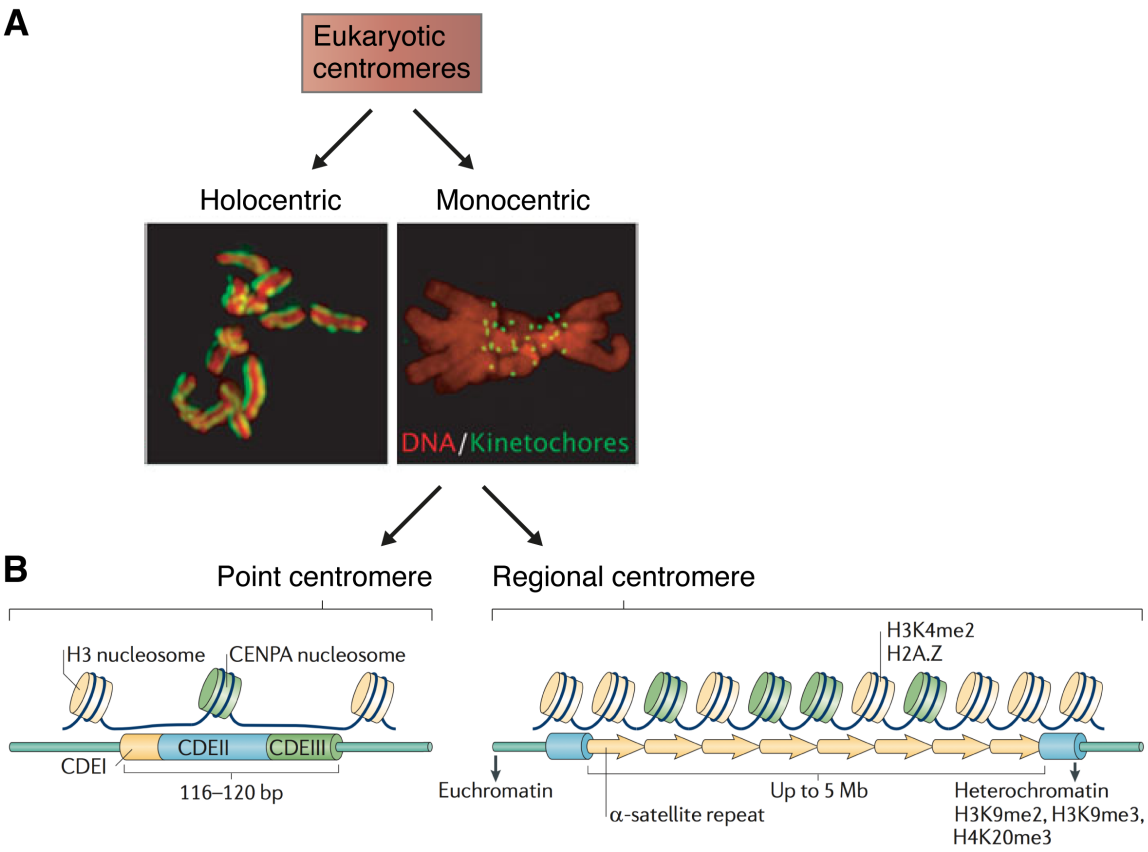

Figure 5. Organization of the centromeric region. (**A**) Types of centromeres in eukaryotes. *Left*, holocentric chromosomes in a *C. elegans* embryo. *Right*, monocentric chromosomes in a vertebrate cultured cell. Illustration adapted from (Oegema and Hyman, 2006). (**B**) Basic characteristics of point and regional centromeres. Regional centromeres, as found in primates, are built from α-satellite DNA repeats and contain multiple CENP-A nucleosomes. Canonical histones in the centromere regions are methylated. Point centromeres, as found in budding yeast are composed of three conserved centromere DNA elements (CDE) and contain only one CENP-A nucleosome. Illustration adapted from (Verdaasdonk and Bloom, 2011).

CENP-A is essential for the localization of all known KT components in vertebrate cells (Liu et al., 2006; Régnier et al., 2005) and artificial targeting of CENP-A to an ectopic chromosomal *locus* is sufficient to form operational KT-like structures that can bind MTs and direct chromosome segregation (Barnhart et al., 2011; Heun et al., 2006; Mendiburo et al., 2011). Thus, assembly of functional KTs starts with the targeted chromatin deposition of CENP-A nucleosomes, which occurs in a cell cycle regulated manner. In vertebrate cells, during DNA replication, existing CENP-A nucleosomes are distributed between the replicated sister chromatids and become replenished at centromeres, other than the canonical histone H3 nucleosomes not in S phase, but in G1 (Figure 6A) (Jansen et al., 2007). This cell cycle restriction is ensured by a mechanism integrating signals from CDKs and polo-like kinase 1 (Plk1), which control the regulated recruitment and function of the dedicated CENP-A deposition machinery (Figure 6B) (McKinley and Cheeseman, 2014). This includes as the key factors the Mis18 complex (Mis18α, Mis18β, Mis18BP1/KNL2) and the CENP-A chaperone HJURP in vertebrate cells (Fujita et al., 2007; Foltz et al., 2009; Hayashi et al., 2004; Maddox et al., 2007). While CDK activity suppresses assembly of the Mis18 complex during G2, S phase, and early mitosis, the decline of CDK activity at the onset of anaphase allows Plk1 to trigger the assembly of the Mis18 complex, which “licenses” the loading of CENP-A in late telophase (McKinley and Cheeseman, 2014; Silva et al., 2012). Subsequently, HJURP is recruited in early G1, which specifically recognizes CENP-A by the CATD and drives its incorporation into centromeric heterochromatin (Black et al., 2007; Barnhart et al., 2011; Foltz et al., 2009). Finally, after newly synthesized CENP-A has been deposited, it is stabilized in late G1 by the centralspindlin component

MgcRacGAP and RSF1 (McKinley and Cheeseman, 2015). Mechanisms that eliminate CENP-A nucleosomes loaded to non-centromeric sites complement this targeted deposition pathway to ensure maintenance of centromere identity (Collins et al., 2004; Conde e Silva et al., 2007; Hewawasam et al., 2010; Ranjitkar et al., 2010).

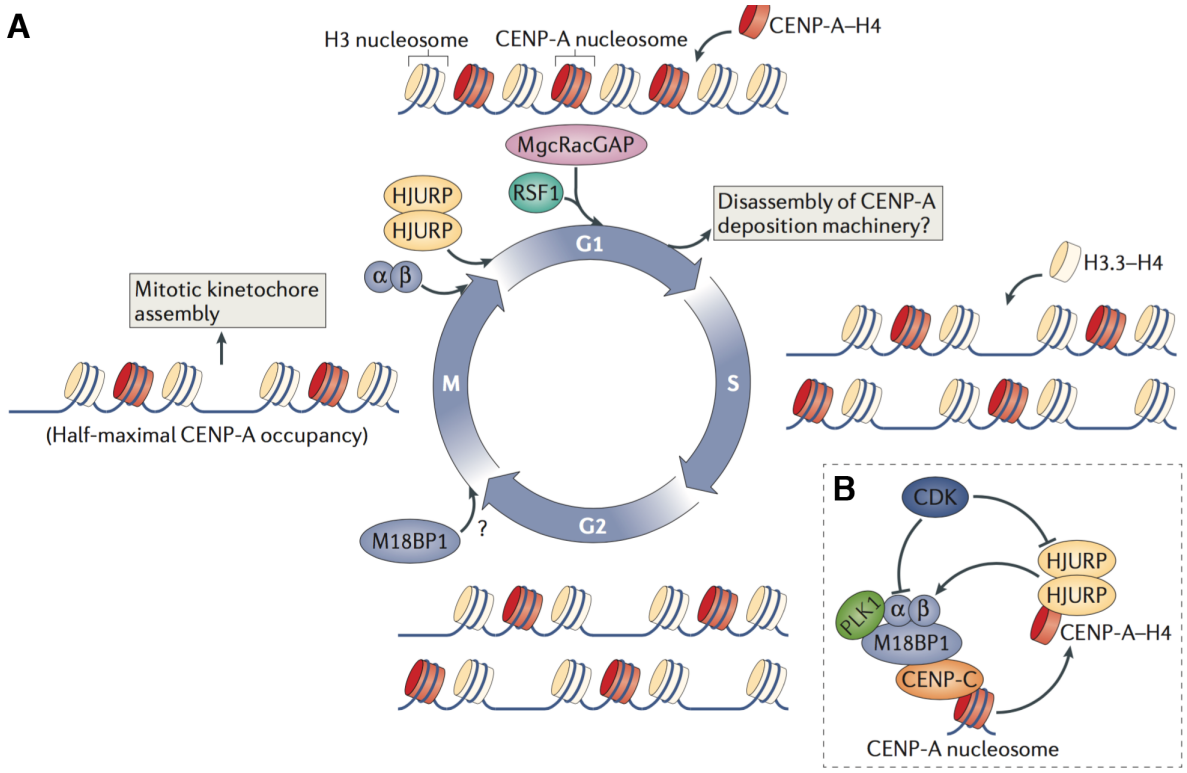

Figure 6. CENP-A deposition during the cell cycle. (**A**) In S phase, existing CENP-A nucleosomes are distributed between the replicated sister chromatids and gaps are filled with canonical histone H3. The resulting mixed CENP-A/H3 chromatin supports KT assembly during mitosis. By mitosis, Mis18BP1 is recruited to centromeres, followed by Mis18α and Mis18β at mitotic exit. Loading of new CENP-A nucleosomes is mediated by a HJURP dimer, which is recruited during early G1 phase, and drives CENP-A loading throughout the first hours of G1. New CENP-A is stabilized in late G1 by MgcRacGAP and RSF1. (**B**) CDK activity prevents CENP-A incorporation in S, G2, and M phases by inhibiting Mis18 complex assembly and HJURP recruitment. In G1, Plk1 binds to and phosphorylates the Mis18 complex to license CENP-A incorporation. Illustration adapted from (McKinley and Cheeseman, 2015).

Although CENP-A is the key factor for the specification of the KT assembly site, it is not strictly sufficient for the formation of functional KTs in vertebrate cells (Gascoigne et al., 2011; Van Hooser et al., 2001). Accordingly, there are additional proteins needed to direct the formation of fully operational KTs. Besides CENP-A, a subset of 16 chromatin-proximal proteins, termed the constitutive centromere-associated network (CCAN), localizes to centromeres in vertebrate cells throughout the cell cycle and provides a platform for ensuing outer KT protein assembly (Perpelescu and Fukagawa, 2011). Among the 16 CENPs, CENP-C and CENP-T are required in parallel for KT formation and define two non-redundant pathways for the recruitment of the core MT attachment proteins of the outer KT, the KMN (KNL-1-Mis12-Ndc80) network (Figure 4A) (Cheeseman et al., 2006; Gascoigne et al., 2011; Rago et al., 2015). Both CENP-C and CENP-T as part of the CENP-T-W-S-X complex can bind directly to DNA (Hori et al., 2008; Sugimoto et al., 1994). CENP-C also interacts with CENP-A nucleosomes and thereby contributes to the targeted deposition of CENP-A (Carroll et al., 2010; Hori et al., 2013). Targeting of N-terminal segments of CENP-C or CENP-T to a non-centromeric site is sufficient to build functional KT-like structures in absence of CENP-A that recruit the KMN network (Hori et al., 2013; Rago et al., 2015). Interestingly, in chicken DT40 cells these CENP-C and CENP-T fragment-derived KT structures also localize Bub1 and promote accumulation of Aurora B and Survivin, components of the chromosomal passenger complex (CPC), as well as of histone H3-pT3 in the area comprised between the ectopic targeting sites, indicating that CPC centromere localization is subordinate to KT assembly (Hori et al., 2013). The KMN complex is recruited by CENP-C and CENP-T in a reversed functional configuration. CENP-C directly binds

to the four-subunits Mis12 complex, which, in turn, interacts with KNL-1 and promotes the binding to the four-subunit Ndc80 complex, while CENP-T directly interacts with the Ndc80 complex and promotes the recruitment of the KNL-1/Mis12 complex (Nishino et al., 2012; Petrovic et al., 2010; Rago et al., 2015; Screpanti et al., 2011). CENP-T additionally provides an indirect interaction with the Ndc80 complex through CENP-I as part of the CENP-H-I-K subcomplex (Kim and Yu, 2015). Similar to the CENP-A deposition, the assembly of these KMN recruitment pathways is cell cycle regulated, such that the core MT binding site is timely assembled when cells enter mitosis. Specifically, the Ndc80 complex is spatially separated from the CCAN during interphase through nuclear exclusion. As the nuclear envelope breaks down, Ndc80 can access chromosomes and CDK1 promotes its subsequent binding to CENP-T through direct phosphorylation of CENP-T at multiple sites (Gascoigne and Cheeseman, 2013; Rago et al., 2015). In addition, Aurora B phosphorylates the Mis12 subunit Dsn1 and increases its binding affinity for CENP-C (Figure 7) (Kim and Yu, 2015; Rago et al., 2015).

The KMN complex, in turn, serves as a scaffold for a number of additional proteins, including SAC components (e.g. Bub1, Bub3, BubR1), regulatory proteins (e.g. PP1), motor proteins (e.g. CENP-E, Dynein), as well as non-motor microtubule-associated proteins (MAPs) that dynamically associate with the KT. Prominent among the latter are the Dam1 complex in yeast and the Ska complex in vertebrates, which have both been proposed to act synergistically to the KMN network in the generation of KT-MT connections (Varma and Salmon, 2012). Collectively, these pathways contribute to the assembly of a functional outer KT interface that mediates chromosome attachment to MTs.

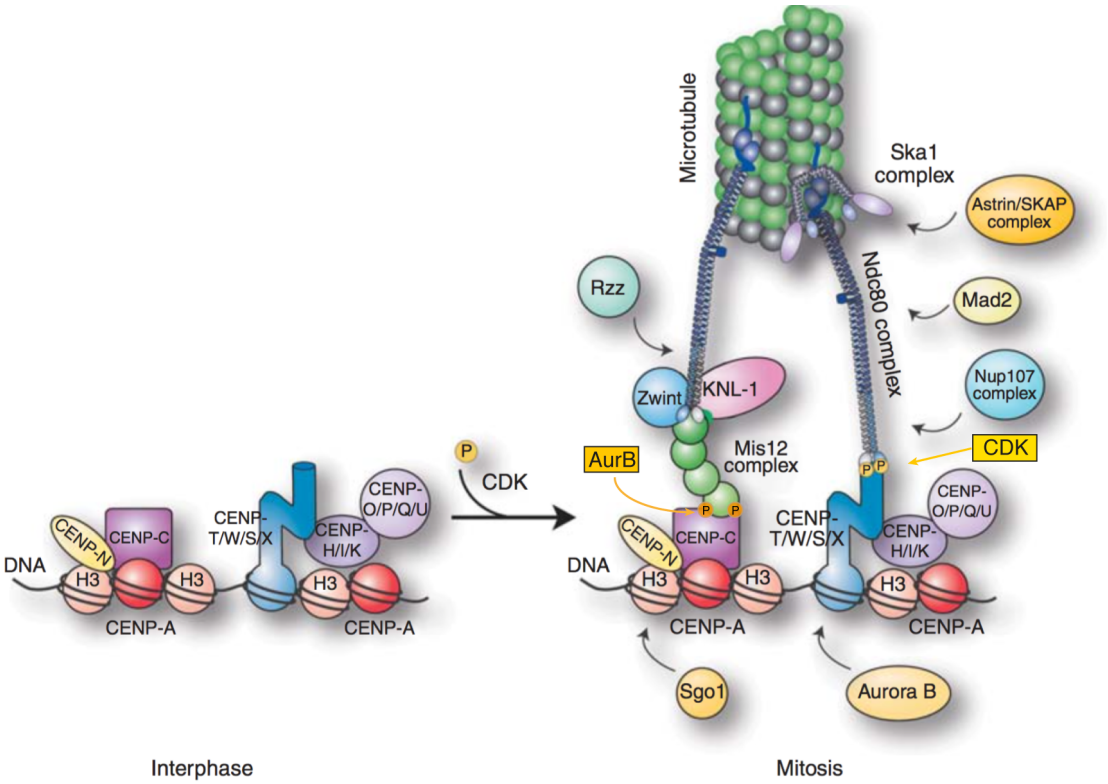

Figure 7. Assembly of the outer KT. CENP-A and the CCAN proteins are present at centromeres throughout the cell cycle**.** At mitotic entry, CDK phosphorylation promotes the assembly of the outer KT downstream of CENP-A and the CCAN. CENP-C and the CENP-T-W-S-X complex contribute via two parallel pathways to the recruitment of the KMN network (see text for detail). Illustration adapted from (Cheeseman, 2014).

Kinetochore-microtubule attachment

Dynamic behavior of microtubules

To understand how MTs attach to KTs, one needs to know about their inherent structural and dynamic properties. MTs are the main structural and functional units of the mitotic spindle. Their basic building blocks are α-/β-tubulin heterodimers arranged head-to-tail in linear protofilaments, which associate laterally to form 25 nm diameter cylindrical tubes. MTs *in vivo* and MTs nucleated *in vitro* from centrosomes comprise predominantly 13 protofilaments. The asymmetry of tubulin heterodimers makes the MT lattice polar, with a faster growing plus-end and a slower growing minus-end. β-tubulin monomers are exposed at the plus-end (usually at KTs in KT-MTs) and α-tubulin at the minus-end (usually at the spindle poles) (Figure 8A) (Desai and Mitchison, 1997).

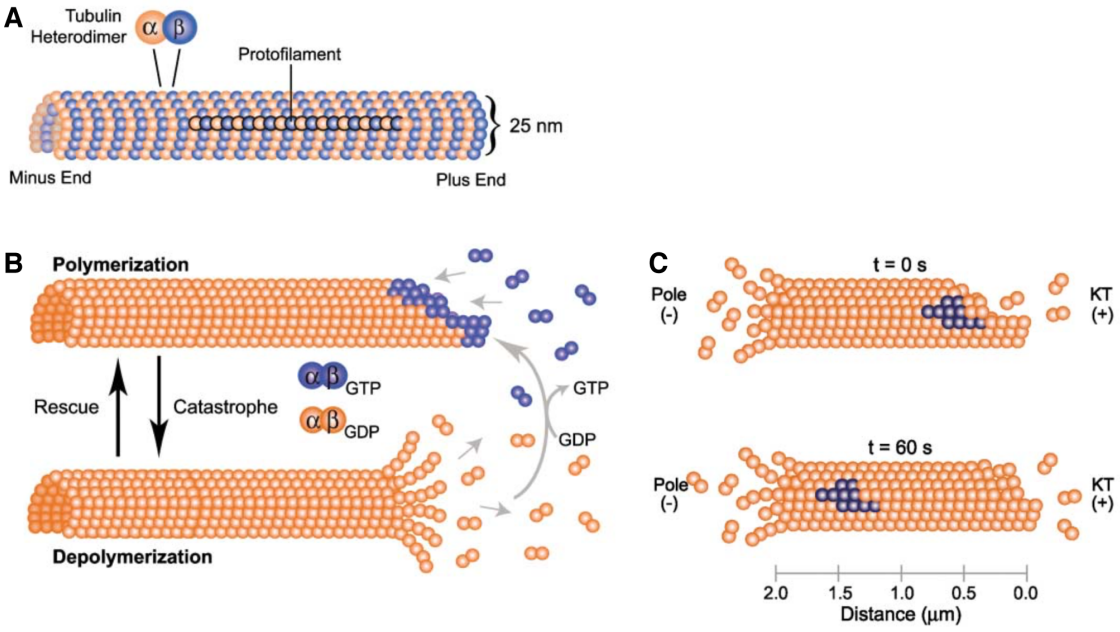

Figure 8. Structure and dynamic behavior of MTs. (**A**) MT structure. (**B**) MT dynamic instability. Although MTs exhibit dynamic instability at both ends, the plus-ends are more dynamic than the minus-ends. In the spindle, dynamic instability occurs primarily at the plus-ends, as the minus-ends are often capped at the centrosome. (**C**) MT treadmilling behavior. In the spindle, a similar behavior referred to as MT flux occurs due to net subunit addition at plus-ends and net loss at minus-ends. Illustration adapted from (Kline-Smith and Walczak, 2004).

MTs exhibit a specialized non-equilibrium dynamic behavior, termed dynamic instability, in which MT plus-ends switch stochastically between phases of slow growth and rapid shrinkage (Mitchison and Kirschner, 1984). The switch from growth to shrinkage is referred to as catastrophe, and the reverse transition as rescue (Figure 8B). This behavior is powered by the energy of polymerization-triggered GTP hydrolysis on β-tubulin; the resulting GDP-bound heterodimer has a slightly kinked conformation in comparison to the GTP-dimer but is forced into a straight conformation within the MT lattice (Wang and Nogales, 2005). Thus, the energy of GTP hydrolysis is stored as mechanical strain within the MT lattice, which triggers more rapid dissociation of GDP-bound than GTP-bound heterodimers at the MT plus-end. Because of a lag between subunit incorporation and nucleotide hydrolysis, a MT end exists in a polymerizing state, when the rate of addition of GTP-bound tubulin dimers exceeds the rate of GTP hydrolysis, forming a GTP cap. Loss of this cap, either by small random changes in the rates of tubulin binding and GTP hydrolysis or by external factors, leads to the exposure of GDP-bound heterodimers at the MT end and release of the stored mechanical strain, causing the protofilaments to bend outward and the MT to rapidly depolymerize (Brouhard and Rice, 2014; Cheeseman and Desai, 2008; Desai and Mitchison, 1997).

Another dynamic non-equilibrium MT behavior, termed treadmilling, results from the differences in the subunit affinities at the two MT ends (Margolis and Wilson, 1978). It describes the net subunit addition at the plus-end and the balanced net subunit loss from the minus-end of a MT, which causes an intrinsic flow of tubulin subunits (Figure 8C). A similar treadmilling-like steady state behavior, termed poleward MT flux, occurs in KT-MTs and interpolar MTs of animal metaphase

spindles, where MT disassembly at the spindle poles and balanced plus-end assembly at the spindle equator cause poleward movement of tubulin subunits. In contrast to treadmilling, which results from the intrinsic properties of MTs, poleward MT flux is driven by MT-associated motors and other MAPs that regulate tubulin addition and removal at both MT ends (Rogers, 2005).

A number of different MAPs have been implicated in the regulation of KT-MT dynamics. For example, kinesin-related proteins such as the kinesin-13/Kin-I family member mitotic centromere associated kinesin (MCAK) can promote MT depolymerization and catastrophe, and TOG domain containing proteins such as ch-TOG/XMAP215 or cytoplasmic linker protein (CLIP)-associated proteins (CLASPs) can promote MT polymerization or rescue (Akhmanova and Steinmetz, 2008).

Initial kinetochore-microtubule interaction is a stochastic and error prone process

The discovery that MT plus-ends undergo periodic transitions between phases of growth and shrinkage has led rapidly to the search-and-capture model, which represents the prevailing guiding principle for spindle assembly in somatic vertebrate cells containing centrosomes (Kirschner and Mitchison, 1986; Heald and Khodjakov, 2015). According to this model, the attachment of KTs to the nascent spindle occurs largely stochastically in that KTs capture centrosome-nucleated MTs, exploring the cytoplasm by their dynamic instability behavior, as they grow into their vicinity (Figure 9A). A Ran-GTP concentration gradient formed around chromosomes thereby helps to “guide” the MTs towards them and increases, together with other mechanisms such as the sweeping movements of the growing MTs (termed pivoting), the

efficiency of the search-capture process (Kalinina et al., 2012; Wollman et al., 2005; Weaver and Walczak, 2015).

Since sister KTs are initially oriented in variable positions relative to the two poles of the growing spindle, the chance encounter with MTs gives rise frequently to KT attachments that are not bioriented (Figure 9B and 9C). Some of these are transient attachment intermediates that can normally occur in the course of biorientation. These include monotelic attachments, in which only one sister KT binds to MTs from one spindle pole, and lateral attachments, in which KTs attach to the side wall (the lattice) of spindle MTs. Lateral attachments involve the molecular motors Dynein (which is minus-end directed) and CENP-E (which is plus-end directed) and are important for the spatial positioning of chromosomes to spindle poles and the spindle equator, respectively. They are thought to be converted to end-on attachments when MT ends shrink to the KT and are grasped by outer KT components, such as the Ndc80 complex (Barisic et al., 2014; Kapoor et al., 2006; Kops et al., 2010; Shrestha and Draviam, 2013). Besides these normal attachment intermediates, sister KTs can also engage in two different erroneous configurations, including syntelic and merotelic. In the syntelic attachment state, both sister KTs interact with MTs emanating from the same spindle pole, while in the merotelic state, a single KT of a sister pair connects to both poles (Figure 9C). Merotelic attachments are particularly problematic because they evade detection by the SAC and can lead to lagging chromosomes during anaphase (Cimini et al., 2002; Salmon et al., 2005). Lagging chromosomes, in turn, contribute to chromosome instability (CIN) in cancer cells and constitute a potential source for structural chromosome aberrations and DNA damage (Crasta et al., 2012; Janssen et al., 2011; Thompson and Compton,

2008). Thus, such malorientations must be converted to bioriented attachments to ensure faithful chromosome segregation.

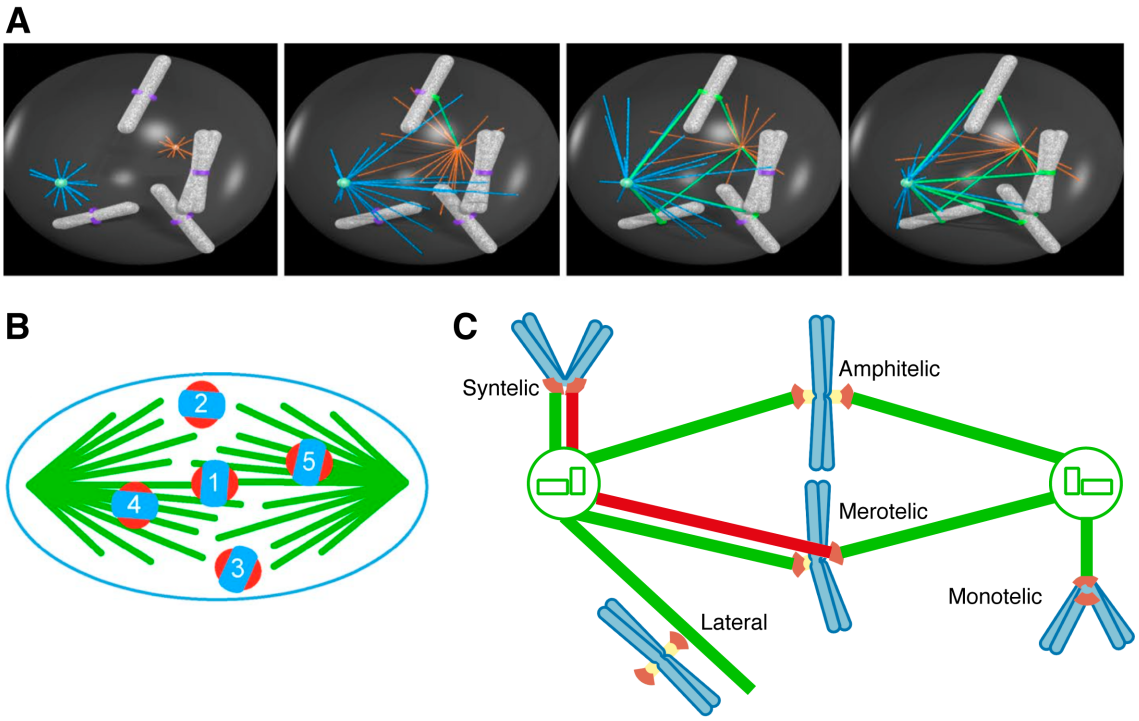

Figure 9. Chromosome attachment to the mitotic spindle by stochastic MT search-and-capture. (**A**) Classical search-and-capture model of spindle assembly. MT arrays (blue and orange) nucleated at the two centrosomes explore the cytoplasm by their dynamic instability behavior until they encounter a KT (magenta) and get partially stabilized (indicated by color change of KTs and MTs to green). (**B**,**C**) Variable initial sister KT positions during search-and-capture can lead to different attachment configurations. Sister KTs oriented midway between the spindle poles and with their axis aligned favorably have a reasonable chance for forming bioriented/amphitelic attachments (1). Sister KTs that do not face the poles may form merotelic attachment errors (2 and 3). Sister KTs close to the poles that are exposed to a high density of MTs from one pole may become oriented in a syntelic (4) or monotelic (5) fashion. Illustrations adapted from (Heald and Khodjakov, 2015) and (Khodjakov and Pines, 2010).

The spindle assembly checkpoint

Unattached and tensionless (i.e. laterally attached and monooriented) sister KTs activate the spindle assembly checkpoint (SAC), a regulatory mechanism that delays the initiation of anaphase to provide sufficient time for the conversion of these attachments to bioriented attachments (Collin et al., 2013; Kapoor et al., 2000; Magidson et al., 2015; Rieder et al., 1995). The SAC was originally discovered in budding yeast by genetic screens for mutants that failed to arrest in mitosis in the presence of spindle poisons (Hoyt et al., 1991; Li and Murray, 1991; Weiss and Winey, 1996). The core components of the SAC include Mad1, Mad2, BubR1/Mad3, Bub1, Bub3, and Mps1. In higher eukaryotes, checkpoint function also depends on the RZZ (Rod-Zw10-Zwilch) complex (Stukenberg and Burke, 2015). These proteins accumulate at unattached or tensionless KTs to initiate SAC signaling and are depleted following bipolar attachment (Musacchio and Salmon, 2007).

The molecular mechanisms by which the checkpoint machinery monitors the attachment status of KTs are not well understood. Several constituents of the outer KT that directly bind MTs are known to interact with SAC components, including Ndc80, KNL1, and CENP-E (Martin-Lluesma et al., 2002; Mao et al., 2003; Kiyomitsu et al., 2007; Yamagishi et al., 2012). Current evidence suggests that engagement of some of these factors with MTs may regulate the availability of binding sites for checkpoint components through direct competition with MT binding and/or through conformational and biochemical changes that follow intra-KT tension or stable MT occupancy (which is subordinate to establishment of tension) (Aravamudhan et al., 2015; Etemad et al., 2015; Hiruma et al., 2015; Maresca and Salmon, 2009; Tauchman et al., 2015; Ji et al., 2015).

While it remains unclear how exactly the SAC senses the attachment status, the nature of the downstream effector signal of the SAC that delays anaphase onset is becoming increasingly clear. Unattached or tensionless KTs catalyze the formation of a diffusible inhibitor, termed the mitotic checkpoint complex (MCC). This complex targets and inhibits the E3 ubiquitin ligase anaphase-promoting complex/cyclosome (APC/C) through inactivation of Cdc20, a critical coactivator of the APC/C. The APC/C, in turn, triggers mitotic exit and sister chromatid separation by polyubiquitinylation of Cyclin B and Securin (an inhibitor of the enzyme Separase, which cleaves cohesin complexes), thereby promoting their rapid proteasomal degradation (Figure 10) (Musacchio, 2015).

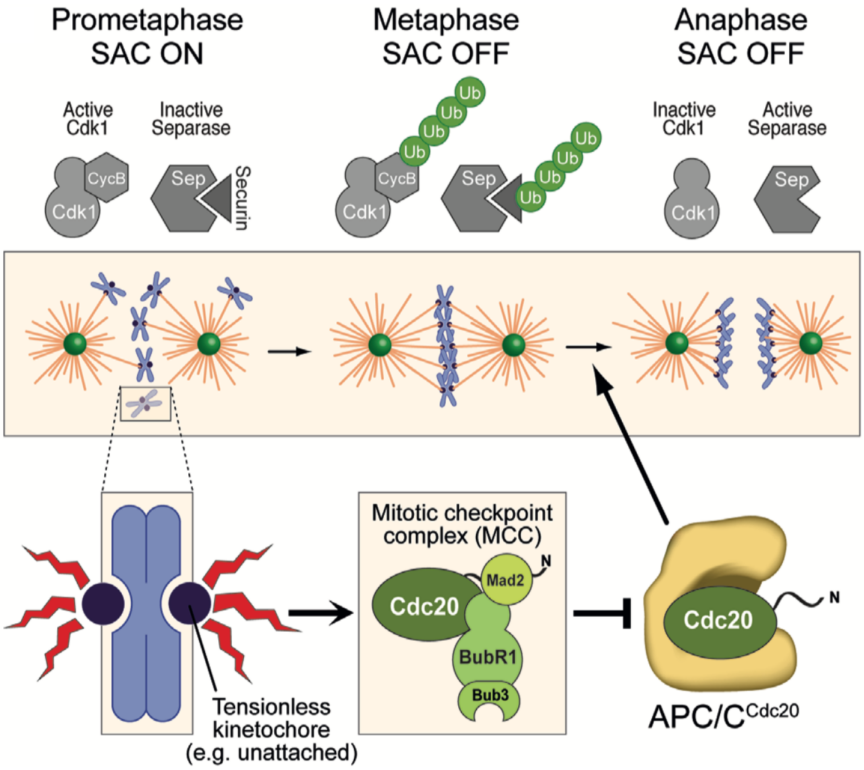

Figure 10. The spindle assembly checkpoint. Unattached or tensionless KTs promote assembly of the MCC. The MCC binds to the APC/C in complex with a second Cdc20 molecule (which can act both as APC/C coactivator and as MCC subunit) and inhibits its activity (Izawa and Pines, 2015). Upon bipolar attachment, APC/C^{Cdc20} activation triggers Securin and Cyclin B ubiquitinylation (Ub) and proteolysis. This leads to activation of Separase and inactivation of CDK1, which enables chromatid separation and mitotic exit. Illustration adapted from (Krenn and Musacchio, 2015).

A key step in the assembly of the MCC, which contains Mad2, BubR1/Mad3, Bub3, and Cdc20 (Hardwick et al., 2000; Sudakin et al., 2001), is the KT-based formation of Mad2:Cdc20 complexes. Mad2 adopts two conformations: an inactive open (O-Mad2) conformation when unbound in the cytoplasm and an active closed conformation when liganded with Mad1 or Cdc20 (Luo and Yu, 2008). Mad2 is held in the closed conformation at KTs by the interaction with Mad1. Mad1-bound C-Mad2 recruits additional cytosolic O-Mad2 and enhances through dimerization the ability of Mad2 to bind Cdc20, thereby catalyzing the formation of C-Mad2:Cdc20 complexes. The resulting C-Mad2:Cdc20 complexes diffuse away from KTs and subsequently assemble with Bub3 and BubR1 the MCC. Upon KT release, C-Mad2:Cdc20 may further promote the conversion of O-Mad2 to C-Mad2:Cdc20 complexes in the cytoplasm, amplifying the effector signal (De Antoni et al., 2005; Mapelli et al., 2007; Mapelli and Musacchio, 2007).

Once bipolar attachments are formed, additional proteins act to silence SAC signaling. These include Dynein, which "strips off" checkpoint proteins from KTs (Howell et al., 2001), and the Mad2-binding protein p31^{comet}, which triggers "capping" of the Mad1:C-Mad2 KT template and MCC dissociation, in concert with the AAA-ATPase TRIP13 (Eytan et al., 2014; Hagan et al., 2011; Mapelli et al., 2006; Westhorpe et al., 2011). In addition, KT targeting of protein phosphatases is important to oppose and revert phosphorylation events made by checkpoint kinases (Foley and Kapoor, 2013; Stukenberg and Burke, 2015).

Although the SAC can "buy" time for biorientation, it does not directly prevent or correct attachment errors *per se*. Accordingly, other mechanisms are required for these essential tasks.

Mechanisms promoting chromosome biorientation

The prevalence of attachment errors is determined by the rate at which they form and the rate at which they are corrected. The efficiency of correction must thereby exceed the frequency at which new errors are formed by the stochastic capture of MTs. Otherwise, errors will accumulate and may lead to chromosome missegregation and aneuploidy (Cimini, 2008; Godek et al., 2014).

Avoidance of attachment errors

Several mechanisms are known to increase the likelihood that sister KTs encounter MTs from opposite spindle poles. Most of these help to exploit the back-to-back arrangement of sister KTs that favors MT capture of the KT facing away from the opposite pole (Indjeian and Murray, 2007; Nicklas, 1997; Lončarek et al., 2007). For example, lateral attachments and the concerted action of minus-end directed motors and polar ejection forces have been suggested to promote, by angular rotation, pre-alignment of sister KTs on the nascent spindle, such that the sister KTs face opposite poles (Figure 11). The enlargement of the outer KT layer prior to end-on attachment thereby increases the surface for efficient lateral capture of MTs and improves the rotation angle (Magidson et al., 2015). Motor movements and polar ejections forces on the chromosomes arms also contribute to favorably arrange chromosomes relative to the spindle poles (Kops et al., 2010; Magidson et al., 2011; Walczak et al., 2010). Another mechanism that may provide a bias towards bioriented attachment is based on the activity of KTs and chromatin to nucleate MTs, which are assembled into polarized bundles, termed preformed K-fibers (Khodjakov et al., 2003; Maiato et al., 2004a; Meunier and Vernos, 2015). KT-derived MTs are thought to extend away

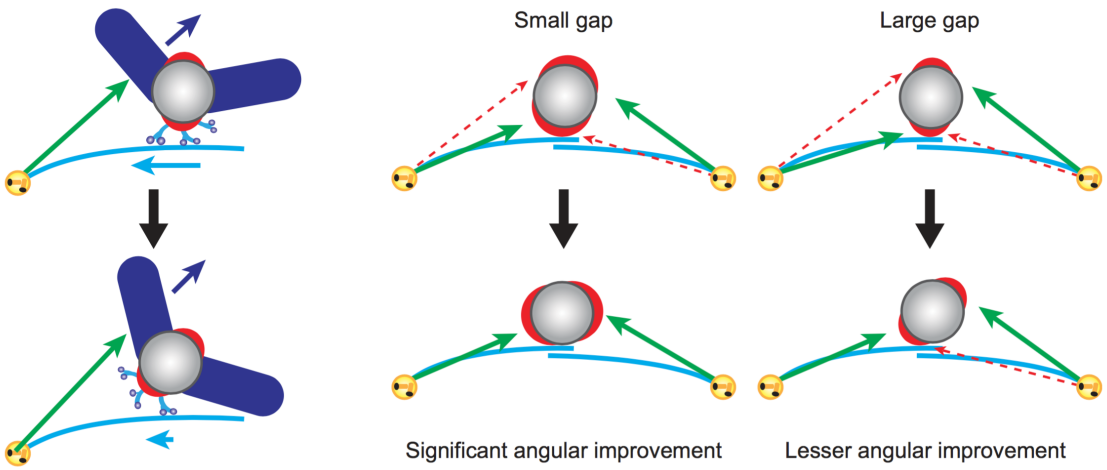

Figure 11. Model for prealignment of sister KTs by angular rotation due to lateral attachment. *Left*, polar ejection forces (chromokinesins) acting on the chromosome arms and opposing inward forces generated at the KT (e.g. by Dynein) rotates the centromere so that the sister KTs become favorably oriented toward opposite spindle poles. *Right*, larger KTs (small gap between sister KTs) support a more significant rotation, whereas rotation of smaller KTs (large gap) is limited because small KTs lose direct contact with MTs, dampening the inward force. Illustration adapted from (Magidson et al., 2015).

from KTs with their minus-ends organized in pole-like structures that contain Dynein and NuMA, which, in turn, facilitate KT loading onto the lattice of spindle pole-derived MTs (Goshima et al., 2005; Khodjakov et al., 2003; Stukenberg and Burke, 2015). Computer simulations have suggested that these pre-formed K-fibers increase the efficiency of MT capture and may, similar to lateral attachments, reduce the formation of attachment errors by rotating chromosomes, so that sister KTs become aligned with the spindle pole-to-pole axis (Paul et al., 2009). Finally, mechanisms that ensure the formation of a bipolar spindle array, such as the regulated duplication of centrosomes and their timely separation at NEBD help to keep attachment error rates low (Ganem et al., 2009; McHedlishvili et al., 2012; Silkworth et al., 2012).

Error correction: Targeted release *versus* indiscriminate turnover

The removal of improper attachments after they have formed is enabled by the turnover of KT-MTs, that is, continuous cycles of MT detachment, depolymerization, repolymerization, and reattachment (Zhai et al., 1995). This dynamic exchange of KT-MTs contributes to the correction of attachment errors likely by two mechanisms (Godek et al., 2014). In one, the KT-MT turnover rate is enhanced specifically on improperly attached KTs, leading to the selective release of attachment errors. Such a targeted regulation may be the main strategy for the correction of syntelic attachments (Lampson et al., 2004; Salimian et al., 2011). Unlike merotelic malorientations, syntelic attachments interfere with chromosome congression and are clearly distinguishable from bipolar attachments, as they produce only low intra-KT as well as centromeric tension and activate the SAC (Musacchio and Salmon, 2007). Moreover, it has been observed that syntelic attachment shifts the sister KTs towards one side of the centromere, abrogating their back-to-back geometry (Lončarek et al., 2007). On the other hand, a global regulation of the KT-MT turnover without discriminating between properly and improperly oriented KT-MTs may be a major mechanism for the correction of merotelic attachment errors. In line with this view, suppression of the overall dynamics of KT-MTs both in prometaphase and metaphase has been shown to elevate the frequency of merotelic attachments in human cultured cells. Stimulation of the global KT-MT turnover, in turn, was found to reduce the missegregation rate in tumor cell lines with hyperstable KT-MTs (Bakhoum et al., 2008; 2009). The value of regulating the KT-MT turnover of all KTs becomes apparent, when considering that the release of maloriented MTs from KTs is likely the rate-limiting step for error correction (Nicklas and Ward, 1994) and that

the back-to-back geometry of sister KTs provides a bias for MT capture from opposite poles. In this view, promoting the turnover of both bioriented and merotelic KT-MTs would distinctly favor the accumulation of bioriented attachments. Indeed, computer modeling has highlighted that “indiscriminate” KT-MT turnover can provide strong error correction activity for back-to-back oriented sister KTs with a geometrical constraint for MT capture (Zaytsev and Grishchuk, 2015). Considering also that chromosomes acquire merotelic attachments at highest frequency during spindle formation in early prometaphase, but can subsequently congress to the spindle equator (Cimini, 2003), such a global correction mechanism may be particularly beneficial for merotelic error correction during later stages of mitosis, when sister KTs are favorably aligned with the spindle pole axis. Hence, elevating the KT-MT turnover rate of all KTs should improve the error correction efficiency. Yet, excessive KT-MT dynamics would prevent KTs from attaining an adequate number of MTs for satisfaction of the SAC as well as stable load-bearing K-fiber attachments. On the other hand, too slow turnover again raises the frequency of attachment errors. Accordingly, the “dynamic range” of KT-MT attachments must be kept within a narrow window, in order to satisfy the requirements for proper biorientation and faithful chromosome segregation (Figure 12) (Bakhoum and Compton, 2012; Zaytsev and Grishchuk, 2015).

To achieve such a narrow “dynamic range” for KT-MT attachments, both the strength of the grip of KTs on the MT lattice and the polymerization and depolymerization dynamics of KT-MTs within the KT binding sites must be precisely controlled during the course of mitosis. Although these two mechanical properties can be regulated independently from each other (Amaro et al., 2010), they are

closely related. For example, it was found that if the binding affinity between the Ndc80 complex and the MT lattice is too high, MT plus-end dynamics is suppressed (DeLuca et al., 2006). Thus, the grip on the KT-MT lattice must be kept “loose” enough to allow for fluid KT-MT plus-end dynamics.

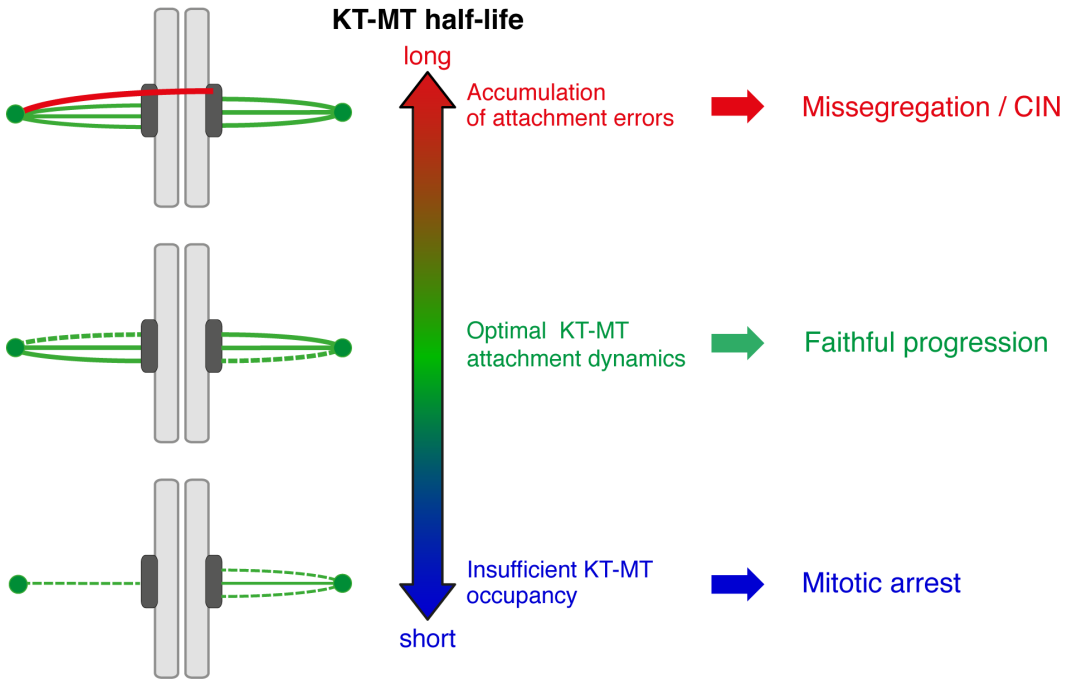

Figure 12. Relation between KT-MT attachment dynamics and chromosome segregation fidelity. KT-MT attachment stability and plus-end dynamics must fall within a narrow range to ensure faithful progression into anaphase. A sufficient degree of KT-MT attachment instability and plus-end turnover is required for error correction and force generation for chromosome movements, respectively. Too transient interactions between KTs and MTs result in insufficient MT occupancy at KTs and persistent SAC activity (*bottom*), whereas overly strong and static interactions cause the accumulation of improper attachments (e.g. merotelic attachments), which in turn can lead to chromosome missegregation and chromosomal instability (CIN) (*top*).

Molecular control of KT-MT attachment

At the molecular level, control of KT-MT attachment depends largely on the interplay between kinases and phosphatases, which regulate KT composition and MT-binding properties of their KT substrates (Godek et al., 2014). In addition, there is evidence that mechanical tension *per se* can impact KT-MT attachment by activating a "catch-bond" mechanism (Sarangapani and Asbury, 2014).

Aurora B kinase

One of the key regulators of both KT-MT attachment stability and plus-end dynamics is the conserved serine/threonine kinase Aurora B. Perturbation of Aurora B function through small-molecule inhibitors increases both syntelic and merotelic attachments and suppresses KT-MT plus-end turnover in mammalian cultured cells (Cimini et al., 2006; Ditchfield, 2003; Hauf et al., 2003). Conversely, an increase of Aurora B (Ipl1) activity by its overexpression in budding yeast has been shown to cause continuous disruption of all KT-MT attachments (Muñoz-Barrera and Monje-Casas, 2014). Prior to anaphase, it is found along chromosome arms and becomes enriched at the inner centromere as part of the chromosomal passenger complex (CPC), that also includes Borealin, the inner centromere protein (INCENP), and Survivin (Carmena et al., 2012). Functionally relevant pools of the kinase or of its phosphorylated forms have also been reported to localize to spindle MTs (Tseng et al., 2010; Banerjee et al., 2014) and KTs prior to anaphase (Posch et al., 2010; DeLuca et al., 2011; Petsalaki et al., 2011; Bekier et al., 2015). At KTs, Aurora B differentially phosphorylates KT proteins that bind MTs, including the KMN network, the Dam1 complex, and the Ska complex, to decrease their MT-binding activity and to actively promote MT catastrophe

(Lampson et al., 2004; Welburn et al., 2010; Umbreit et al., 2012; Sarangapani et al., 2013; Schmidt et al., 2012; Chan et al., 2012). Moreover, the kinase regulates the dynamics of KT-MTs by controlling the localization and activity of various MT-associated proteins, such as MCAK and CENP-E (Tanno et al., 2010; Ditchfield, 2003), which can modulate directly or indirectly the dynamics of KT-MT attachments (Bakhoum et al., 2009; Wordeman et al., 2007; Maffini et al., 2009). MCAK and CENP-E, in turn, also have an important function in chromosome alignment (Kline-Smith, 2003; Tanno et al., 2010; Kapoor et al., 2006; Auckland and McAinsh, 2015). Finally, Aurora B is in an antagonistic relationship with protein phosphatases, including protein phosphatase 1 (PP1) and PP2A-B56 families, which oppose the phosphorylation of Aurora B substrates and reportedly also directly influence the activity state of Aurora B (Krenn and Musacchio, 2015; Sugiyama et al., 2002a). These functions are not only crucial for the reorientation of improperly attached KTs during establishment of biorientation in early mitosis, but also to sustain an adequate degree of KT-MT attachment dynamics to allow for fluid MT plus-end turnover for chromosome movements and error correction in late mitosis (Bakhoum et al., 2009; Cimini et al., 2006; DeLuca et al., 2011; Tanno et al., 2015).

The Ska complex

Among the various KT targets of Aurora B, the spindle and KT-associated (Ska) complex is recognized as an important factor for the stability of K-fibers and as a potential functional equivalent of the yeast Dam1 complex that couples chromosome movement to MT plus-end depolymerization (Hanisch et al., 2006; Gaitanos et al., 2009; Raaijmakers et al., 2009; Welburn et al., 2009; Schmidt et al., 2012). The Ska

complex is present in vertebrates but is absent in fungi and *D. melanogaster*, although apparent homologues of complex subunits can be found in other insects, as well as in nematodes and plants. In vertebrates, the Ska complex consists of three subunits (Ska1, Ska2 and Ska3) and localizes to both spindle MTs and outer KTs after NEBD. While it stays associated with spindle MTs throughout mitosis, the complex becomes maximally enriched at bioriented KTs in late prometaphase/metaphase and leaves the KTs in telophase (Raaijmakers et al., 2009; Chan et al., 2012; Jeyaprakash et al., 2012). Accumulation of Ska at the KT-MT interface is important to confer cold-stability to K-fibers and this function is opposed by Aurora B activity (Chan et al., 2012). Besides its role in fostering K-fiber stability, Ska has been implicated in chromosome alignment and timely metaphase-to-anaphase transition (Hanisch et al., 2006; Schmidt et al., 2012; Abad et al., 2014). The latter role possibly reflects a function of Ska in silencing the SAC or in facilitating the activity of the APC/C (Daum et al., 2009; Sivakumar et al., 2014).

Aim of this work

Here, we focused on a functional interplay between the Ska complex and Aurora B kinase, with the aim of understanding the mechanisms that generate stable yet dynamic KT-MT attachments, which are essential for chromosome biorientation and error-free chromosome segregation.

First, we used siRNA-mediated depletion and high-resolution live-cell microscopy combined with laser-induced photoactivation and KT tracking to reveal that the Ska complex is not only required for K-fiber stability, but also for chromosome biorientation and control of KT-MT dynamics. As these functions overlapped with those previously described for Aurora B, we hypothesized that the Ska complex may act to mediate faithful mitotic progression by regulating Aurora B activity. We set out to test this hypothesis, in a second step, using cell-based and biochemical assays. Finally, having established that the Ska complex stimulates the activity of Aurora B, we asked how Ska is able to promote maturation of K-fiber attachments once biorientation is achieved, given that Aurora B antagonizes this function.

Results

The Ska complex is required for error-free chromosome segregation

We sought to gain novel insights into Ska complex function by reexploring the consequences of Ska depletion in HeLa S3 cells using high-resolution time-lapse microscopy. Asynchronously growing cells stably expressing histone H2B–GFP were cotransfected with siRNAs against two different Ska subunits (Ska1 and Ska3) to achieve specific targeting of the Ska complex and were filmed 36-40 h after transfection. As reported previously (Hanisch et al., 2006; Daum et al., 2009; Gaitanos et al., 2009; Welburn et al., 2009), Ska-depleted cells displayed prominent early mitotic defects including (i) a late prometaphase delay with occasional loss of chromosomes from the spindle equator and rotation and/or widening of the equatorial plate, (ii) a similar late prometaphase arrest with subsequent chromosome scattering (cohesion fatigue), and (iii) a complete chromosome congression failure (Figure 12A). While cells showing chromosome scattering and alignment defects underwent in the majority of cases mitotic cell death, the remaining cells (~75% of the population; Figure 13A) were eventually able to progress into anaphase. Strikingly, when we analyzed chromosome behavior in these cells, we observed a marked increase in the frequency of segregation errors. Specifically, 21% of the anaphases in Ska-depleted cells displayed lagging chromosomes, as compared to 3% in control cells (Figure 12B and 12C). Live-cell analysis showed that these lagging chromosomes occasionally segregated, either as whole chromosomes or as fragments after chromosome breakage, into micronuclei (data not shown). Consistently, micro-nucleated cells occurred with a twofold higher frequency, when measured in

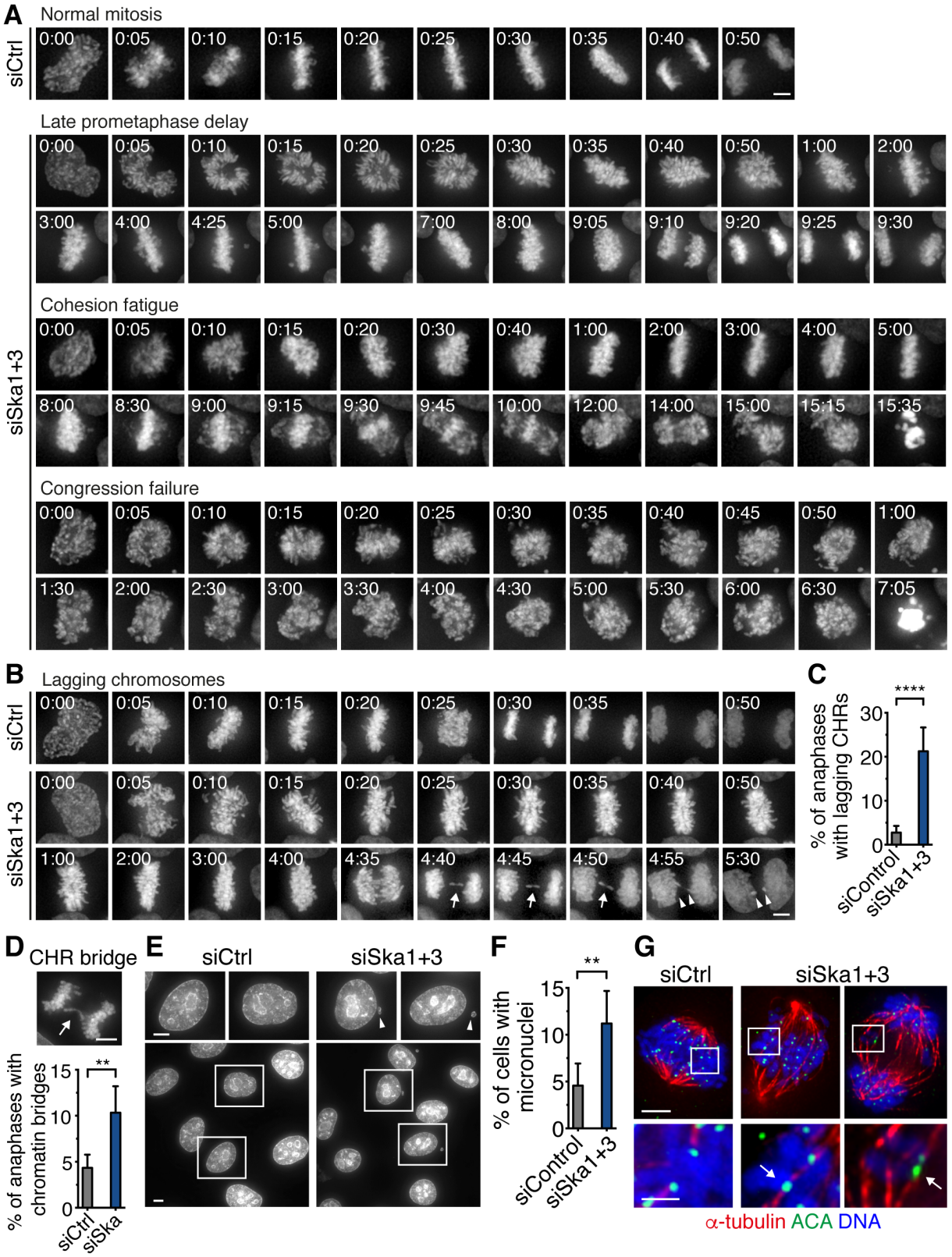

Figure 12. The Ska complex is required for error-free chromosome segregation. (**A**) Selected images from time-lapse imaging sequences of HeLa S3 H2B–GFP cells treated with control or Ska1 and Ska3 siRNAs for 36–40 h before imaging that illustrate previously described Ska RNAi phenotypes. (**B**) Lagging chromosome Ska depletion phenotype. *Top*, mitotic progression of a siControl cell. *Bottom*, example of a siSka1+3 cell showing a lagging chromosome and subsequent chromosome breakage. The arrows point at the lagging chromosome, arrowheads highlight the

chromosome fragments. Scale bar, 5 *μ*m. (**C**) Percentage of anaphase cells with lagging chromosomes. Bars represent mean ± 95% confidence interval (CI) ($n \geq 300$ anaphase cells per condition from $N = 4$ independent experiments). (**D**) Representative image and quantification of anaphase cells with chromatin bridges. Bars represent mean ± 95% CI ($n \geq 275$ anaphase cells per condition from $N = 3$ independent experiments). (**E**) Nuclear integrity of siControl or siSka1+3 cells in interphase 48 h after siRNA transfection. Cells were fixed and stained for DNA with Hoechst dye. Scale bars, 5 *μ*m. (**F**) Percentage of micronucleated interphase cells. Bars represent mean ± 95% CI ($n = 1500$ cells per condition from $N = 3$). (**G**) siControl or siSka1+3 transfected cells were treated after 48 h with the Mps1 inhibitor reversine for 20–25 min to force anaphase entry, followed by 5 min incubation at 4°C to depolymerize non-KT-MTs. Cells were fixed and immunostained with the indicated antibodies. *Left*, optical section of a siControl cell before anaphase onset. A bioriented sister KT pair is depicted in the enlarged crop. *Right*, optical sections of two siSka1+3 cells with merotelic attachments before and after anaphase onset. Merotelic-oriented sister KTs are highlighted by arrows in the enlarged crops. Scale bars, 5 *μ*m (*upper panel*) and 1 *μ*m (*lower panel*). Asterisks show statistical significance (Student's *t*-test, unpaired). **** $P \leq 0.0001$; ** $P \leq 0.01$.

fixed cells (11% versus 5%, for Ska depletion and control cells, respectively) (Figure 12E and 12F). In addition to lagging chromosomes and micronuclei, we also detected chromatin bridges at lower but elevated frequencies upon Ska depletion (10% versus 4%) (Figure 12D). The leading cause of lagging chromosomes in anaphase is merotelic KT orientation (Cimini et al., 2001; 2002), while chromatin bridges may arise from unresolved merotelic attachments or other premitotic defects (Gisselsson, 2008; Steigemann et al., 2009). To confirm that lagging chromosomes in Ska-depleted cells are a result of merotely, we sought to analyze the attachment status on these chromosomes. In order to enrich Ska-deficient cells in anaphase and depolymerize non-KT-MTs that occlude precise assessment of KT-MT interactions, cells were treated with an inhibitor of the checkpoint kinase Mps1 and cold. Under these experimental conditions, KTs on lagging chromosomes, identified by a single anti-centromere-antibody (ACA) signal, often appeared with MT contacts oriented toward both spindle poles, consistent with persistent merotelic attachment (Figure 12G). Together, these data suggest a role of the Ska complex in correction or prevention of merotelic attachments, thus revealing a novel phenotypic aspect of Ska loss-of-function.

Loss of the Ska complex abolishes the control of KT-MT dynamics

Correction of attachment errors relies on the detachment and depolymerization of inappropriately oriented MTs from KTs. Consequently, this process is dependent on factors governing the kinetics of MT polymerization and depolymerization at KTs (Zhai et al., 1995; Bakhoum and Compton, 2012). To test whether the Ska complex promotes error correction by modulating KT-MT dynamics, we examined MT plus-end turnover in absence of Ska using HeLa K cells stably expressing photo-activatable GFP–α-tubulin and histone H2B–mRFP (Amaro et al., 2010). In comparison to HeLa S3 cells, these cells were more sensitive to double depletion of Ska complex subunits, as seen by higher frequencies of cell death and elevated mitotic timings (Figure 13A). To increase cell viability but achieve comparable knockdown efficiencies, assays with this cell line were performed with Ska3 single-siRNA treatment (Figure 13A and 13B) (Gaitanos et al., 2009). We measured tubulin turnover at MT plus-ends by fluorescence dissipation after photoactivation. GFP was

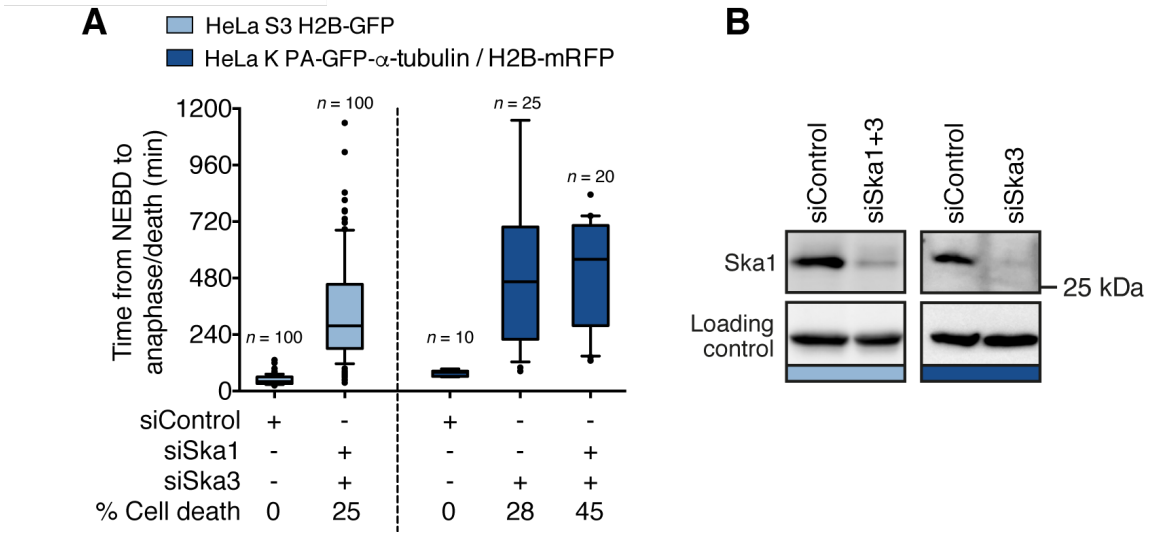

Figure 13. Efficiency of Ska complex depletion in HeLa K PA-GFP–α-tubulin/H2B–mRFP and HeLa S3 cells. (**A**) Box-and-whisker plot showing the elapsed time between NEBD and anaphase onset/mitotic cell death after the indicated siRNA treatments. The number of cells (*n*) analyzed is given above each box. Percentage of mitotic cell death is displayed below the plot. (**B**) Western blot anaylsis of mitotic cell extracts of HeLa S3 H2B–GFP cells (*pale blue*) or HeLa K PA-GFP–α-tubulin/H2B–mRFP cells (*dark blue*) treated with the indicated siRNAs for 48 h. Note that depletion of any Ska complex subunit leads to destabilization of the entire complex.

activated along a line close to the chromosome mass in cells with a late prometaphase chromosome arrangement and the decrease of fluorescence in the activated regions was followed over time (Figure 14A). Both in control- and Ska-depleted cells the fluorescence dissipation was biphasic and best fit by a double-exponential curve ($R^2 > 0.99$) (Figure 14B), with the fast phase reflecting free non-KT-MTs and the slow phase representing the more stable K-fiber population (Mitchison, 1989; Zhai et al., 1995). Knockdown of the Ska complex increased the fraction of non-KT-MTs within K-fibers (from 52% in control cells to 67% in Ska3-depleted cells) (Figure 14D), in line with previous cold sensitivity assays (Hanisch et al., 2006; Gaitanos et al., 2009). Moreover, Ska-deficiency caused a ~1.8-fold increase in the half-life of KT-MTs relative to control-depleted cells (368s versus 202s for siSka3 and control cells, respectively), while half-lives of non-KT-MTs remained similar in each case (14s versus 12s for siSka3 and control cells, respectively) (Figure 14C). Similar results were obtained when targeting the Ska complex with Ska1 single-siRNA treatment (Figure 14A–D). Thus, the Ska complex is required both to attain and/or maintain K-fibers with a normal number of MTs and to sustain the plus-end turnover of KT-MTs.

We also measured poleward MT flux by determining the rates of the pole-directed movement of fluorescent marks away from the chromosome mass. We found that the average poleward tubulin transport was markedly increased in spindles of Ska-depleted cells as compared to control spindles (1.62 μm/min versus 0.94 μm/min for siSka3 and control cells, respectively) (Figure 14E). This finding is in agreement with previous reports suggesting a direct correlation between high MT flux rates and long MT half-life (Buster et al., 2007; McHedlishvili et al., 2012).

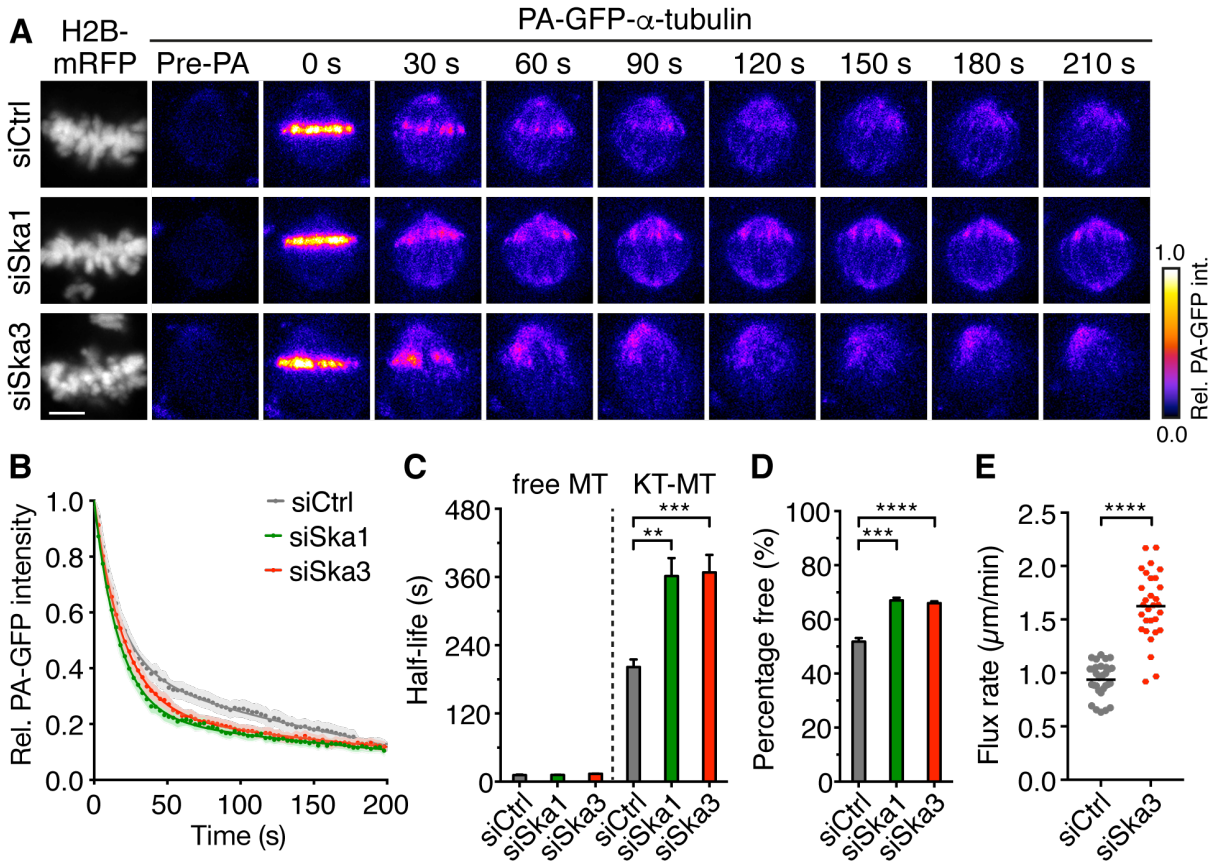

F **Table.** Double exponential decay curve fitting parameters

Double exp. fit: $I_t = P_{fast}\ exp\ (-K_{fast}\ t) + P_{slow}\ exp\ (-K_{slow}\ t)$			
	siCtrl	siSka1	siSka3
n (fibers)	111	83	111
n (cells)	32	23	31
N (experiments)	3	2	3
P_{fast}	0.52	0.67	0.66
K_{fast}	0.060	0.058	0.049
$t_{1/2}$ (fast) = ln(2) / K_{fast}	11.6	11.9	14
K_{slow}	0.00344	0.00192	0.00188
$t_{1/2}$ (slow) = ln(2) / K_{slow}	202	362	368

Figure 14. Loss of the Ska complex slows the KT-MT plus-end turnover and decreases the number of MTs within K-fibers. (**A**) Live cell fluorescence images (pseudo-colored heat maps) before and after photoactivation of HeLa K cells stably expressing photoactivatable (PA)-GFP–α-tubulin and histone H2B–mRFP treated with control, Ska1 or Ska3 siRNAs for 48 h. (**B**) Quantification of the fluorescence intensity decay of the activated regions over time. Relative GFP intensities were fitted to a double exponential equation corresponding to fast (free MT) and slow MT (KT-MT) populations (see Experimental Procedures for detail). Shaded areas represent the 95% CI. (**C**,**D**) Bar graphs illustrating fitting parameters obtained from **B**. (**C**) Half-life of free MTs and KT-MTs. (**D**) Percentage of the free MTs. Bars represent mean ± 95% CI. (**E**) Scatter plot showing poleward MT flux rates in cells treated as in **A**. Each dot represents the average cellular flux calculated from ≥ 3 K-fibers per cell (*n* = 30 cells per condition from *N* = 3 independent experiments). The horizontal lines depict mean. (**F**) Table showing sample sizes and fitting parameters related to **B**. Asterisks show statistical significance (Student's *t*-test, unpaired). **** P ≤ 0.0001; *** P ≤ 0.001; ** P ≤ 0.01 ns. Scale bar, 5 μm.

In addition, based on live-cell tracking analysis of HeLa K cells stably expressing EGFP-CENP-A (a marker for KTs), we found that sister KT oscillations (i.e. sister KT movements along the spindle axis) and sister KT breathing (i.e. changes in the distance between sister KTs) were clearly impaired in Ska-deficient cells, consistent with the abrogated control of KT-MT plus-end turnover (Figure 15A–C).

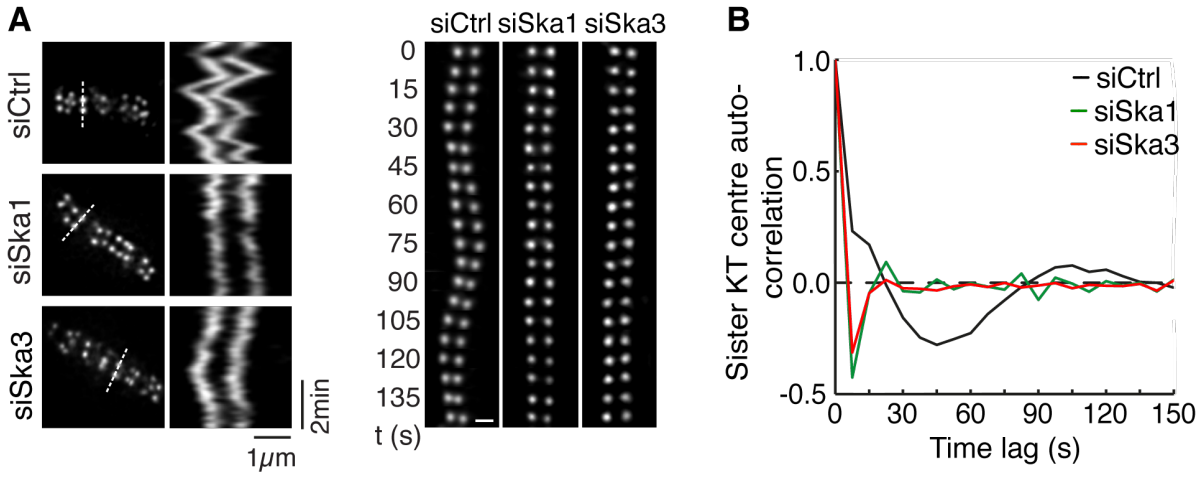

C **Table.** Number of KT pairs analyzed by 3D KT tracking

	siCtrl	siSka1	siSka3
n (sister-KT pairs)	1512	1043	1654
n (cells)	49	32	58
N (experiments)	3	2	3

Figure 15. Ska depletion abrogates sister KT oscillations and breathing. (**A**) Kymographs (left) and live-cell stills (*right*) of single sister KT oscillations in living HeLa K cells stably expressing EGFP–CENP-A treated for 48 h with control, Ska1 or Ska3 siRNAs. Scale bars, 1 μm. (**B**) Quantification of sister KT oscillations using automated sister KT tracking. The graph shows the autocorrelation function of KT oscillations in siControl (black line), siSka1 (green line), and siSka3 (red line) cells. The autocorrelation function was calculated by combining all aligned sister KT pairs for each condition. The first negative lobe in siControl cells indicates the half-period of the mean oscillation period and its depth indicates the regularity of the oscillations. The second positive lobe indicates the full period. Note that a negative value at a short time lag is indicative of random motion (Jaqaman et al., 2010). (**C**) Table showing the number of sister KTs analyzed for calculating the autocorrelation function.

Ska regulates KT-MT dynamics and chromosome alignment through KT localization of the Aurora B effectors MCAK and CENP-E

To determine how the Ska complex controls KT-MT plus-end turnover, we next investigated whether Ska depletion alters the distribution of proteins implicated in the regulation of KT-MT dynamics. Interestingly, we found that Ska depletion impaired inner KT localization, but not spindle pole association, of the Aurora B downstream effector MCAK in HeLa S3 cells (Figure 16A and 16B), without affecting its total protein levels (Figure 16C). A similar reduction in MCAK inner KT levels was observed in the chromosomally stable, non-transformed cell line MCF10A following Ska knockdown (Figure 16D and 16E). Notably, this effect on MCAK KT localization is not a consequence of changes in KT-MT plus-end dynamics or occupancy since MCAK associates with the inner KT/centromere independently of MTs (Figure 16F and 16G) (Kline-Smith, 2003; Andrews et al., 2004). Conversely, depletion of MCAK did not produce a major effect on Ska3 KT localization, placing the Ska complex upstream of MCAK (Figure 16H and 16I). Immunoprecipitation assays from mitotic HeLa S3 cells failed to reveal MCAK in Ska1 immunoprecipitates (Figure 16J), suggesting that the Ska complex is required to support MCAK localization to the inner KT independently of a physical interaction.

We also found that KT localization of CENP-E, another Aurora B effector reportedly required to promote KT-MT plus-end turnover (Maffini et al., 2009), was reduced in Ska-depleted cells, to a similar extent as upon direct inhibition of Aurora B (Figure 17A and 17B).

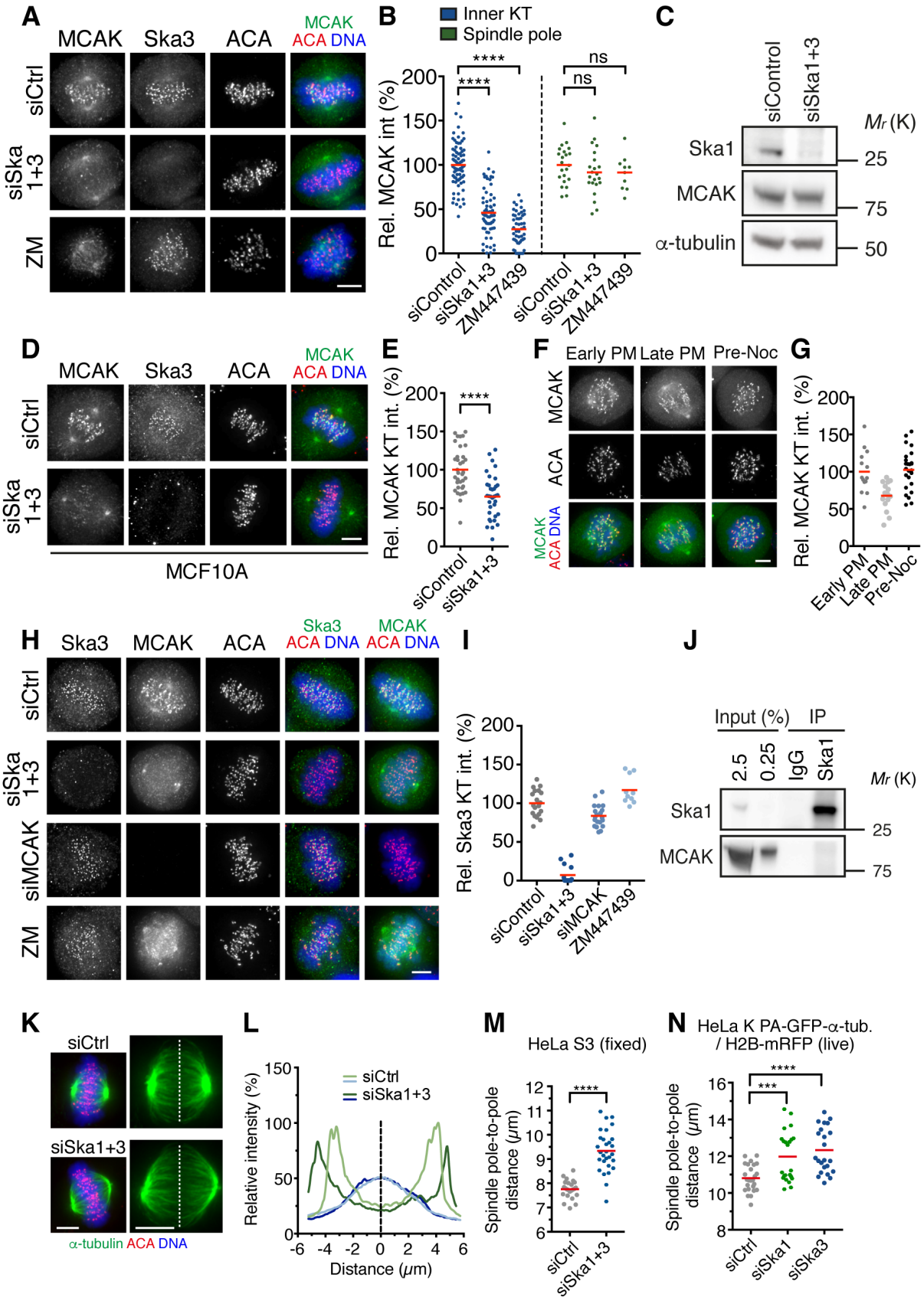

Figure 16. KT localization of MCAK and spindle length are dependent on the Ska complex. (**A**,**B**) Immunofluorescence images (**A**) and quantification (**B**) of relative MCAK intensities at inner KTs and spindle poles in HeLa S3 cells treated for 48 h with control, Ska1 and Ska3, or control siRNAs and the Aurora B inhibitor ZM447439 for 1 h (n = 10–77 cells per condition from $N \geq 2$ independent

experiments). (**C**) Western blot analysis of MCAK levels in mitotic HeLa S3 cell extracts 48 h after siRNA transfection. (**D**,**E**) Immunofluorescence images (**D**) and quantification (**E**) of relative MCAK intensities at the inner KTs in MCF10A cells treated with control or Ska1 and Ska3 siRNAs. (**F**,**G**) Mitotic cells from asynchronously growing HeLa S3 cells were washed-out and cells were treated for 16–18 h with DMSO or nocodazole (0.33 μM). Immunofluorescence images (**F**) and quantification (**G**) of relative MCAK inner KT levels in DMSO-treated early and late prometaphase (PM) cells or in cells subjected to pre-mitotic nocodazole treatment (n = 14–25 cells per condition). (**H**,**I**) Immunofluorescence images (**H**) and quantification (**I**) of relative Ska3 KT intensities in HeLa S3 cells treated with control, Ska1 and Ska3, MCAK siRNAs or control siRNAs and ZM447439 for 1 h (n = 10–20 cells per condition). (**J**) Immunoprecipitates (IP) from an extract of STLC-arrested mitotic HeLa S3 cells, obtained using anti-Ska1 antibodies or control IgGs, were analyzed by Western blotting using antibodies against Ska1 and MCAK. (**K**–**N**) Spindle elongation in Ska-deficient cells. (**K**) Representative immunofluorescence images showing spindle length in fixed HeLa S3 cells treated for 48 h with control or Ska1 and Ska3 siRNAs. (**L**) Linescan of the tubulin (green) and DNA fluorescent intensity (blue) of the cells shown in **K.** (**M**) Quantification of the spindle length in fixed HeLa S3 cells (n = 24–29 cells per condition from N = 3). (**N**) Scatter plots showing the spindle length distribution in live HeLa K PA-GFP–α-tubulin/histone H2B–mRFP cells treated for 48 h with control, Ska1, or Ska3 siRNAs (n = 23–25 cells per condition from $N \geq 2$). Spindle length was measured as pole-to-pole distance in cells with fully aligned chromosomes. Each dot in the depicted scatter plots represents one cell. Horizontal lines indicate mean. Asterisks show statistical significance (Student's t-test, unpaired). **** $P \leq 0.0001$; *** $P \leq 0.001$; ns, non-significant. Scale bars, 5 μm.

To delineate the significance of the reduction of MCAK and CENP-E at KTs, we examined whether additional functions associated with these two proteins were perturbed in Ska-depleted cells. MCAK is a potent depolymerizer of MTs (Hunter et al., 2003), and selective loss of the inner KT MCAK pool may not only lead to a slower tubulin turnover, but also to misbalanced MT assembly at KTs. Consistent with this idea, we observed elongated spindles in Ska-deficient cells (Figure 16K–N), in line with previous reports showing a role of MCAK in governing spindle length (Wordeman et al., 2007; Domnitz et al., 2012). Besides the function of CENP-E in promoting KT-MT plus-end dynamics, it has a well-established role in mediating chromosome congression (Auckland and McAinsh, 2015). We therefore monitored chromosome alignment following recovery from monastrol washout. While control cells efficiently aligned chromosomes at the spindle equator, the proportion of Ska-depleted cells with misaligned chromosomes following spindle bipolarization was clearly increased, similar as in CENP-E-depleted or Aurora B-inhibited cells (Figure 17C and 17D). We conclude that Ska contributes to the regulation of KT-MT

dynamics, spindle length, and chromosome alignment and/or correction of syntelic attachment errors likely through the KT localization of MCAK and CENP-E, respectively.

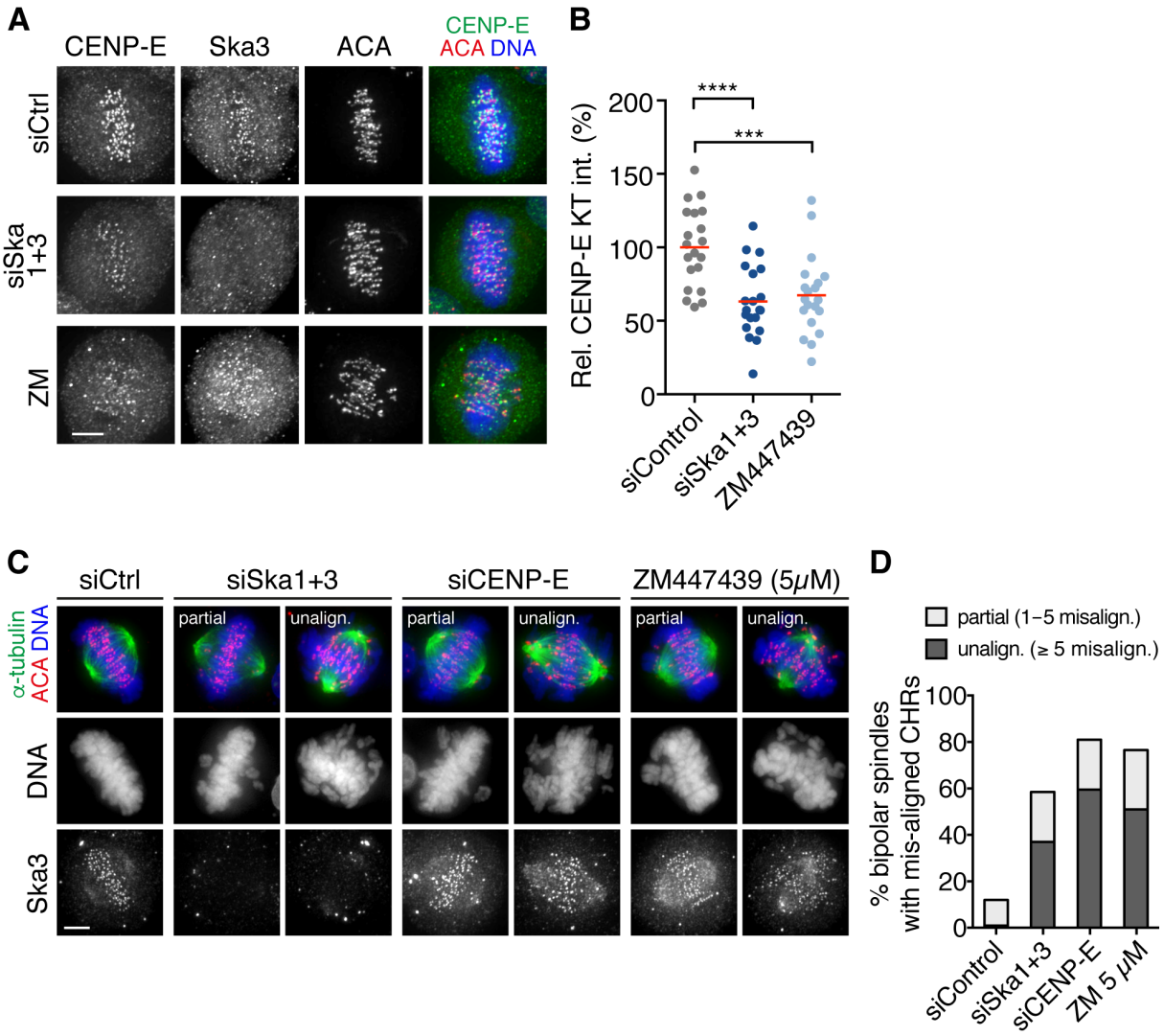

Figure 17. KT localization of CENP-E and chromosome alignment are dependent on the Ska complex. (**A**,**B**) Immunofluorescence images (**A**) and quantification (**B**) of relative CENP-E KT intensities in HeLa S3 cells treated for 48 h with control, Ska1 and Ska3, or control siRNAs and the Aurora B inhibitor ZM447439 (5 μM) for 1 h (n = 20 cells per condition from N = 1 experiment). (**C**,**D**) HeLa S3 cells were transfected with control, siSka1 and Ska3 or CENP-E siRNAs, incubated for 12 h, and treated with thymidine for 24 h. After thymidine release, the cells were incubated in fresh medium for 6 h before addition of the Eg5 inhibitor monastrol for 4 h to induce monopolar spindles. Ten hours after thymidine release, monastrol was washed out and cells were incubated 1 h in medium containing MG132 to allow spindle bipolarization before fixation. Immunofluorescence images (**C**) and quantification (**D**) of chromosome alignment in cells with bipolar spindles (n = 100 cells per condition from N = 1).

The Ska complex is required for Aurora B activity

Previously, the Ska complex has been identified as an Aurora B substrate (Chan et al., 2012). Now we find that several of the phenotypes observed after Ska depletion (i.e. merotely, lagging chromosomes, suppressed KT-MT plus-end turnover, and chromosome alignment defects) are highly reminiscent of previously described consequences of Aurora B loss-of-function (Cimini et al., 2006; DeLuca et al., 2011; Ditchfield, 2003; Hauf et al., 2003). Moreover, MCAK and CENP-E KT localization are both dependent on Aurora B activity (Figure 16A and 16B; Figure 17A and 17B) (Andrews et al., 2004; Lan et al., 2004; Tanno et al., 2010; Murata-Hori and Wang, 2002; Ditchfield, 2003). Hence, we reasoned that the Ska complex might govern Aurora B activity. In support of this hypothesis, we found that Ska depletion in HeLa S3 cells caused a significant decrease in the phosphorylation of histone H3 on both serine 10 (H3-pS10) and serine 28 (H3-pS28) (Figure 18A–D), an Aurora B substrate localizing along chromosome arms (Goto et al., 2002). Treatment of cells with the Aurora B kinase inhibitor ZM447439 confirmed the specificity of these phosphorylation signals (Figure 18A–D). Similar results on H3-pS10 were obtained by targeting the Ska complex with a panel of different siRNAs (Figure 18G and 18H) and complementation of the depleted Ska complex subunits by transient expression of their siRNA-resistant versions partially rescued H3-S10 phosphorylation (Figure 18E and 18F), attesting to specificity. Furthermore, we also observed a drop in H3-pS10 levels in U2OS and MCF10A cells (which are transformed and aneuploid and non-transformed and near-diploid, respectively) (Figure 18I–L). In contrast, RPE-1 cells (also non-transformed and near-diploid) showed at most marginally reduced H3-pS10 levels (Figure 18M), presumably because of incomplete Ska complex depletion

(Figure 18N and 18O). Ska knockdown also suppressed Aurora B phosphorylation in living HeLa K cells stably expressing either a centromere-targeted (CENP-B fused) or a chromatin-targeted (histone H2B-fused) fluorescence resonance energy transfer (FRET) sensor for Aurora B activity (Fuller et al., 2008), albeit to a lesser extent than direct inhibition of Aurora B (Figure 19A–D). Collectively, these data indicate that the Ska complex promotes Aurora B activity in cells to facilitate KT-MT dynamics and prevent the accumulation of attachment errors.

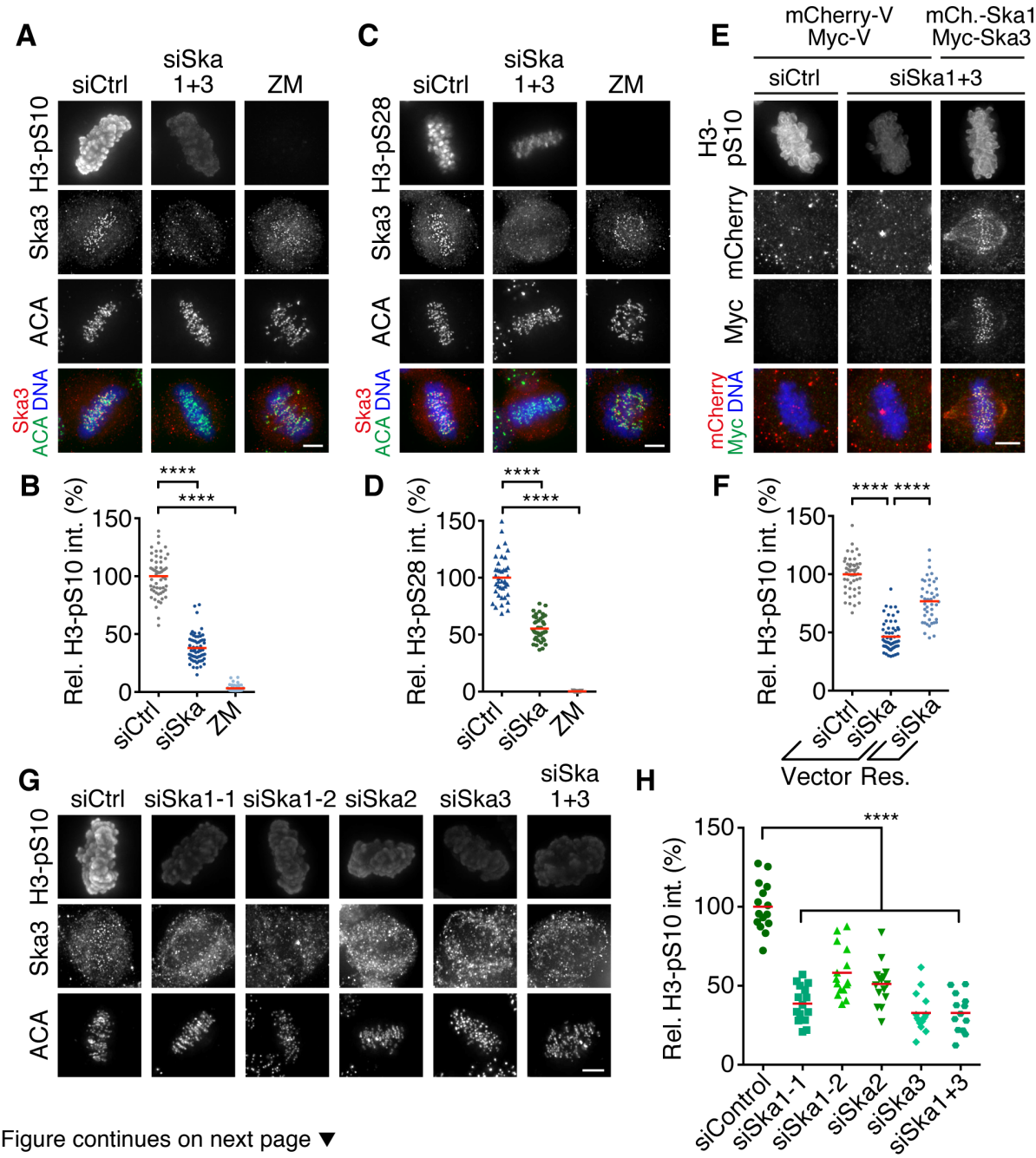

Figure continues on next page ▼

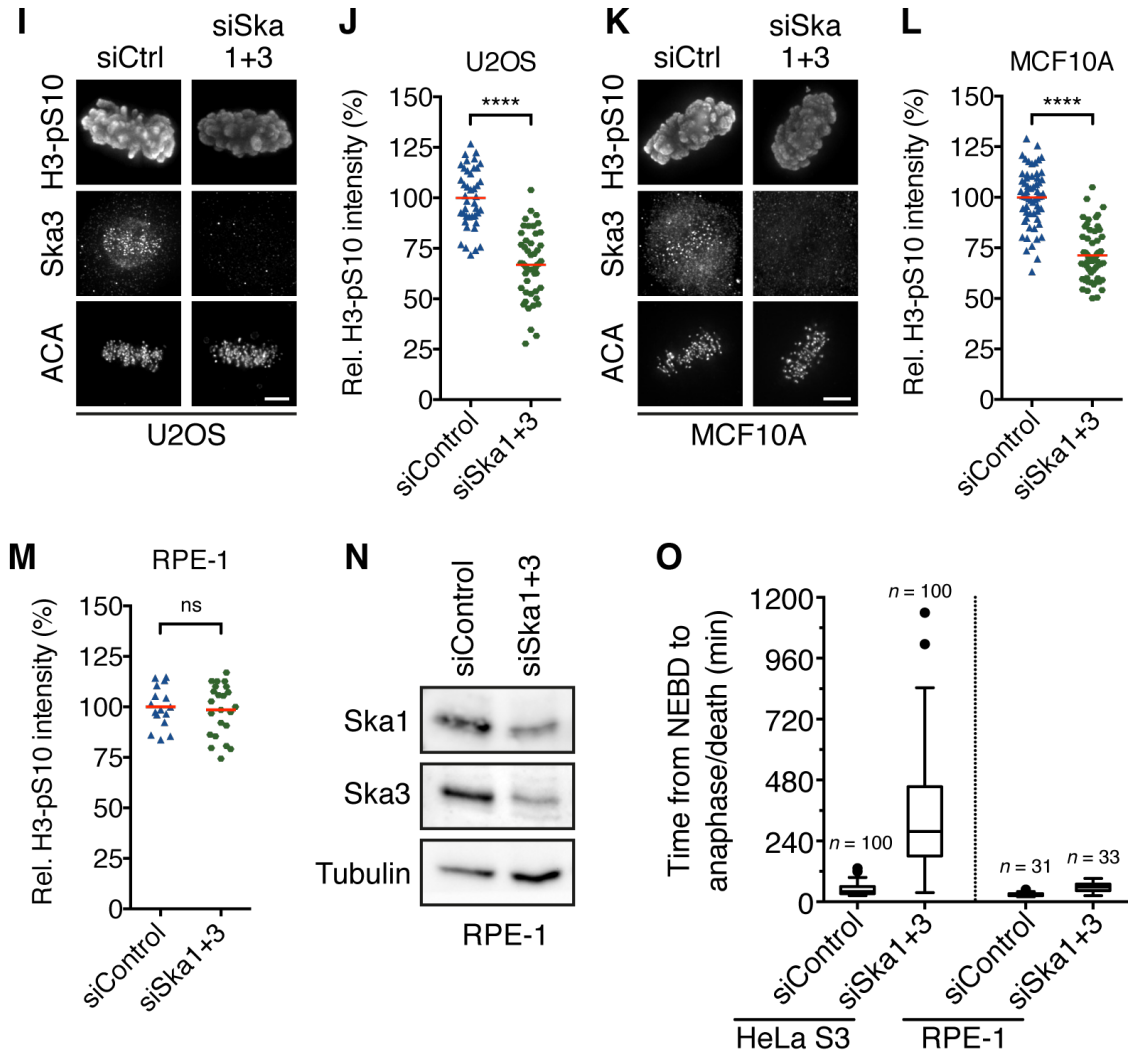

Figure 18. The Ska complex is required for Aurora B kinase-mediated histone H3 phosphorylation. (**A**,**B**) Immunofluorescence images (**A**) and quantification (**B**) of relative histone H3-pS10 intensities in HeLa S3 cells treated for 48 h with control or Ska1 and Ska3 siRNAs. The Aurora B inhibitor ZM447439 was added to siControl cells 1 h before fixation (n = 47–61 cells per condition from N = 3 independent experiments). (**C**,**D**) Immunofluorescence images (**C**) and quantification (**D**) of relative H3-pS28 intensities in HeLa S3 cells treated as in **A** (n = 35–40 cells per condition from N = 2). (**E**,**F**) HeLa S3 cells were depleted of endogenous Ska1 and Ska3 or treated with control siRNAs, synchronized by a double thymidine arrest, and rescued by transfection with siRNA-resistant mCherry-Ska1 and Myc-Ska3 (Res.) or empty mCherry- and Myc-Vectors (Vector), fixed and stained with the indicated antibodies. (**F**) Relative H3-pS10 intensities in cells treated as in **E** (n = 44–59 cells from N = 2). (**G**,**H**) Immunofluorescence images (**G**) and quantification (**H**) of relative H3-pS10 intensities in HeLa S3 cells treated for 48 h with control or the indicated panel of siRNAs targeting the Ska complex (n = 13–15 cells per condition). (**I**–**M**) Relative H3-pS10 intensities in U2OS (**I** and **J**; n = 42–49 cells per condition from N = 3), MCF10A (**K** and **L**; n = 60 cells from N = 3), and RPE-1 cells (**M**; n = 16–23 cells from N = 2) treated for 48 h with control or Ska1 and Ska3 siRNAs. (**N**) Western blot analysis of Ska1 and Ska3 levels in mitotic RPE-1 cell extracts. Note the incomplete depletion of Ska1 and Ska3. (**O**) Box-and-whisker plot of the elapsed time between NEBD and anaphase onset/mitotic cell death after the indicated siRNA treatments. The number of cells (n) analyzed is given above each box. For comparison, the data for HeLa S3 H2B–GFP cells is shown. Note that transfection of RPE-1 H2B–GFP cells with Ska siRNAs causes only a minor delay in mitotic progression compared to HeLa S3 H2B–GFP cells. Horizontal lines in the scatter plots depict mean. Asterisks show statistical significance (Student's t-test, unpaired). **** $P \leq 0.0001$; ns, non-significant. Scale bars, 5 μm.

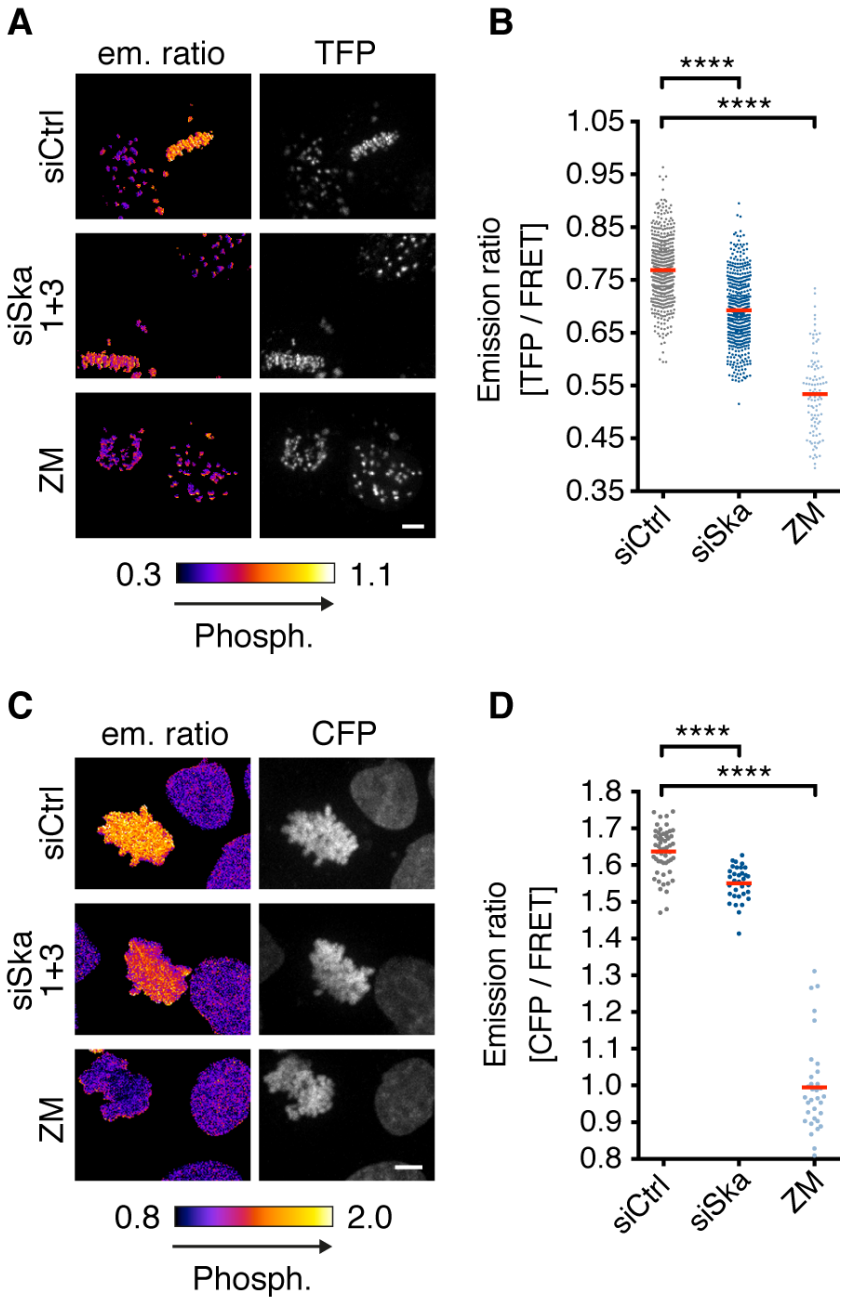

Figure 19. Ska depletion suppresses Aurora B activity at centromeres and chromatin in living cells. (**A**–**D**) Live-cell images of HeLa K cells stably expressing an Aurora B FRET sensor targeted to inner KTs/centromeres (**A**,**B**) or chromatin (**C**,**D**) 48 h after transfection with control or Ska1 and Ska3 siRNAs**.** The FRET sensors were completely dephosphorylated in siControl cells treated with the Aurora B inhibitor ZM447439 30 min before imaging. Shown are emission ratio images (TFP/YFP or CFP/YFP), color-coded as indicated by the color scale, and images for sensor localization (TFP or CFP emission). (**B**) Scatter plot showing TFP/YFP emission ratios calculated for individual aligned KTs in siControl and siSka1+3 cells (n = 500 KTs from 50 cells each from N = 2) or mostly unaligned KTs in ZM447439 treated cells (n = 100 KTs from 10 cells from N = 1). (**D**) CFP/YFP emission ratios calculated for individual siControl and siSka1+3 cells with aligned chromosomes (n = 33–55 cells from N = 3) or ZM447439 treated cells with mostly unaligned chromsomes (n = 33 cells from N = 1). Horizontal lines in the scatter plots depict mean. Asterisks show statistical significance (Student‘s t-test, unpaired). **** P ≤ 0.0001. Scale bars, 5 μm.

The Ska complex promotes Aurora B activity in a MT-dependent manner

Most of the functions of the Ska complex have been linked to its ability to directly associate with spindle MTs. To see whether the Ska complex also requires its MT-binding capability to enhance Aurora B activity, we depleted endogenous Ska1 in HeLa cells stably expressing mutant versions of RNAi resistant GFP-Ska1 lacking either a basic patch in the MT-binding surface of Ska1 (Ska1$^{R155A, R236A, R245A}$) or the entire MT-binding domain (MTBD) (Ska1$^{\Delta MTBD}$; residues 1-131) (Schmidt et al., 2012). These mutants both make the full Ska complex MT-binding deficient *in vitro* without affecting complex formation; in intact cells they fail to localize to spindle MTs but not KTs (Schmidt et al., 2012; Abad et al., 2014). While cells expressing wild-type Ska1 showed after Ska1 depletion H3-pS10 and MCAK KT levels that were indistinguishable to control cells, expression of Ska1$^{R155A, R236A, R245A}$ and Ska1$^{\Delta MTBD}$ failed to restore wild-type levels of these two Aurora B activity markers (Figure 20A–D). These results indicate that the Ska complex promotes Aurora B activity in a MT-dependent manner.

GFP fluorescence intensities of wild-type Ska1 and Ska1$^{R155A, R236A, R245A}$ at KTs were comparable, whereas the Ska1$^{\Delta MTBD}$ KT levels were on average ~40% lower (Figure 20H). Although expressed at lower levels, Ska1$^{\Delta MTBD}$ also produced a significant decrease in H3-S10 phosphorylation and a modest reduction in the staining intensity of MCAK at KTs in presence of the endogenous proteins (Figure 20E–G). This falls in line with a previously described dominant negative effect of this mutant and likely reflects dimerization of the Ska complex (Schmidt et al., 2012). In contrast, Ska1$^{R155A, R236A, R245A}$ had no apparent dominant-negative effect on Aurora B activity (Figure 20F and 20G), possibly because MT-binding of the Ska complex

depends on a dimeric arrangement of the Ska1 MTBD (Abad et al., 2014), and the Ska1$^{R155A,\ R236A,\ R245A}$ domain may be still capable to support a functional conformation of the endogenous MTBD. Alternatively, the Ska1 MTBD may be involved in the binding and/or activation of Aurora B.

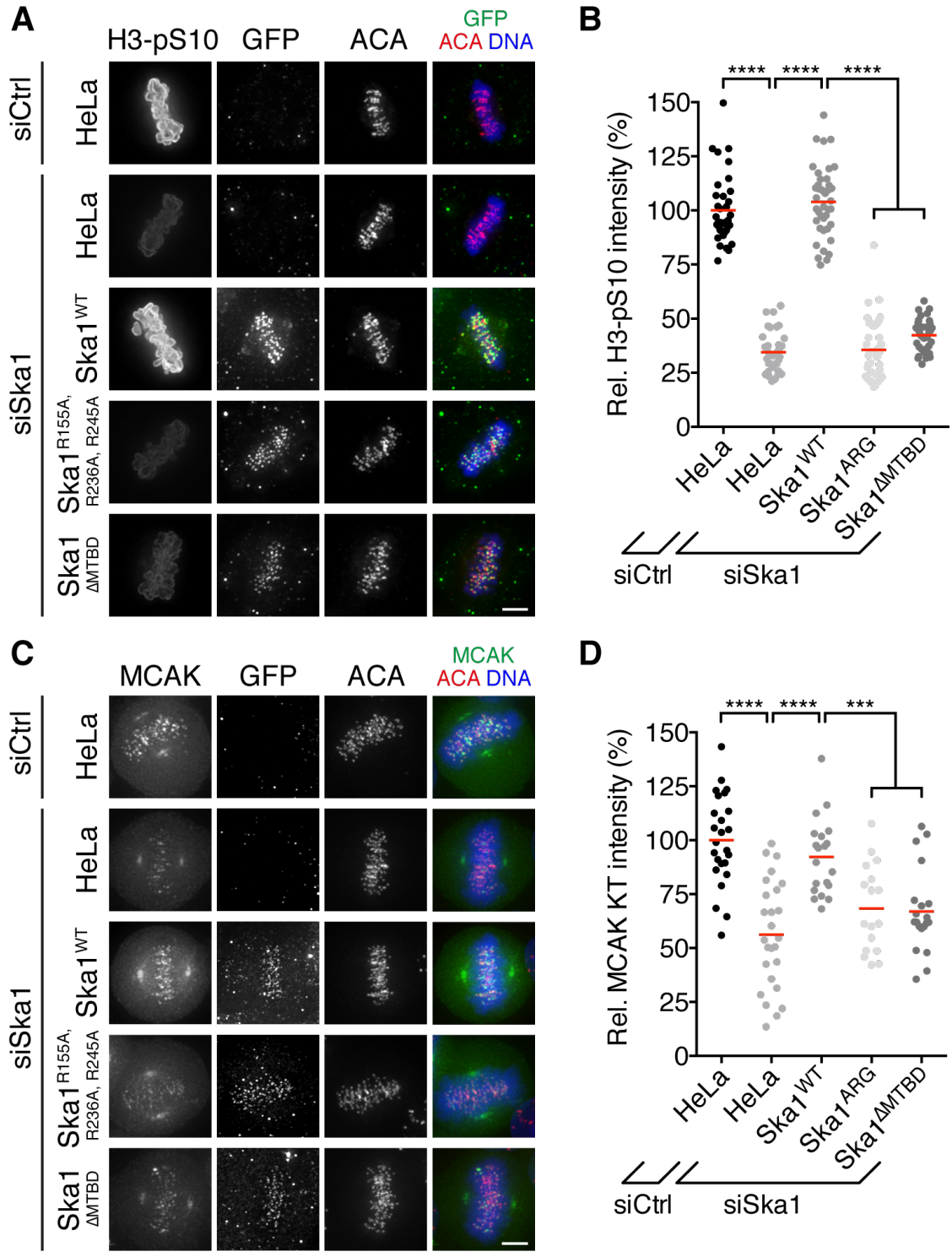

Figure continues on next page ▼

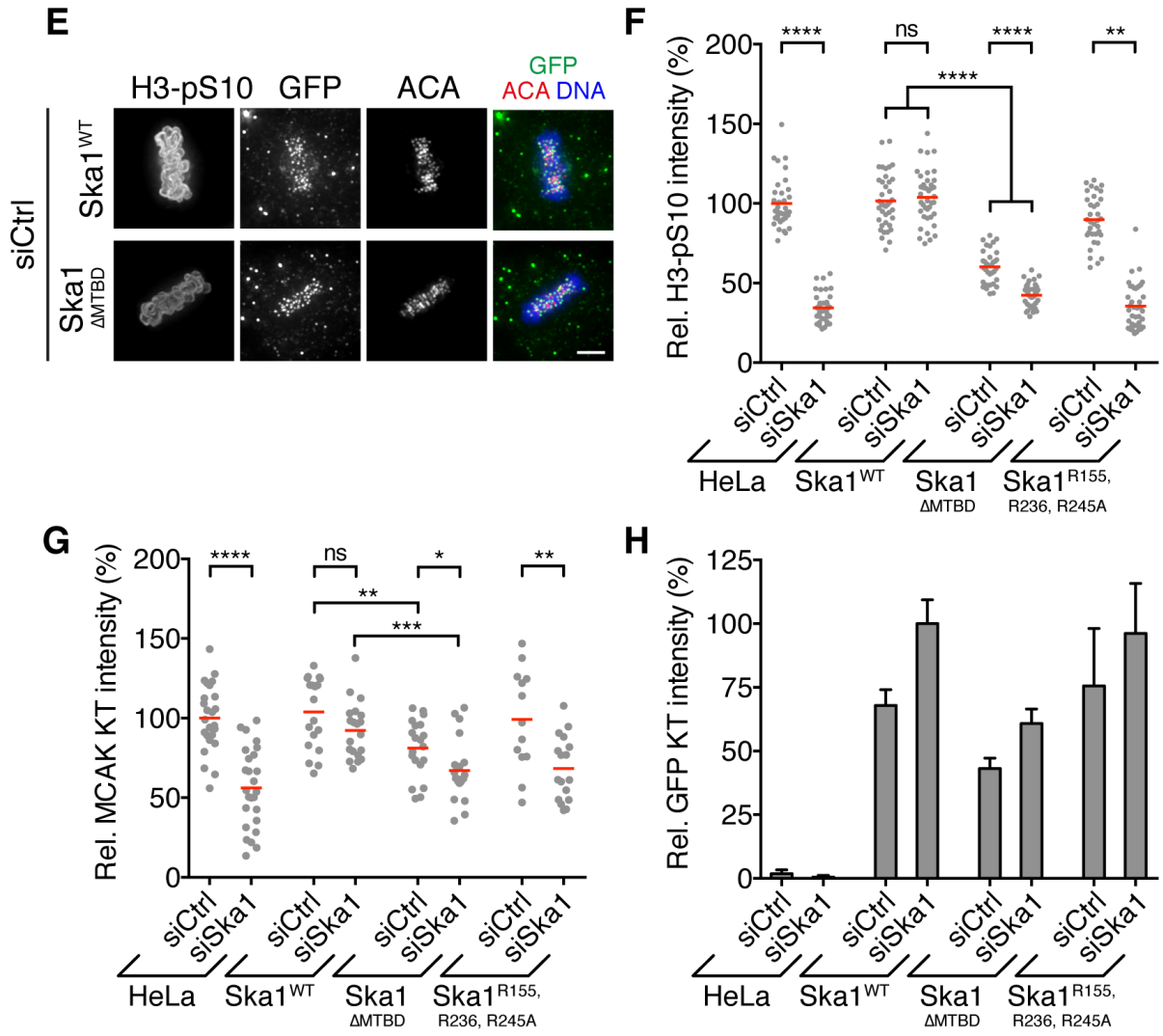

Figure 20. The MT-binding capability of the Ska complex is required for Aurora B activity.
(**A**,**B**) Immunofluorescence images (**A**) and quantification (**B**) of relative histone H3-pS10 intensities in HeLa cells stably expressing GFP-tagged and siRNA-resistant wild-type Ska1 (WT) or the MT-binding deficient mutants Ska1$^{R155A,\ R236A,\ R245A}$ (ARG) and Ska1$^{1-131}$ (ΔMTBD), respectively, treated for 48 h with control or Ska1 siRNAs (n = 35–40 cells per condition from N = 2 independent experiments). (**C**,**D**) Immunofluorescence images (**C**) and quantification (**D**) of relative MCAK KT intensities in cells treated as in **A** (n = 17–26 cells from N = 1). Note that due to the simultaneous cell permeabilzation and fixation spindle association of GFP-Ska1^{WT} is not apparent in all cells. (**E**–**G**) Dominant negative effect of the Ska1$^{1-131}$ (ΔMTBD) mutant on H3-pS10 and MCAK KT levels. (**E**) Immunofluorescence images of histone H3-pS10 levels in HeLa cells stably expressing GFP-tagged and siRNA-resistant wild-type Ska1 (WT) or Ska1$^{1-131}$ (ΔMTBD) treated for 48 h with control siRNAs. Scatter plots showing the entire quantification of relative H3-pS10 intensities (**F**) and MCAK KT intensities (**G**) in cells treated as in **A**. Horizontal lines in the scatter plots depict mean. (**H**) Bar graphs showing the average GFP-Ska1 fusion protein levels at KTs in the corresponding stable cell lines. Bars represent mean ± 95% CI. Asterisks show statistical significance (Student's t-test, unpaired). **** P ≤ 0.0001; *** P ≤ 0.001; ** P ≤ 0.01; * P ≤ 0.05; ns, non-significant. Scale bars, 5 μm.

The Ska complex is necessary to maintain centromere localization of Aurora B but promotes Aurora B activity independently of its centromere targeting

Having shown that the Ska complex depends on its MT-binding capability to promote Aurora B activity, we next sought to determine the underlying molecular mechanism by which the Ska complex governs Aurora B activity. Previous work suggested that concentration of the chromosomal passenger complex (CPC) at the inner centromere contributes to Aurora B kinase activity by transactivation (Kelly et al., 2007; 2010; Wang et al., 2011a). We therefore asked whether the Ska complex might regulate Aurora B activity via centromere recruitment of the CPC by facilitating its MT-dependent transport (Banerjee et al., 2014). We found that Ska depletion in HeLa S3 cells displaced Aurora B from mitotic centromeres to a more diffuse distribution on chromatin (Figure 21A and 21B). Notably, this was primarily seen in Ska-depleted cells with scattered chromosomes, while cells with aligned chromosomes showed only a minor decrease in centromeric Aurora B (Figure 21A, 21B and 21E). Similar results were obtained for the CPC subunit Borealin, indicating mislocalization of the entire CPC (Figure 21D and 21F). In contrast, Ska knockdown did not affect total CPC protein levels in mitosis or CPC complex formation (Figure 22A–C). Furthermore, CPC displacement from centromeres not only correlated with the alignment status of Ska-depleted cells, but also with a decrease in Haspin kinase-dependent phosphorylation of histone H3 on threonine 3 (H3-pT3, Figure 21A and 21C), a chromatin mark important to target the CPC to the inner centromere (De Antoni et al., 2012; Wang et al., 2012).

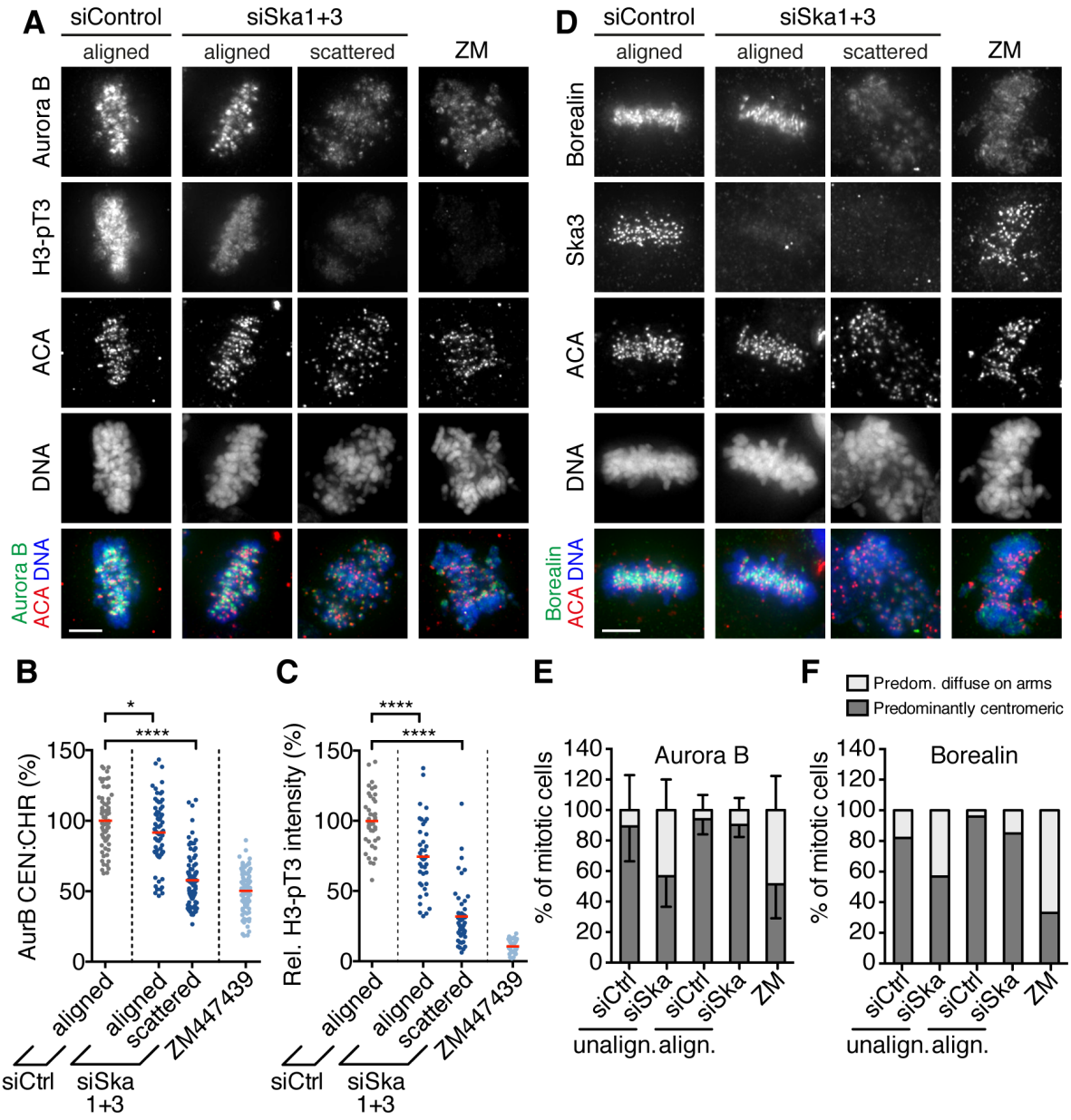

Figure 21. The Ska complex is necessary to maintain CPC centromere localization. (**A**) HeLa S3 cells treated for 48 h with control, Ska1 and Ska3, or control siRNAs and ZM447439 for 1 h were pre-extracted, fixed and stained with the indicated antibodies. (**B**) Quantification of Aurora B centromere enrichment. The signal intensity at centromeres (CEN) was divided by the intensity at chromosome arms (CHR) (n = 66–97 cells per condition from N = 4). (**C**) Relative histone H3-pT3 intensities in cells treated as in **A**. (**D**) Borealin localization in cells treated as in **A**. (**E**,**F**) Classification of Aurora B and Borealin localization in cells treated as in **A** displaying unaligned/scattered or aligned chromosomes. (**E**) Aurora B localization pattern. Bars represent mean ± 95% CI (n = 250–300 cells per condition from N = 3 independent experiments). (**F**) Borealin localization pattern. (n = 50–100 cells per condition from N = 1 experiment). Asterisks show statistical significance (Student's t-test, unpaired). **** P ≤ 0.0001, * P ≤ 0.05. Scale bars, 5 μm.

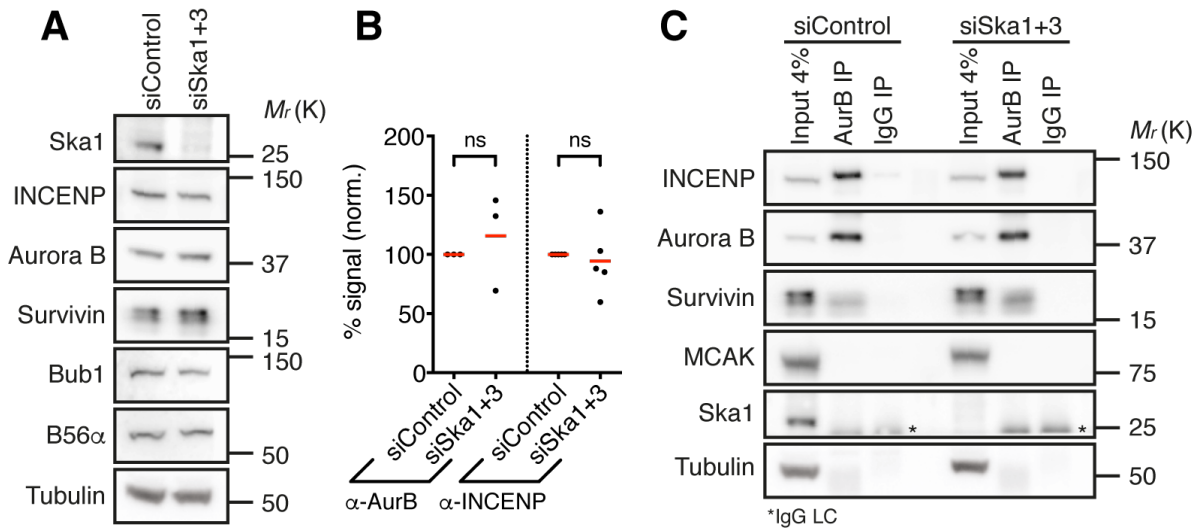

Figure 22. CPC stability and complex formation remains intact following Ska depletion. (**A**) Western blot analysis of the stability of CPC complex subunits (Aurora B, INCENP, and Survivin) and CPC-related proteins (Bub1, PP2A-B56α) in mitotic HeLa S3 cell extracts 48 h after transfection with control or Ska1 and Ska3 siRNAs. α-tubulin is shown as loading control. (**B**) Scatter plot showing the corresponding quantification of the relative Aurora B and INCENP signal intensities from **C** normalized against α-tubulin (*N* = 3–5). ns, non-significant. (**C**) Coimmunoprecipitation analysis of CPC complex formation. Mitotic HeLa S3 cell extracts prepared from cells treated for 48 h with control or Ska1 and Ska3 siRNAs were subjected to immunoprecipitation (IP) with Aurora B or control antibodies (IgG), prior to Western blotting with the indicated antibodies. IgG LC, IgG light chain.

As chromosome scattering in Ska-deficient cells can be a consequence of cohesion fatigue (Figure 12A) (Daum et al., 2009; Sivakumar et al., 2014) and both Haspin and CPC centromere localization depend on cohesion (Yamagishi et al., 2010; Carretero et al., 2013), we tested if perturbation of Aurora B activity might be a secondary effect of cohesion fatigue. However, cohesion fatigue induced by either proTAME (Lara-Gonzalez and Taylor, 2012) or MG132 (Daum et al., 2011) did not decrease Aurora B activity, as determined by H3-pS10, although it caused a similar reduction in the centromere enrichment of Aurora B as seen in Ska-depleted cells (Figure 23A–D). Likewise, phosphorylation of the Haspin chromatin mark H3-pT3 was only mildly reduced in cells that underwent chromosome scattering upon prolonged proTAME or MG132 treatment, when compared to Ska-depleted cells (Figure 23B and 23D), indicating that cohesion fatigue and Ska deficiency likely

contribute to Aurora B centromere displacement through different pathways. To rule out that the loss of Aurora B activity in Ska-depleted cells is due to perturbation of Haspin kinase activity, we examined the effects of intra-mitotic inhibition of Haspin kinase on H3-S10 phosphorylation using 5-iodotubercidin (5-ITu). Consistent with previous reports we found that, although Haspin kinase activity is necessary for concentration of Aurora B at centromeres (Figure 23E and 23F; 23H), it is dispensable for maintenance of Aurora B activity towards H3-S10 (Figure 23E and 23G) (Wang et al., 2012). These results indicate that suppression of Aurora B activity in Ska-depleted cells is not a primary consequence of CPC displacement from centromeres by cohesion fatigue or perturbation of Haspin kinase activity. Instead, loss of Aurora B activity in Ska-deficient cells might be the underlying cause of CPC centromere displacement. In support of this interpretation, Aurora B activity is required for CPC centromere enrichment through feedback regulation of Haspin activity, as seen by centromere delocalization of Aurora B and Borealin as well as loss of H3-T3 phosphorylation in cells treated with ZM447439 (Figure 21A–F) (Wang et al., 2011b).

To further corroborate the notion that the Ska complex contributes to Aurora B activity independently of its centromere targeting, we constitutively tethered Aurora B to the inner KT through expression of a fusion protein comprising the DNA-binding domain of centromere protein B (CENP-B^{1-158}; CB) and a truncation of the inner centromere protein ($INCENP^{48-918}$) devoid of the N-terminal centromere localization domain (CB^{DBD}-INCENP; (Liu et al., 2009). Although CB^{DBD}-INCENP targeted to the inner KT and drove Aurora B accumulation at KTs in Ska-depleted cells as efficiently as in control cells (Figure 24A and 24B), expression of CB^{DBD}-INCENP failed to fully

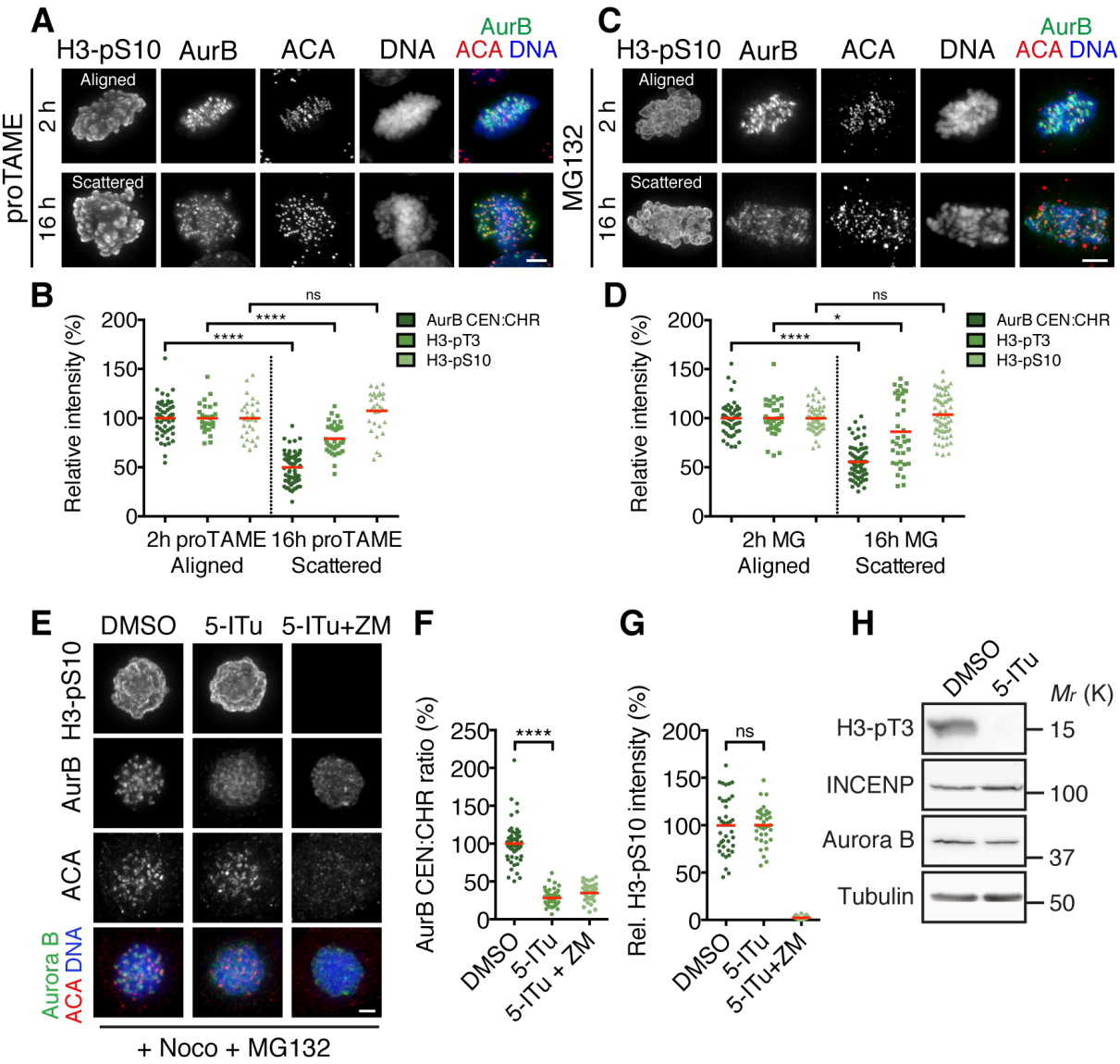

Figure 23. Suppression of Aurora B activity in Ska-deficient cells is not a consequence of cohesion fatigue or perturbation of Haspin kinase activity. (**A**–**D**) Cohesion fatigue induced by a prolonged metaphase arrest does not suppress Aurora B activity at chromosome arms despite its centromere displacement. (**A**) Immunofluorescence images of histone H3-pS10 and Aurora levels in HeLa S3 cells treated for 2 or 16 h with the APC/C inhibitor proTAME. (**B**) Quantification of the relative Aurora B, histone H3-pS10 and histone H3-pT3 intensities in proTAME treated cells (n = 30–65 cells per condition from N = 2). Only cells with scattered chromosome upon 16 h of proTAME treatment were quantified. (**C**) H3-pS10 and Aurora B levels in HeLa S3 cells treated for 2 or 16 h with the proteasome inhibitor MG132. (**D**) Quantification of the relative Aurora B, histone H3-pS10 and histone H3-pT3 intensities in MG132 treated cells (n = 35–67 cells per condition from N = 2). Only cells with scattered chromosome upon 16 h of MG132 treatment were quantified. (**E**–**H**) Haspin activity and Aurora B centromere enrichment is dispensable for maintenance of Aurora B activity at chromosome arms. HeLa S3 cells were treated with nocodazole (3.3 μM) for 50 min before MG132 was added for 10 min followed by 1.5 h treatment with DMSO (as negative control), the Haspin inhibitor 5-iodotubercidin (5-ITu) or 5-ITu and ZM447439 (as positive control). Shown are the corresponding immunofluorescence images (**E**) and scatter plots of the relative Aurora B (**F**) and H3-pS10 intensities (**G**), respectively. (**H**) Validation of Haspin kinase inhibition by Western blotting. HeLa S3 cells were synchronized in mitosis with nocodazole (3.3 μM) for 6–8 h, treated 10 min with MG132 followed by 1.5 h with DMSO or 5-ITu and whole cell extracts were subjected to Western blotting with the indicated antibodies. Asterisks show statistical significance (Student's t-test, unpaired). **** P ≤ 0.0001; * P ≤ 0.05; ns, non-significant. Scale bars, 5 μm.

restore either MCAK centromere localization (Figure 24C and 24D), or H3-S10 phosphorylation (Figure 24E and 24F). Taken together, these data indicate that the Ska complex is required to maintain the localization of Aurora B at centromeres, but, in addition, governs Aurora B kinase activity at both KTs and chromosome arms largely independently of its centromere accumulation.

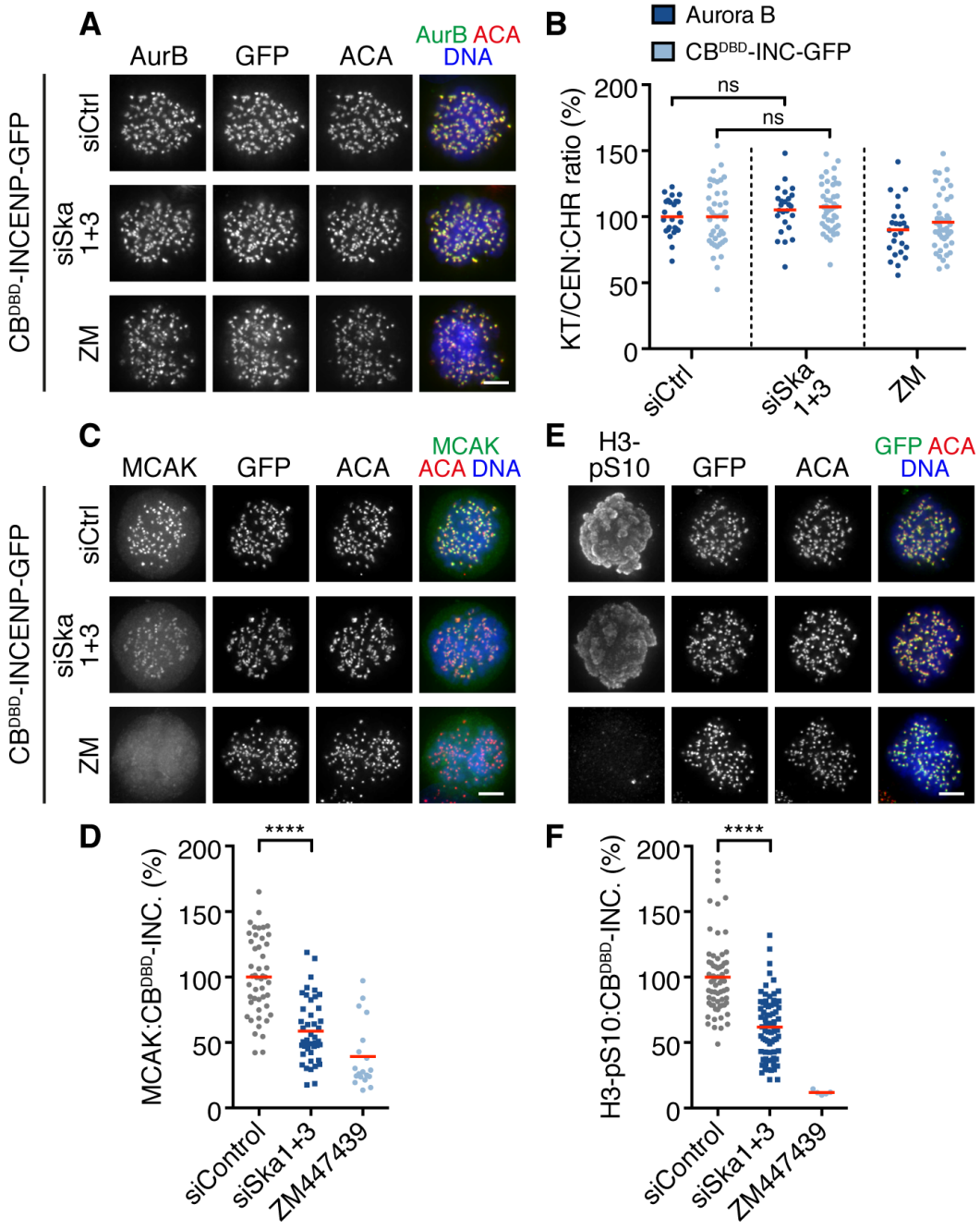

Figure 24. Forcing Aurora B centromere accumulation is not sufficient for control levels of Aurora B activity in Ska-depleted cells. (**A**–**F**) HeLa S3 cells were cotransfected with CENP-B^{DBD}–INCENP–GFP and control or Ska1 and Ska3 siRNAs for 48 h. ZM447439 was added to siControl cells

1 h before fixation. (**A**,**B**) Immunofluorescence images (**A**) and quantification (**B**) of inner KT/centromere enrichment of Aurora B and CENP-B^{DBD}–INCENP–GFP in siControl, siSka1+3, and ZM447439 treated cells expressing CENP-B^{DBD}–INCENP–GFP. The KT/centromere over chromosome arm signal ratios were calculated as described in Figure 21B (n = 25–44 cells per condition from $N \geq 2$). (**C**,**D**) Immunofluorescence images (**C**) and quantification (**D**) of normalized inner KT MCAK fluorescence intensities in siControl, siSka1+3, or ZM447439 treated cells expressing CENP-B^{DBD}–INCENP–GFP. The MCAK signal intensities at KTs were divided by the respective GFP KT over chromosome arm ratios to normalize for differences in the CENP-B^{DBD}–INCENP–GFP expression levels (n = 45–47 cells for siControl and siSka1+3 from N = 2, and n = 19 cells for ZM from N = 1). (**E**,**F**) Immunofluorescence images (**E**) and quantification (**F**) of normalized histone H3-pS10 intensities in siControl, siSka1+3, or ZM447439 treated cells expressing CENP-B^{DBD}–INCENP–GFP. Cellular H3-pS10 intensities were divided by the respective mean GFP KT over chromosome arm ratios (n = 64–72 cells for siControl and siSka1+3 from N = 3, and n = 5 cells for ZM from N = 1). Asterisks show statistical significance (Student's t-test, unpaired). **** $P \leq 0.0001$; ns, non-significant. Scale bar, 5 μm.

The Ska complex stimulates Aurora B kinase activity *in vitro*

We next asked whether the Ska complex might directly promote the catalytic activity of Aurora B. To test this hypothesis, full-length Aurora B, a C-terminal fragment of INCENP containing the IN-box domain (INCENP$^{790\text{-}918}$), which together constitute the catalytic core unit of the CPC (Honda et al., 2003; Sessa et al., 2005), and the Ska complex were separately purified from *E. coli* (Figure 25A–C), and Aurora B activation was examined *in vitro* (Figure 26A–C). Aurora B was preincubated with INCENP$^{790\text{-}919}$ in presence of the reconstituted Ska complex or equimolar amounts of bovine serum albumin (BSA), as negative control for molecular crowding, before γ-^{32}P-ATP (adenosine triphosphate) and recombinant histone H3 as substrate were added to initiate the kinase reaction. Compared to preincubation with BSA, the Ska complex markedly enhanced histone H3 and INCENP$^{790\text{-}918}$ phosphorylation rates (Figure 26A and 26B) as well as Aurora B autophosphorylation (Figure 26C). Similar results were obtained when BSA was omitted (Figure 26D) and BSA had a negligible effect on Aurora B autophosphorylation (Figure 26E), ruling out that BSA interfered with Aurora B activation. Likewise, incubation of the Ska complex with γ-^{32}P-ATP and histone H3 but without Aurora B and INCENP$^{790\text{-}918}$ did not increase incorporation of ^{32}P into histone H3, confirming the absence of other copurifying bacterial kinases (Figure 26F). Together, these results show that the Ska complex is able to stimulate

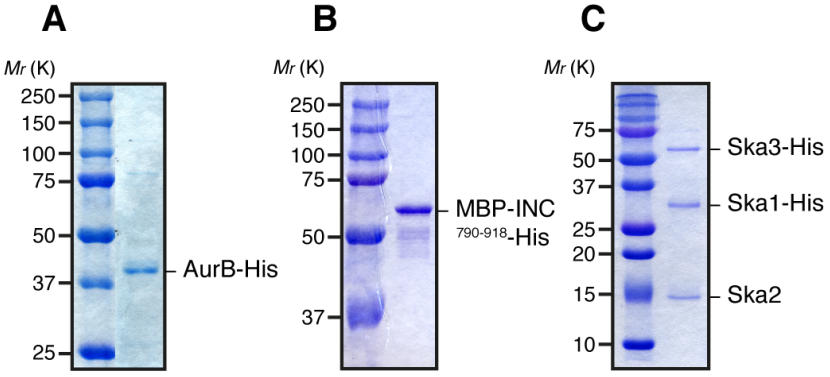

Figure 25. Purity of Aurora B, INCENP$^{790\text{-}918}$ (IN-Box), and the Ska complex. (**A**–**C**) Coomassie-stained gels of recombinant Aurora B-His (**A**), MBP-INCENP$^{790–919}$-His (**B**), and the Ska complex (**C**), expressed and purified from *Escherichia coli*.

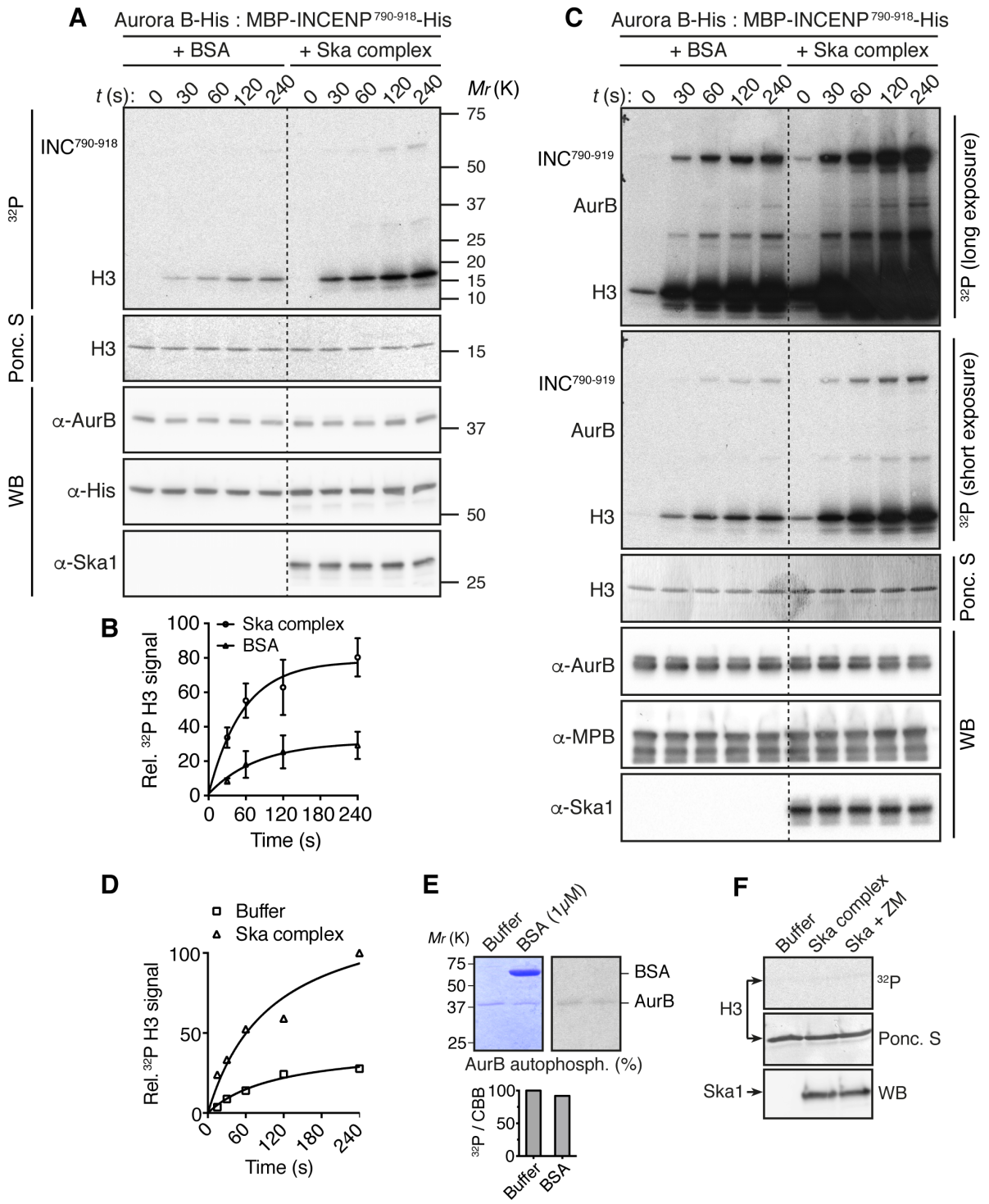

Figure 26. The Ska complex promotes the catalytic activity of Aurora B within the CPC core complex *in vitro*. (**A**) Ska complex-dependent activation of Aurora B. Time course kinase assay with Aurora B–His (0.5 μM) and MBP–INCENP$^{790–919}$–His (0.5 μM) pre-incubated for 30 min at 30°C with Ska complex (1 μM) or equimolar amounts of bovine serum albumin dissolved in Ska complex dialysis buffer (BSA, 1 μM), as control, before addition of histone H3 and γ-^{32}P–ATP. (**B**) Quantification of Aurora B activity by densitometric scanning of the histone H3 ^{32}P signals. Signals were normalized to H3 protein levels monitored by Ponceau S staining (Ponc. S) and Aurora B levels detected by Western blotting (WB). Signal intensities are expressed relative to the first time-point. Data represent mean ± 95% SD from $N = 3$ experiments. (**C**) Time course assay showing Aurora B autophosphorylation after prolonged exposure time. (**D**,**E**) BSA does not interfere with Aurora B activity. (**D**) Time course assay in which BSA was omitted in the control reaction. Shown is the quantification of the relative histone H3

^{32}P signal intensities normalized to the histone H3 and Aurora B protein levels. (**E**) Aurora B–His (0.5 μM) was pre-incubated 30 min at 30°C in presence or absence of BSA (1 μM), before incubation with γ-^{32}P–ATP for another 30 min. Autophosphorylation of Aurora B was visualized by autoradiography (^{32}P) and the Aurora B levels by Coomassie (CBB) staining. The bar graph shows the quantification of the ^{32}P autophosphorylation signals normalized to the Aurora B levels measured by CBB staining. (**F**) The Ska complex preparation does not contain histone H3-directed kinase contaminants. Histone H3 was incubated with Ska complex dialysis buffer (*left lane*), Ska complex (1 μM, *middle lane*) or Ska complex and the Aurora B kinase inhibitor ZM447439 (1 μM and 10 μM, respectively, *right lane*) for 30 min at 30°C in the presence of γ-^{32}P–ATP. Incorporation of ^{32}P into histone H3 was monitored by autoradiography (^{32}P), levels of histone H3 and the Ska complex were visualized by Ponceau S staining and Western blotting, respectively.

the kinase activity of Aurora B within the CPC core complex. They further suggest that Ska directly interacts with the CPC core complex. Consistently, the Ska complex associated with Aurora B *in vitro* (Figure 27A) and we reproducibly found the CPC subunits Aurora B, INCENP and Survivin in endogenous Ska1 immunoprecipitates from mitotic HeLa S3 cells (Figure 27B). However, we failed to clearly detect Ska complex subunits in reverse immunoprecipitation assays using INCENP or Aurora B antibodies (Figure 27C and Figure 22C), possibly because of differences in the binding pool size representation of the two complexes. Having shown that Ska directly associates with Aurora B, we further asked whether the Ska complex could promote Aurora B activity independently of INCENP$^{790\text{-}918}$, phosphorylation of which had previously been shown to be required for maximal Aurora B activation (Honda et al., 2003; Sessa et al., 2005). Indeed, incubation of increasing amounts of the Ska complex with Aurora B enhanced kinase autophosphorlyation in a dose-dependent fashion. In comparison, incubation with histone H3 only led to a marginal increase in Aurora B ^{32}P incorporation, presumably reflecting an unspecific stimulation of Aurora B autophosphorylation (Figure 28A and 28B). Similar results were obtained in a time-course assay, in which histone H3 was replaced with a buffer control to exclude a possible inhibitory effect of histone H3 on Aurora B activity (Figure 28C and 28C)

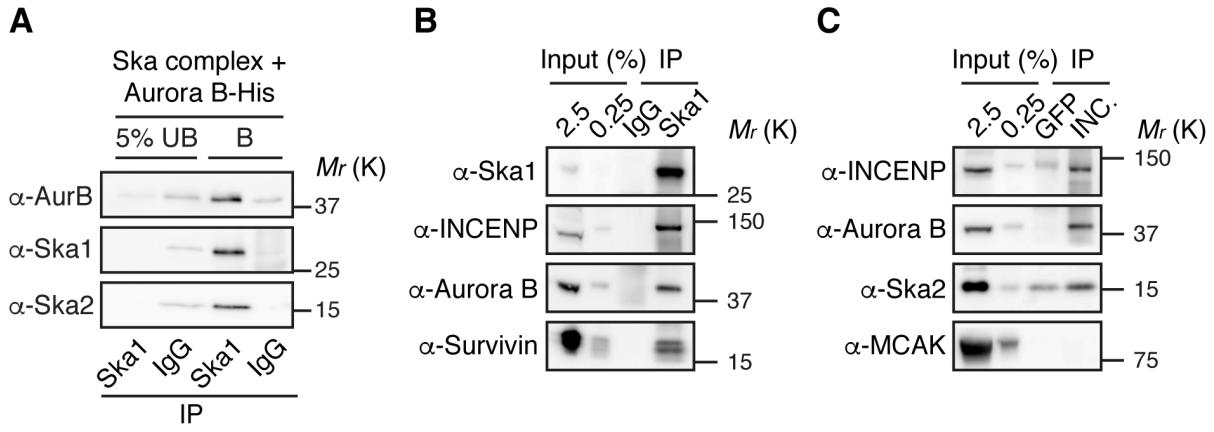

Figure 27. The Ska complex directly interacts with Aurora B. (**A**) *In vitro* binding of the Ska complex and Aurora B. Aurora B–His was incubated with recombinant Ska complex before pull-down with anti-Ska1 antibody- or control antibody (IgG)-coupled beads. Aurora B and the Ska complex subunits Ska1 and Ska2 were visualized in the unbound (UB) and bound (B) fractions by Western blotting. (**B**) Coimmunoprecipitation of Ska1 and the CPC from cells. Immuno-precipitates (IP) from mitotic HeLa S3 cell extracts, obtained using anti-Ska1 antibodies or control antibodies (IgG), were analyzed by Western blotting against the indicated proteins. (**C**) Immunoprecipitates obtained using anti-INCENP antibody-coupled or control antibody-coupled (GFP) beads were analyzed by Western blotting against the indicated proteins.

(Rosasco-Nitcher et al., 2008). We also tested whether the Ska complex can influence the autocatalytic activity of other mitotic kinases. Specifically, we assessed autophosphorylation of Plk1 and Mps1; the former is also able to phosphorylate the Ska complex *in vitro* (Appendix Figure 33). Compared to Aurora B, incubation with the Ska complex produced only a minor increase in the autophosphorylation of these two kinases (Figure 28E and 28F), confirming that the effect on Aurora B autophosphorylation is for the most part specific.

Our results imply that the Ska complex fosters an active conformation or transactivation of Aurora B without modulating the interaction of the kinase with the INCENP IN-box domain. To explore a role of transactivation, we tested if the presence of soluble antibodies recognizing the N-terminal maltose-binding protein (MBP) tag of INCENP$^{790\text{-}919}$, whose divalent antigen binding sites are expected to force dimerization and transactivation of the Aurora B–INCENP$^{790\text{-}919}$ complex (Kelly et al., 2007), would alleviate the effect of the Ska complex on Aurora B activity.

Consistent with our finding that ectopic concentration of Aurora B at centromeres by a CB^{DBD}-INCENP fusion is not sufficient to bypass the requirement of Ska for full Aurora B activity in intact cells (Figure 24C–F), anti-MBP antibodies did not diminish the promoting effect of the Ska complex on Aurora B catalytic activity *in vitro*, arguing against the notion that Ska facilitates Aurora B transactivation by inducing its local proximity or dimerization (Figure 29). Notably, and contrary to a previous finding with soluble anti-INCENP antibodies in *Xenopus* egg extracts (Kelly et al., 2007), anti-MBP antibodies also did not stimulate the catalytic activity of human Aurora B *per se* (Figure 29), possibly because the human CPC core complex already exists predominantly as a dimer in solution (Elkins et al., 2012). We conclude that the Ska complex can directly associate with Aurora B and stimulate its catalytic activity *in vitro*, independently of modulating the interaction of the kinase with its primary activator, the INCENP IN-box domain, and apparently independently of induced proximity or dimerization.

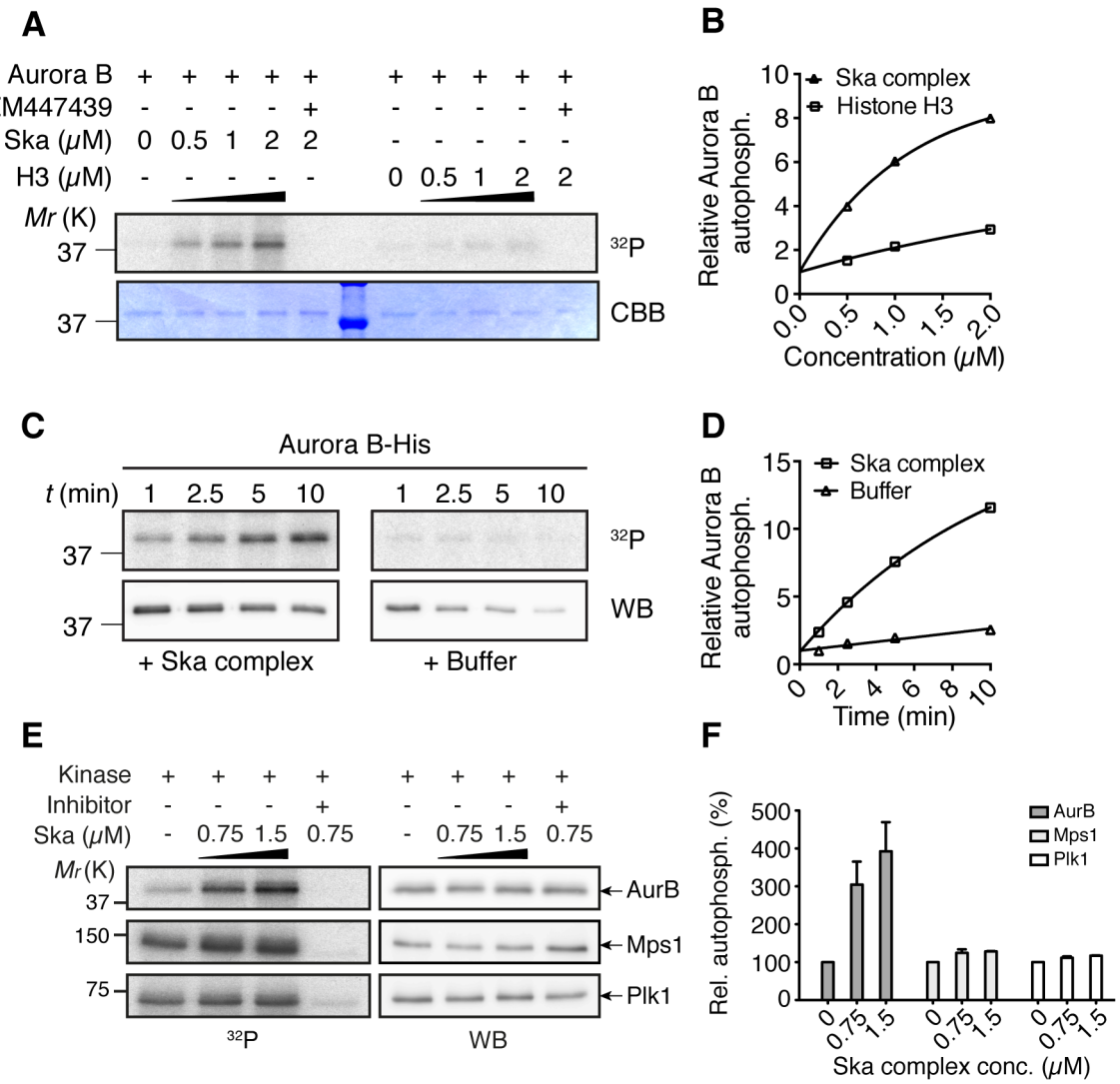

Figure 28. The Ska complex stimulates Aurora B autophosphorylation. (**A**) End-point autophosphorylation kinase assay. Aurora B–His (0.5 μM) was pre-incubated 30 min at 30°C with the Ska complex or recombinant histone H3, as control, at the indicated concentrations before incubation with γ-^{32}P–ATP for another 30 min. Autophosphorylation of Aurora B was detected by autoradiography (^{32}P) and the Aurora B levels were visualized by Coomassie brilliant blue (CBB) staining. (**B**) Quantification of Aurora B autophosphorylation by densitometric scanning of the ^{32}P signals. Signal intensities are expressed relative to the first concentration. (**C**) Time-course autophosphorylation assay. Aurora B–His (0.5 μM) was pre-incubated 30 min at 30°C with Ska complex (1 μM) or Ska complex dialysis buffer, as control, before addition of γ-^{32}P–ATP to start the kinase reactions. Reactions were stopped at the indicated time-points. Autophosphorylation of Aurora B was detected by autoradiography (^{32}P), levels of Aurora B by Western blotting (WB). (**D**) Corresponding quantification of the relative Aurora B autophosphorylation signals normalized to the Aurora B protein levels. (**E**) End-point autophosphorylation assay with Mps1 and Plk1. The kinases were pre-incubated 30 min at 30°C with purified Ska complex at the indicated concentrations before incubation with γ-^{32}P–ATP for another 30 min. Shown are autoradiographs of the autophosphorlyation signals (^{32}P) and Western blots of the kinase protein levels (WB). (**F**) Quantification of the relative autophosphorylation signals. Bars represent mean ± SEM (N = 2 experiments).

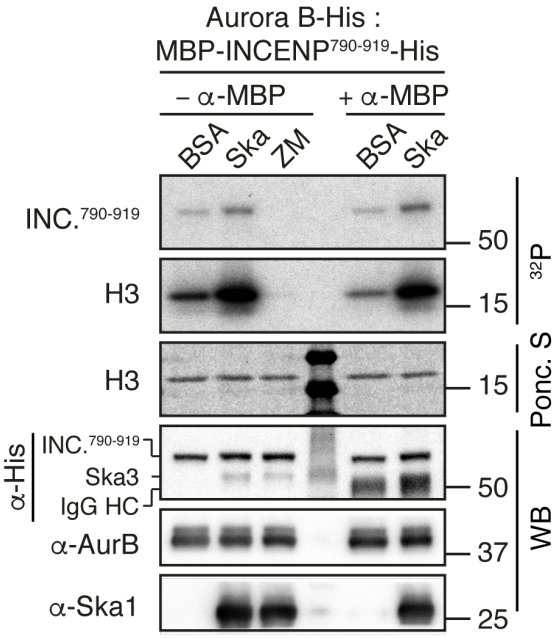

Figure 29. The Ska complex does not stimulate Aurora B activity by dimerization/induced proximity. Pre-incubation with soluble anti-MBP antibodies does not alleviate Ska complex-meadiated Aurora B activation. Aurora B–His (0.5 μM) and MBP–INCENP$^{790–919}$–His (0.5 μM) were pre-incubated 30 min at 30°C with Ska complex (1 μM) or purified bovine serum albumin (BSA, 1 μM) in presence or absence of monoclonal anti-MBP antibodies (0.25 μM), before addition of recombinant histone H3 and γ-^{32}P–ATP. Kinase reactions were stopped after 240 s. Phosphorylation of INCENP$^{790–919}$ and histone H3 was visualized by autoradiography (^{32}P), protein levels by Ponceau S staining (Ponc. S) and Western blotting (WB), respectively.

PP1 protects the Ska complex from Aurora B phosphorylation to enable its accumulation on bioriented KTs

Previous work has established that timely accumulation of the Ska complex at the KT-MT interface following chromosome biorientation is important for stabilizing K-fibers and that Aurora B opposes this function by lowering the binding affinity of the complex for both its outer KT receptor, the KMN network, and MTs (Chan et al., 2012; Jeyaprakash et al., 2012; Schmidt et al., 2012; Abad et al., 2014). The data presented here further suggest that the Ska complex, in turn, promotes Aurora B activity, presumably on the mitotic spindle and/or at KTs (see discussion). So, how is the Ska complex able to accumulate at the KT-MT interface and stabilize K-fibers

upon chromosome biorientation, if it also stimulates the Aurora B kinase that antagonizes this function? One possibility is that KT recruitment of phosphatases counteracting Aurora B might protect the Ska complex from Aurora B phosphorylation. To test this hypothesis, we arrested HeLa S3 cells in prometaphase using STLC (an Eg5 inhibitor) or in metaphase using MG132, subjected the cells to short treatment with the protein phosphatase 1 (PP1) and protein phosphatase 2 (PP2) inhibitor okadaic acid (OA) in presence or absence of ZM447439 (ZM) and examined KT levels of the Ska complex by immunofluorescence. In line with previous measurements in untreated cells (Chan et al., 2012), Ska3 immunofluorescence was about twofold higher at metaphase KTs in MG132-arrested cells than at prometaphase KTs in STLC-arrested cells, confirming that the Ska complex accumulates at KTs after biorientation (Figure 30A and 30B). Treatment of prometaphase (STLC-arrested) cells with the phosphatase inhibitor OA had little effect on the KT levels of Ska3, while coinhibition of Aurora B with ZM caused an increase of Ska3 staining intensity to levels seen in metaphase (MG132-treated) control cells (Figure 30A and 30B), confirming that Aurora B activity promotes the dissociation of Ska from KTs in prometaphase. In striking contrast, phosphatase inhibition by OA in metaphase (MG132-arrested) cells reduced staining of Ska3 at KTs to levels similar to prometaphase (STLC-treated) control cells; furthermore, simultaneous inhibition of Aurora B with ZM reverted this effect, indicating that phosphatase activity balances the influence of Aurora B on Ska KT binding (Figure 30A and 30B). Notably, we did not observe that tension across the centromeres was negatively affected in MG132-arrested cells by short OA treatment, as indicated by inter-KT distance measurements. This suggest that the effect on Ska3 KT localization

is not a consequence of changes in the spatial separation of Ska at the outer KT to Aurora B at the inner centromere and indicate that Ska and Aurora B may still functionally interact downstream of centromeric tension (Figure 30C). We conclude that either PP2 or PP1 balances Aurora B activity at the outer KT to enable timely enrichment of the Ska complex after chromosome biorientation.

The PP2 family member PP2A has been implicated in regulating the establishment of initial KT-MT contacts (Foley et al., 2011), while PP1 has been shown to stabilize attachments by opposing Aurora B activity upon biorientation (Liu et al., 2010). We therefore reasoned that PP1 is most likely to reverse Aurora B phosphorylation of the Ska complex to facilitate its KT association. To test this, we made use of a KNL1 mutant ($KNL1^{RSFV/AAAA}$) devoid of the PP1 binding site, which prevents targeting of PP1 to the outer KT, but is proficient in MT binding (Liu et al., 2010). Replacement of endogenous KNL1 with $KNL1^{RSFV/AAAA}$ resulted in a loss of Ska3 from KTs to a similar extent as observed in OA-treated metaphase cells, while expression of wild-type KNL1 reverted this effect (Figure 30D and 30E). These results show that PP1 counteracts Aurora B to allow the accumulation of the Ska complex at KTs upon biorientation. Altogether, these data prompt us to propose the model illustrated in Figure 30F. We propose a feedback mechanism in which Ska limits its own enrichment at KTs and/or spindle MTs by promoting Aurora B activity, ensuring a high degree of KT-MT dynamics prior to establishment of biorientation, while PP1 antagonizes this feedback regulation at KTs once biorientation is achieved, allowing Ska to stabilize proper K-fiber attachments.

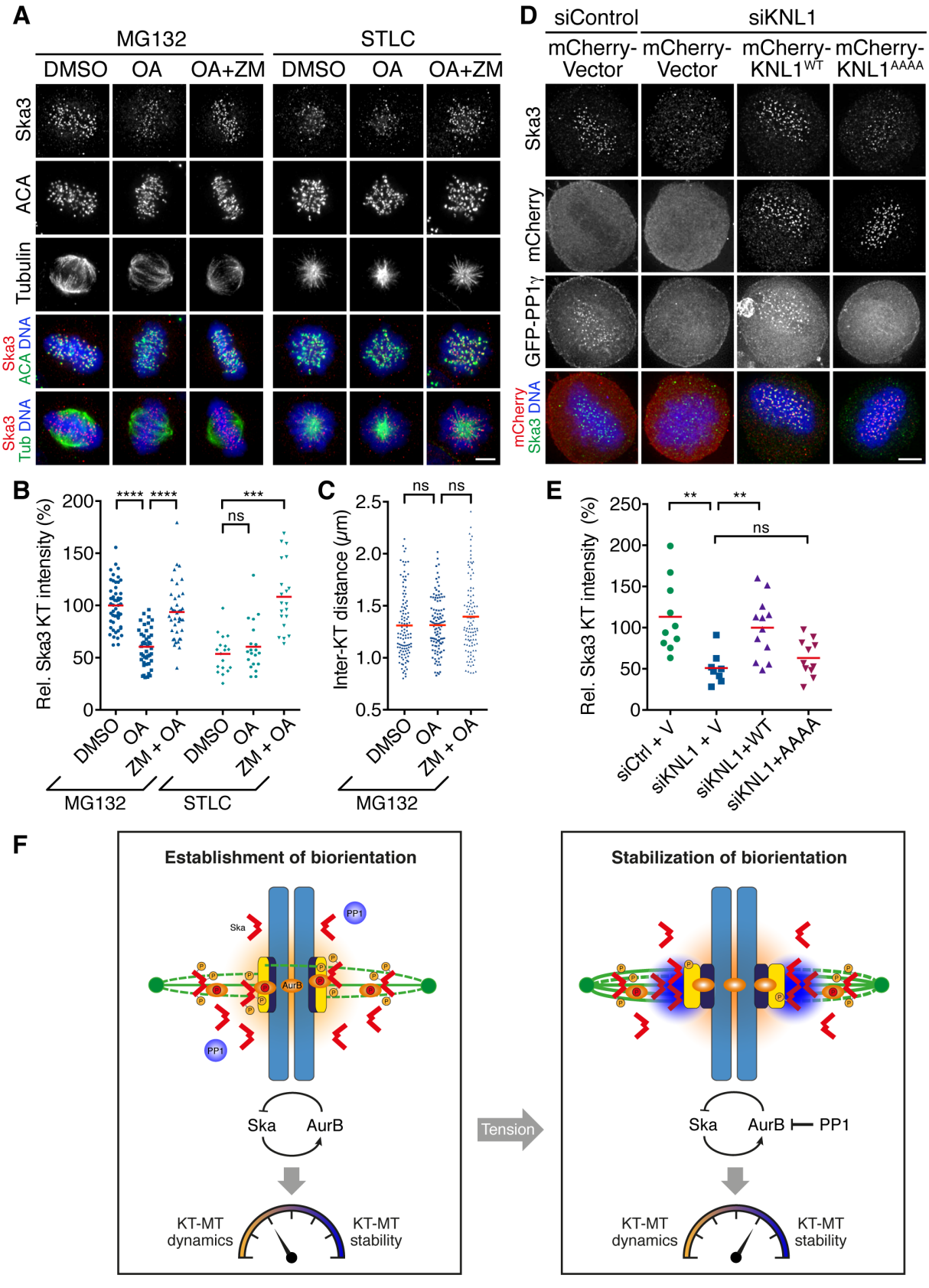

Figure 30. PP1 opposes Aurora B activity to enable Ska complex enrichment on bioriented KTs. (**A**) Asynchronously growing HeLa S3 cells were arrested in metaphase with MG132 (MG) or in early prometaphase with STLC for 2–3 h and treated for 20 min with the indicated combinations of the PP1 and PP2 inhibitor okadaic acid (OA) and the Aurora B inhibitor ZM447439 (ZM). Dimethylsulfoxide (DMSO) treatment served as negative control. Cells were fixed and stained with the indicated

antibodies. (**B**) Quantification of relative Ska3 KT intensities in cells treated as in **A** (n = 41–51 from N = 2 for MG132-treated cells, and n = 18–20 cells from N = 1 experiment for STLC-treated cells) (**C**) Scatter plot showing inter-KT distances in cells treated as in **A** (n = 110 sister-KT pairs per condition from 10 cells). (**D**) HeLa S3 cells were transfected with siRNA-resistant wild-type (WT) mCherry-KNL1 or PP1-binding-deficient mCherry-KNL1$^{RVSF/AAAA}$ together with GFP-PP1γ, before depletion of endogenous KNL1. (**E**) Quantification of relative Ska3 KT intensities in cells treated as in **D** (n = 8–11 cells per condition). (**F**) Model for the regulation of KT-MT attachment dynamics during chromosome biorientation by the feedback loop between the Ska complex and Aurora B (see discussion for details). The Ska complex promotes Aurora B activity at KTs and/or on the spindle, which, in turn, limits the accumulation of Ska at these sites during establishment of biorientation. This ensures a high degree of KT-MT attachment instability and dynamics to facilitate efficient reorientation of improper MTs through MT turnover. Upon biorientation, PP1 KT recruitment outweighs the feedback loop between Ska and Aurora B at KTs, enabling Ska KT accumulation and further maturation of K-fibers. Ongoing stimulation of Aurora B on the spindle may ensure an optimal dynamic behavior of KT-MTs for correction of merotelic attachments and chromosome movements in late mitosis.

Discussion

In this thesis, we discovered a novel function of the Ska complex. Specifically, we find that the Ska complex is not only a substrate of Aurora B kinase, but also regulates the activity of this key enzyme. We show that the Ska complex interacts with Aurora B and promotes, in a MT-dependent manner, both Aurora B substrate phosphorylation and effector localization in cells. We also demonstrate that Ska directly binds to Aurora B and stimulates its catalytic activity within the CPC core complex *in vitro*. Furthermore, we reveal hitherto concealed phenotypic aspects of Ska depletion, including suppressed KT-MT plus-end dynamics as well as chromosome biorientation and segregation defects, which distinctly resemble consequences of Aurora B partial loss-of-function. Finally, we demonstrate that PP1 antagonizes Aurora B activity at KTs to enable Ska KT accumulation once biorientation is achieved, which allows the Ska complex to promote K-fiber maturation.

Ska depletion phenocopies aspects of Aurora B loss-of-function

Using high-resolution time-lapse microscopy we find that the Ska complex is required to prevent lagging chromosomes in anaphase and micronuclei formation. In agreement with previous studies, we also confirm an implication of the Ska complex in chromosome congression, maintenance of chromosome alignment and timely metaphase to anaphase transition – phenotypes that are likely to be attributed to different degrees of Ska knockdown (Gaitanos et al., 2009). Some of these phenotypes are highly reminiscent of those previously described for Aurora B

inhibition. Specifically, partial inhibition of Aurora B has been shown to correlate with an increased frequency of merotely and lagging chromosomes, underlying a decrease in KT-MT turnover (Cimini et al., 2004), while a more pronounced impairment of Aurora B function has been linked to chromosome alignment defects (Kallio et al., 2002; Ditchfield, 2003; Hauf et al., 2003). Our work shows that perturbation of Ska complex function by RNAi similarly slows KT-MT turnover, providing an explanation for the appearance of lagging chromosomes and merotelic attachments. In addition, Ska-deficiency also causes pronounced chromosome alignment defects. Consistently, we find that KT localization of MCAK and CENP-E – both prominent downstream effectors of Aurora B that promote KT-MT plus-end dynamics and chromosome alignment (Kline-Smith, 2003; Bakhoum et al., 2008; Tanno et al., 2010; Murata-Hori and Wang, 2002; Ditchfield, 2003; Kapoor et al., 2006; Maffini et al., 2009) – are perturbed upon Ska depletion.

The Ska complex regulates KT-MT dynamics through Aurora B

The selective loss of MCAK from inner KTs explains the dampening of the KT-MT plus-end turnover and the faster MT poleward flux in Ska-deficient cells (Wordeman et al., 2007). Reduced MCAK depolymerase activity at KTs lowers the catastrophy frequency and leads to increased tubulin supply at the MT plus-ends. The latter, in turn, may be compensated by upregulation of spindle pole associated depolymerase activities, assuming that KT-MT plus-ends and minus-ends are mechanically linked. In line with the abrogated control of KT-MT dynamics, we also observed a disruption of regular sister KT oscillations in Ska-depleted cells. Although we cannot discount the possibility that the latter effect may reflect a reported function of the Ska complex

in coupling MT depolymerization to chromosome movements (Schmidt et al., 2012), our finding that Ska1 MT-binding deficient mutants do not restore wild-type KT levels of MCAK suggests that this phenotype may instead be a consequence of suppressed Aurora B activity.

The Ska complex plays a dual role in the regulation of KT-MT dynamics and K-fiber maturation

Our data further indicate that the Ska complex may influence KT-MT stability and dynamics in multiple ways. Specifically, we find that Ska is not only required for KT-MT plus-end turnover, but also for K-fibers with a normal number of MTs. The latter may mirror a role of the Ska complex in promoting the coherence and stabilization of MT arrays within K-fibers by laterally cross-linking the lattice of individual MTs at the KT-MT interface. This notion is supported by the findings that the Ska complex has the ability to bundle MTs both in cells and *in vitro* and that the complex becomes enriched at the KT-MT interface upon chromosome biorientation (Welburn et al., 2009; Chan et al., 2012). An inter-MT cross-linking function also matches the W-shaped structure of the Ska complex, which spans a diameter of ~35 nm and thus exceeds the diameter of ~25 nm of individual MTs (Jeyaprakash et al., 2012). Moreover, Ska likely promotes MT recruitment during K-fiber maturation either by providing additional MT-binding sites within the outer KT (King and Nicklas, 2000), by enhancing the MT-binding affinity of the Ndc80 complex (Schmidt et al., 2012), and/or by facilitating MT capture through CENP-E (McEwen et al., 2001), thereby enabling KTs to attain and maintain a normal complement of MTs. Thus, we propose

that the Ska complex plays a dual role in the control of KT-MT dynamics via Aurora B and in the formation and stabilization of K-fibers.

Where does the Ska complex promote Aurora B activity?

Inner centromere localization of Aurora B prior to anaphase is a prominent and conserved feature in eukaryotic model organisms, indicating that this localization is crucial for kinase activation and function. However, ample evidence suggests that not all Aurora B functions strictly rely on its centromere localization. Most strikingly, it has been shown that impairment of centromere targeting of Aurora B in chicken DT40 cells and budding yeast does not associate with extensive chromosome biorientation defects that cause cell inviability (Yue et al., 2008; Campbell and Desai, 2013). Moreover, centromere accumulation of the kinase in human cells is not essential for the establishment and maintenance of histone H3-S10 phosphorylation, although centromere concentration of Aurora B can enhance the rate of H3-S10 phosphorylation (Wang et al., 2010; 2012). Accordingly, there must be subcellular sites distinct to the centromere, where Aurora B activation can, at least partially, occur. In line with this view, we find that the Ska complex that localizes to outer KTs and spindle MTs is required for Aurora B phosphorylation of histone H3 and inner KTs substrates, despite significant centromere levels of Aurora B (in cells with aligned chromosomes) or forced Aurora B centromere concentration (by CB^{DBD}-INCENP expression). Moreover, we also observed that delocalization of Aurora B from centromeres (by Haspin depletion or inhibition) did not alleviate the effect of Ska knockdown on H3-pS10 (data not shown). Finally, we show that Ska depends on its MT-binding capability to promote Aurora B activity. Together, these data support the

hypothesis that Ska facilitates Aurora B activation either on the mitotic spindle or at KTs in a MT-dependent manner, but not at centromeres. In agreement with this notion, pools of Aurora B have been directly observed both on the metaphase spindle and proximal to KTs in the presence of spindle poisons in human tissue culture cells (Tseng et al., 2010; Bekier et al., 2015). Moreover, phosphorylated forms of Aurora B have been detected at KTs, most apparently under conditions of low phosphatase activity (Posch et al., 2010; DeLuca et al., 2011; Petsalaki et al., 2011). Interestingly, at KTs, Aurora B autophosphorylation of threonine 232 within the activation loop was shown to depend on KNL1, one of the outer KT KMN network components, which, in turn, is an upstream requirement for Ska KT localization (Caldas et al., 2013; Chan et al., 2012). In contrast to the Ska complex, however, KNL1 seems dispensable for Aurora B activity towards H3-S10 (Caldas et al., 2013). This may suggest that Ska stimulates Aurora B activity on the mitotic spindle rather than at KTs, but further evaluation is required to provide conclusive evidence on where Ska promotes Aurora B activity. Proximity ligation assays and Ska mutants that are selectively deficient in KT but not MT binding could help to address this question.

Mechanism of Aurora B activation by the Ska complex

Maximal activity of Aurora B arises from several regulatory mechanisms, including the autophosphorylation within its activation segment (Yasui et al., 2004), the binding of the C-terminal INCENP IN-Box around the small lobe of the kinase domain (Sessa et al., 2005), the Aurora B-dependent phosphorylation of the IN-Box on a TSS motif (Honda et al., 2003), the phosphorylation of Aurora B by other kinases (e.g. Chk1) (Petsalaki et al., 2011), the interaction with other proteins (e.g. TD-60) (Rosasco-

Nitcher et al., 2008; Papini et al., 2015), as well as the interplay with phosphatases (Sugiyama et al., 2002b; Foley and Kapoor, 2013). Furthermore, local clustering of Aurora B on centromeric chromatin and MTs has been proposed to stimulate autoactivation of the kinase through transphosphorylation of the IN-box TSS motif and/or yet unknown allosteric mechanisms (Kelly et al., 2007; Tseng et al., 2010; Kelly and Funabiki, 2009). Here we identify the Ska complex, a previously discovered Aurora B substrate, as a novel positive regulator of Aurora B activity. We show that Ska interacts with Aurora B within the CPC and promotes Aurora B substrate phosphorylation in cells. We also show that the Ska complex directly binds to Aurora B and stimulates its kinase activity *in vitro*. How exactly Ska binding promotes Aurora B activity requires further investigation. Yet, we provide several lines of evidence that the Ska complex contributes to Aurora B activity independently of a local clustering/transactivation mechanism. First, ectopic concentration of Aurora B at centromeres is not sufficient to restore control levels of Aurora B substrate phosphorylation in Ska-deficient cells. Second, divalent antibodies targeted against the IN-Box do not abolish Ska-dependent stimulation of the kinase *in vitro* and similar results were obtained with antibodies against the N-terminal tail of Aurora B (data not shown). Third, Aurora B activity in presence of the IN-Box appears to respond in a non-cooperative manner to Ska stimulation *in vitro*. Finally, Ska enhances the catalytic activity of Aurora B regardless of the presence or absence of the INCENP IN-box domain – notably in both cases up to four fold. Together, these data support the notion that binding of the Ska complex to Aurora B promotes the intrinsic autoactivation capability of the kinase, presumably by an allosteric mechanism that differs from that of INCENP.

It is not unprecedented that substrates can regulate their corresponding protein kinases through feedback mechanisms. In fact, this has previously been described as a mechanism for the regulation of the activity of Aurora kinases. In case of Aurora B, this is well exemplified by INCENP, whose direct binding to and subsequent phosphorylation by Aurora B elicits kinase activation (Sessa et al., 2005). In *C. elegans* tousled-like kinase-1 (TLK-1) appears as another example for a substrate that can stimulate Aurora B activity. TLK-1 is reportedly phosphorylated by Aurora B (AIR-2) and triggers, in turn, further activity of Aurora B independently of its own kinase activity, but in an INCENP-dependent manner (Han et al., 2005). Likewise, Aurora A kinase activity is known to be enhanced by some of its substrates. For instance, the MT-associated protein TPX-2 has been reported as a substrate that promotes Aurora A kinase activity (Kufer, 2002; Bayliss et al., 2003; Fu et al., 2015). Thus, substrate activation may constitute an important regulatory mechanism to control the activity and function of Aurora kinases and given their broad range of substrates other substrate regulators may await discovery.

A speculative model for the role of the Ska–Aurora B interplay in the regulation of KT-MT attachment dynamics during biorientation

Chromosome biorientation and accurate chromosome segregation relies on the precise control of the attachment stability and dynamics of KT-MTs. If KT-MTs are too dynamic, KTs fail to attain a stable grip on the KT-MT lattice and thus to generate load-bearing K-fiber attachments with sufficient numbers of MTs that can satisfy the SAC. If they are too static, maloriented KT-MTs cannot be replaced efficiently and force production for chromosome movements is impaired. Likewise, an overly stable

grip on KT-MTs prevents attachment error correction and can suppress KT-MT plus-end dynamics, whereas a too loose grip on KT-MTs leads to weak K-fiber attachments. Thus, there is a requirement for opposing restrictions on both the attachment stability and dynamics of KT-MTs during mitosis. Our present data imply a Ska–Aurora B feedback loop that may contribute to set such essential boundaries on the dynamics of KT-MT attachments. Ska controls its own MT and KT association via Aurora B activity and, *vice versa,* Aurora B activity via its levels of MT and KT enrichment, such as to ensure that the attachment stability and dynamics of KT-MTs fall within an optimal balance for efficient chromosome biorientation (Figure 30F). As Ska levels rapidly rise on spindle MTs and KTs after NEBD (Hanisch et al., 2006; Raaijmakers et al., 2009), Aurora B activity would be driven up. The rise in Aurora B activity, in turn, would increase the phosphorylation rate of Ska, which then limits its further spindle MT and KT accumulation, ensuring that both the concentration of the Ska complex on spindle MTs and KTs and the activity of Aurora B level off at a specific set point (Figure 31).

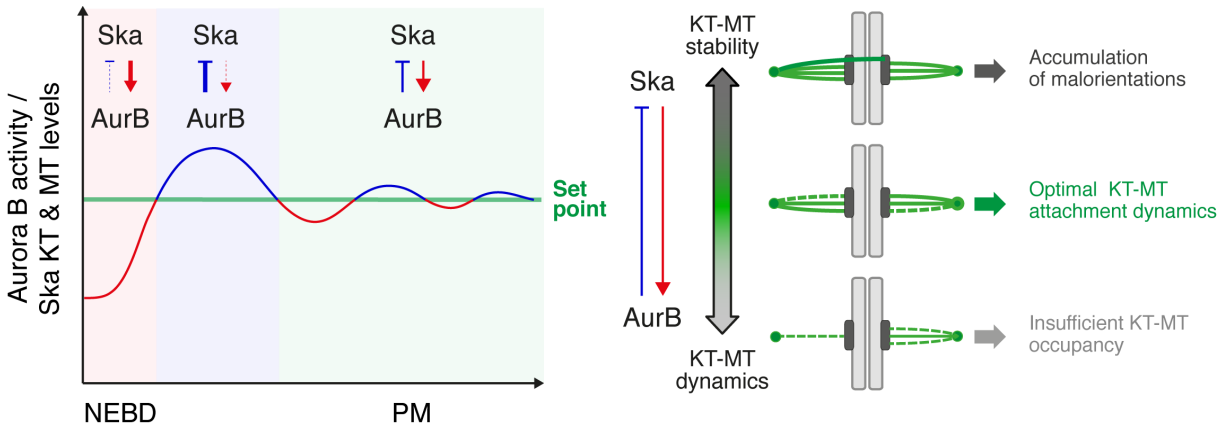

Figure 31. Model for feedback control of KT-MT attachment dynamics by the interplay between Ska and Aurora B. The feedback loop between the Ska complex and Aurora B would ensures that both the levels of Ska on KTs/MTs and the activity of Aurora B level off at a specific set point (*left*) such that KT-MT stability and dynamics fall within an optimal balance during biorientation (*right*). NEBD, nuclear envelope breakdown; PM, prometaphase.

Since the native affinity of the Ska complex for MTs is relatively high (~ 0.3 μM in comparison to ~0.5 μM of the KMN network), the binding equilibrium is expected to favor MT association, which might cause detrimental MT bundling if too high levels of Ska are achieved (Welburn et al., 2009). Thus, limiting the binding of Ska along spindle MTs could be important to achieve a proper K-fiber organization (Nixon et al., 2015). Moreover, confining Ska-dependent MT cross-linking along spindle MTs might facilitate MT dynamics by reducing the physical constraints on the curvature of the GDP lattice of protofilaments. On the other hand, balancing its levels at KTs by Aurora B helps to keep MT attachments sufficiently flexible for the release of maloriented MTs (Chan et al., 2012). Furthermore, the Ska-induced increase in Aurora B activity would promote KT localization of MCAK, which, in turn, coordinately elevates the MT catastrophe frequencies (Wordeman et al., 2007). Together, these mechanisms would ensure a high KT-MT turnover rate during establishment of biorientation (when attachment errors are most frequently made), which promotes the replacement of erroneous KT connections by exploiting the back-to-back arrangement of sister KTs (that provides an intrinsic bias for biorientation) (Nicklas, 1997; Lončarek et al., 2007; Godek et al., 2014; Magidson et al., 2015; Zaytsev and Grishchuk, 2015).

As bioriented attachments are made, small tension-dependent conformational changes within the KT will allow bulk recruitment of PP1 (Wan et al., 2009; Suzuki et al., 2014; Liu et al., 2010; Posch et al., 2010; Campbell and Desai, 2013; Sarangapani and Asbury, 2014). A negative feedback loop of Aurora B on PP1 KT localization prior to establishment of tension may help to prevent premature KT accumulation of Ska and would enable rapid and robust switch-like shifts in the

overall dynamics of KT-MT attachments (Liu et al., 2010). Upon its targeting to KTs, PP1 would then outweigh (at KTs) the positive influence of Ska on Aurora B activity and the negative influence of Aurora B on the localization of Ska, and permit Ska to promote further maturation of K-fiber attachments through its full KT enrichment.

Given that Aurora B activity remains suppressed in Ska-deficient cells upon chromosome alignment, stimulation of Aurora B on the spindle may be ongoing and could contribute to sustain an appropriate dynamic behavior of KT-MTs for merotelic error correction and chromosome movements in late mitosis. In line with this hypothesis, we note that several previous findings suggest that Aurora B activity is important for KT-MT attachment dynamics downstream of tension. First, inhibition of Aurora B kinase activity greatly slows the plus-end turnover and increases the cold stability of KT-MTs in late prometaphase/metaphase without reducing the centromeric stretch (Cimini et al., 2006; Tanno et al., 2015). Second, prevention of Aurora B-dependent phosphorylation of the N-terminal tail of the KMN subunit Ndc80 markedly dampens KT oscillations of bioriented sister KTs (DeLuca et al., 2011). Third, Aurora B phosphorylation of the KMN components KNL1 and Dsn1 at KTs diminish only modestly from early prometaphase to late prometaphase/metaphase (DeLuca et al., 2011; Welburn et al., 2010). Further scrutinization of the functional interplay between the Ska complex and Aurora B will be important for the understanding of how KTs generate, correct, and maintain stable yet dynamic connections to spindle MTs, which are fundamental to preserve genomic stability.

Appendix

Ska1 localization during interphase is regulated by nuclear export

Previous structure-function analyses of Ska1 have revealed different interphase localization patterns of Ska1 truncation mutants. Specifically, an N-terminal Ska1 fragment spanning amino acid 1-132 ($Ska1^{1-132}$, ~15 kDa) localized predominantly to the cytoplasm when transiently expressed in interphase cells (Figure 31A) (Abad et al., 2014), similar to full-length Ska1 (~30 kDa) (Figure 31E). In contrast, the corresponding equal sized C-terminal fragment ($Ska1^{132-255}$, ~14.5 kDa) showed distinctive nuclear localization, hinting on a nuclear export signal (NES) in the first 132 amino acids (Figure 31A) (Abad et al., 2014). Sequence analysis confirmed the presence of a conserved NES in Ska1 encompassing amino acids 52-60 (Figure 31B). Likewise, analysis of Ska2 revealed a NES spanning amino acids 98-103 (~15 kDa), whereas no apparent NES could be detected in Ska3 (~50 kDa) (data not shown). To determine whether Ska1 localization in interphase is controlled by nucleocytoplasmic shuttling, we inhibited CRM1, a major nuclear export receptor, using leptomycin B (Kudo et al., 1999; Hutten and Kehlenbach, 2007). Leptomycin B treatment of living HeLa K cells stably expressing GFP-Ska1 caused a clear nuclear accumulation of the GFP fusion protein (Figure 31C). Similar results were obtained in living RPE-1 cells expressing endogenously tagged GFP-Ska1 (Figure 31D), indicating that Ska1 is actively exported from the nucleus in a CRM1-dependent manner. To further corroborate this finding, we mutated five leucine/isoleucine residues in the identified Ska1 NES to alanine (Figure 31B) and assessed the localization of this mutant following its transient expression in living HeLa S3 cells

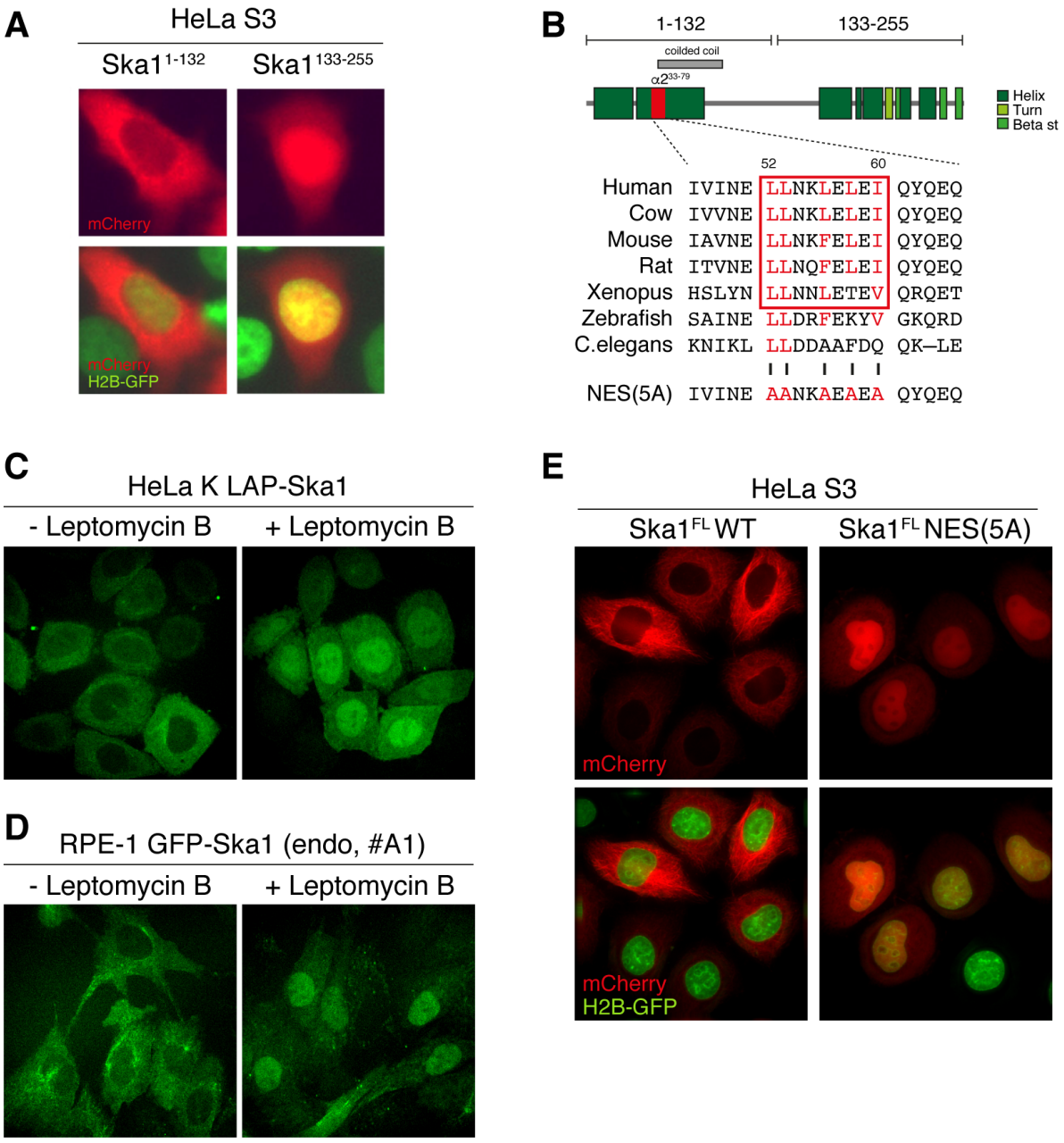

Figure 32. Ska1 localization is controlled by CRM1-dependent nuclear export during interphase. (**A**) HeLa S3 H2B-GFP cells expressing mCherry-Ska1$^{1-132}$ or Ska1$^{133-255}$. This figure was reproduced from (Abad et al., 2014). (**B**) *Top*, schematic representation of the 2° structure of Ska1 with the predicted NES highlighted in red. *Bottom*, alignment of the NES sequence from different species. (**C**,**D**) HeLa K cells stably expressing LAP-Ska1 (**C**) or RPE-1 cells expressing endogenously tagged GFP-Ska1 (**D**) were treated for 2–3 h with leptomycin B (20 nM) before live imaging. (**E**) Live-images of HeLa S3 H2B-GFP cells transiently transfected with mCherry tagged Ska1 wild-type (WT) or Ska1 NES(5A).

stably expressing H2B-GFP. Whereas wild-type Ska1 was predominantly localized to the cytoplasm, Ska1 NES(5A) accumulated in the nucleoplasm (Figure 31E). Together, these data show that Ska1 localization is regulated by nuclear exclusion

during interphase. The biological relevance of this regulation remains to be determined.

Ska3 is phosphorylated by Plk1 on multiple sites *in vitro*

Polo-like kinase 1 (Plk1) has been implicated in the regulation of KT-MT attachment stability and dynamics (Santamaria et al., 2007; Liu et al., 2012) and a prior phosphoproteomic study performed in our lab has suggested that the Ska complex may be regulated by Plk1-dependent phosphorylation (Anna Santamaria, unpublished data). This prompted us to screen for Plk1 target sites on Ska subunits by combining an *in silico* search for the canonical Plk1 motif with a phosphopeptide spotting array. We identified five conserved sites on Ska3 (S34, S124, T229, T328, T342) that were directly phosphorylated by Plk1 *in vitro* (Figure 33A). In comparison, Mps1, that shows a motif preference very similar to Plk1 (Dou et al., 2011; Schubert et al., 2015), did not target any of the twenty-four spotted Ska sites, although it phosphorylated previously established sites in MCAK and Nup98 (Figure 33A). In line with this result, Plk1 but not Mps1 was able to phosphorylate Ska3 within the reconstituted Ska complex (Figure 33B). Two of the identified sites in Ska3 have been previously detected as *in vivo* phosphorylation sites (S34, T229) by mass spectrometry (Nousiainen et al., 2006; Dephoure et al., 2008; Hornbeck et al., 2012). S124, T229, T328 and T342 are all located in the unstructured C-terminal region of Ska3, which is involved in MT binding of the Ska complex (Jeyaprakash et al., 2012). In contrast, S34 sits at a hinge region between the two N-terminal helices of the individual V-shaped Ska complex protomers. Site-directed mutagenesis and rescue

experiments will be needed to explore the potential functional consequences of the Plk1-dependent phosphorylation of Ska3.

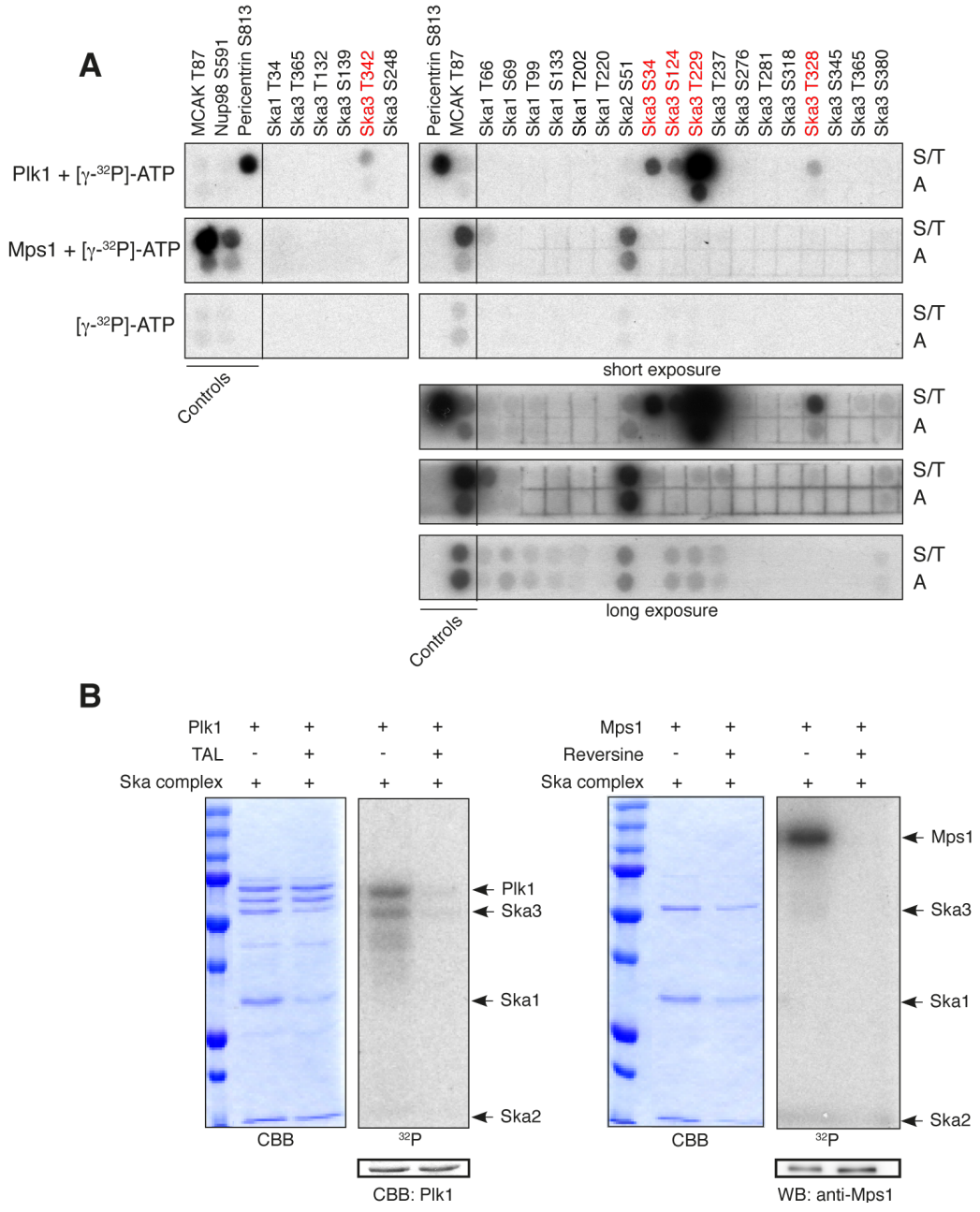

Figure 33. Plk1 phosphorylates Ska3 on multiple sites *in vitro*. (**A**) Selected Ska1, Ska2 or Ska3 peptides containing potential Plk1 phosphorylation sites that conformed to the Plk1 consensus motif (D/E/N/Y/Q)–X–(S/T)–(no P, Φ) (where X is any and Φ is a hydrophobic amino acid) were synthesized on cellulose membranes carrying either the serine or threonine (S/T) phosphoacceptor or an alanine (A) and were used as substrate for Plk1 and Mps1 in *in vitro* kinase assays. As control, peptide spots were incubated without enzymes in the presence of γ-^{32}P–ATP. Positive sites are highlighted in red. (**B**) Plk1 and Mps1 *in vitro* kinase assay on the full-length reconstituted Ska complex. As control, the Plk1 inhibitor TAL and the Mps1 inhibitor reversine, respectively, were included. Note that the Ska complex was present at only half the concentration in the control reactions. Shown are Coomassie stained gels (CBB), the corresponding autoradiographs (^{32}P), and either the cropped Coomassie signal or a Western blot (WB) for the kinase protein levels.

Experimental Procedures

Cell culture, transfection and drug treatments

HeLa S3, HeLa S3 H2B-GFP (Silljé et al., 2006), and U2OS cells were cultured in DMEM-GlutaMAX supplemented with 10% heat-inactivated fetal calf serum (FCS) and penicillin/streptomycin (100 IU/ml and 100 mg/ml, respectively) in a humified incubator at 37°C and 5% CO_2. HeLa Kyoto cells stably expressing PA-GFP–α-tubulin/H2B–mRFP (Amaro et al., 2010) were further maintained in 250 ng/ml puromycin and 500 μg/ml G418. Stable HeLa Kyoto H2B-fused Aurora B FRET reporter (van der Waal et al., 2012), HeLa Kyoto CENP-B-fused Aurora B FRET reporter (a kind gift of Daniel W. Gerlich, IMBA, Vienna, Austria), and stable HeLa Kyoto EGFP-CENP-A cells (Jaqaman et al., 2010) were further maintained in 500 ng/ml puromycin. Stable HeLa LAP-Ska1 cells were maintained in 2 μg/ml blasticidin (Welburn et al., 2009). HeLa cells stably expressing siRNA-resistant GFP-Ska1^{WT}, GFP-Ska1$^{R155A,\ R236A,\ R245A}$ or GFP-Ska1$^{\Delta MTBD}$ (a kind gift from Ian M. Cheeseman, Whitehead Institute, University of California, Berkeley, USA) were cultured as previously described (Schmidt et al., 2012). MCF10A^{ecoR} cells (a kind gift of Tilmann Brummer, ZBMZ, Freiburg i. Br., Germany), authenticated by STR profiling, were grown as previously described (Schnerch and Nigg, 2015). hTERT-RPE-1 wild-type cells and RPE-1 cells expressing endogenously tagged GFP-Ska1 (generated by Anna Santamaria and Fabien Cubizolles) were cultured in DMEM/F12 supplemented with 10% FCS, penicillin/streptomycin, L-glutamine (2 mM) and sodium bicarbonate (0.25%).

Cells were transfected with siRNAs (50–100 nM) using Oligofectamine (Invitrogen) and with plasmid DNA (0.5 mg/ml) using XtremeGene HP (Roche), according to the manufacturers' instructions. The following siRNA duplexes were used: siSka1-1 (5'-CGCTTAACCTATAATCAAA-3'; used throughout the study unless stated otherwise) (Hanisch et al., 2006), siSka3 (5'-AGACAAACATGAACATTAA-3') (Gaitanos et al., 2009), siSka1-2 (5'-GGAGATTTGTGTCAATAAT-3') (Hanisch et al., 2006), siSka2 (5'-GAAATCAAGACTAATCATC-3') (Hanisch et al., 2006), siKNL1 (5'-GGAATCCAATGCTTTGAGA-3') (Liu et al., 2010). A siRNA duplex targeting luciferase (GL2) served as control: siCtrl (5'-CGTACGCGGAATACTTCGA-3'). The pcDNA3.1 plasmids encoding Ska1 and Ska3 in frame with a single mCherry tag and an N-terminal triple-Myc tag, respectively, were generated by Ying Wai Chan. For rescue experiments, a Ska1 siRNA-resistant version was used (Chan et al., 2012), while Ska3 was depleted with a siRNA duplex targeting the 3' UTR (the sequence reported above). Cells were transfected with siRNAs, arrested for 20–22 h with thymidine 24 h after transfection, released into fresh medium for 2 h, transfected with plasmid DNA, followed by a medium change and a second 16 h thymidine block 4 h after transfection, before cells were released into fresh medium for 10–11 h, as previously described (Chan et al., 2012). The mCherry-KNL1 wild type (Addgene plasmid #45224), mCherry-KNL1$^{RSFV/AAAA}$ mutant (Addgene plasmid #45226) and GFP-PP1γ constructs were a kind gift from Michael Lampson (University of Pennsylvania, Philadelphia, USA). Rescue experiments with these constructs were performed as previously described (Liu et al., 2010). The plasmid encoding a fusion protein of CENP-B$^{1–158}$ to human INCENP$^{48–918}$ and EGFP in pcDNA3.1 (Addgene plasmid #45237) (Wang et al., 2011a) was also provided by Michael Lampson

(University of Pennsylvania, Philadelphia, USA). The Ska1 NES(5A) mutant was synthesized by GenScript and was cloned into pDEST-mCherry (a gift from Terje Johanson, University of Tromsø, Norway) (Pankiv et al., 2007) using Gateway cloning (Invitrogen).

The following drugs were used: 5-iodotubericidin (5-ITu, Santa Cruz) at 10 μM, MG132 (Calbiochem) at 10 or 20 μM, leptomycin B (Sigma-Aldrich) at 20 nM, monastrol (Enzo Life Sciences) at 100 μM, nocodazole (Sigma-Aldrich) at 0.33 or 3.3 μM, okadaic acid (Calbiochem) at 1 μM, proTAME (BostonBiochem) at 20 μM, reversine (Enzo Life Sciences) at 0.5 μM, STLC (Tocris Bioscience) at 10 μM, TAL (Bayer Schering Pharma) at 1 μM, thymidine (Sigma-Aldrich) at 2 mM, and ZM447439 (Tocris Bioscience) at 10 μM (except otherwise state).

Photoactivation assay

Photoactivation experiments were carried out in Lab-Tek II chambers (Thermo Fisher Scientific) with Leibovitz L-15 medium containing 10% FCS at 37°C. Photoactivation was performed on bipolar late prometaphase spindles (identified by the H2B–mRFP signal) as described previously (McHedlishvili et al., 2012). In brief, PA-GFP–α-tubulin was activated in a thin stripe just above the chromosome mass using 150 iterations from a 405 nm laser (100%) on a Zeiss LSM 710-FCS confocal microscope. Fluorescence images were captured every 3 seconds for 201 seconds using a 40x/NA1.2 C-apochromat water objective. Fluorescence intensities were measured in Image J at each time frame in circular regions defined by the size of individually activated K-fibers. In average 3–4 high signals on different K-fibers in each cell were measured. Background signal was subtracted for each time frame by

measuring the same pixel area on the opposite side of the photoactivated spindle. Cells that underwent anaphase in this period were discarded. The values were corrected for photobleaching by determining the fluorescence loss in activated cells treated with taxol (10 μM). The average data were fitted to a double-exponential curve $I = P_{fast} \exp(-k_{fast}t) + P_{slow} \exp(-k_{slow}t)$, where I is the proportion of the initial fluorescence intensity, P is the proportion of the fluorescence decay due to the fast or slow process, k is the rate constant for the fluorescence decay of the fast or slow process and t is time. Curve fitting was performed with Prism software (GraphPad). The turnover half-life ($t_{1/2}$) was calculated as $\ln 2/k$ for each fast and slow process. Poleward MT flux rates were manually measured in Image J. Average cellular flux rates were calculated from ≥ 3 K-fibers per cell.

Kinetochore tracking assay

KT tracking experiments with HeLa cells stably expressing EGFP–CENP-A were carried out in Lab-Tek II chambers (Thermo Fisher Scientific) with Leibovitz L-15 medium containing 10% FCS at 37°C. Live-imaging was performed at a temporal resolution of 7.5 seconds for a total 5 min on a DeltaVision system (GE Healthcare) equipped with a 100x/NA1.4 objective, a Photometrics CoolSNAP HQ2 camera and a EGFP/mRFP filter set. KT trajectories were analyzed as described previously (Jaqaman et al., 2010).

Immunofluorescence microscopy, live cell imaging and FRET

For immunofluorescence stainings, cells were grown on uncoated (HeLa, U2OS) or poly-L-lysine-coated (MCF10A, RPE-1) glass coverslips. Cells were simultaneously

fixed and permeabilized for 10 min at room temperature in PTEMF buffer (20 mM PIPES pH 6.8, 4% formaldehyde, 0.2% Triton X-100, 10 mM EGTA, and 1 mM $MgCl_2$). For stainings shown in Figure 18E, 20A, 20E, 21A, 21D, 23A, 23C, and 23E cells were pre-extracted for 2 min in PEM buffer (100 mM PIPES pH 6.8, 10 mM EGTA, and 1 mM $MgCl_2$) with 0.4% Triton X-100 and then fixed for 10 min in 4% formaldehyde in PEM buffer supplemented with 0.2% Triton X-100. Cells were blocked with 3% BSA in PBS for 1 h, incubated with primary antibodies for either 12–16 h at 4°C or 2–3 h at room temperature, washed with PBS/0.1% Tween 20, and incubated with secondary antibodies and Hoechst dye for an additional 1 h at room temperature. Primary antibodies used were: mouse anti-Aurora B (1:500, AIM-1, BD Transductions, 611083, clone 6), rabbit anti-Borealin (1:3000) (Klein et al., 2006), guinea pig anti-mCherry (1:2000, a gift from Peter Scheiffele, Biozentrum, Basel, Switzerland), mouse anti-GFP (1:2000, Abcam, ab1218, clone 9F9.F9), rabbit anti-GFP (1:1000, Abcam, ab290), rabbit anti-histone H3-pS10 (1:1000, Millipore, 06-570), rabbit anti-histone H3-pS28 (1:500, Cell Signaling, 9713P), rabbit anti-histone H3-pT3 (1:200, Cell Signaling, 9714S), rabbit anti-MCAK (1:1000, generated by Zhen Dou against His-MCAK$^{588-725}$), mouse anti-Myc (clone 9E10) (Evan et al., 1985), rabbit anti-Ska1 (1:1000) (Hanisch et al., 2006), mouse anti-Ska3 (1:1, generated by Anna Santamaria; described later), mouse anti–α-tubulin–FITC (1:500, Sigma-Aldrich, F2168, clone DM1A). KTs were identified using human anti-centromere antibodies (1:1000, ACA, ImmunoVision, HCT-0100) and DNA was stained using Hoechst dye (1:5000, Life Technologies).

Images were acquired as 20 μm z-stacks with a step-size of 0.4 μm on a DeltaVision system (GE Healthcare) equipped with a 60x/NA1.42 PlanApo N oil

objective and a Photometrics CoolSNAP HQ2 camera. Images were deconvolved and projected (maximum intensity projection) using SoftWorx software (GE Healthcare) and equally scaled using OMERO software. Quantifications were performed using an automated pipeline, run by CellProfiler software, which involved the following processing steps: manual selection of mitotic cells, generation of KT/centromere and chromatin masks based on thresholding of pixel intensities of stable KT and chromatin marker signals (ACA and Hoechst, respectively), generation of secondary masks for signal and background measurements (KT/centromere intensity, chromatin intensity), measurement of mean signal intensities per cell within these secondary masks and export of reference images for quality control of the image segmentation. Measurements of KT/centromere intensities were corrected by subtraction of the mean intensity of the chromatin mask (background) and were normalized over the mean intensity of ACA or background.

For time-lapse imaging, cells were plated in chambered slides (Lab-Tek II, IBIDI) and filmed in a climate-controlled and humidified environment (37°C and 5% CO_2). High-resolution time-lapse imaging was carried out on a DeltaVision system (GE Healthcare) equipped with a 60x/NA1.42 PlanApo N oil objective and a Photometrics CoolSNAP HQ2 camera. Images were captured with 10% neutral density, 10 ms exposure times and 2× binning in 5 min intervals for 16–18 h with 20 stacks per field spaced 1.5 μm each. Long-term time-lapse imaging was performed on a Nikon Eclipse Ti microscope equipped with a CoolLED pE-1 illumination system and a 20x/NA0.75 plan apochromat air objective. Images were captured with 20 ms exposure times in 4 min intervals for 48 h with 1 stack per field.

FRET experiments were performed on a 3i spinning disk confocal system (Intelligent Imaging Innovations) based on a Zeiss Axio Observer stand equipped with a Photometrics Evolve 512 back-illuminated EMCCD camera, a 63x/NA1.4 plan apochromat oil objective and diode lasers, run by SlideBook software. CFP or TFP was excited with a 440 nm diode laser and CFP or TFP fluorescence emission (CFP_{em} or TFP_{em}) and YFP ($FRET_{em}$) fluorescence emission was acquired sequentially in z-stacks of 20–30 μm with a step-size of 2 μm. For the chromatin-targeted sensor, mean CFP and YFP fluorescence intensities were measured in circular regions within the chromatin mass using Image J software, and background-subtracted $CFP_{em}/FRET_{em}$ ratios were calculated and normalized to the mean of all interphase cells of one experimental replicate. For the centromere-targeted sensor, CFP and YFP emissions were aligned by minimizing the mean square difference of intensities between the two images using the StackReg plugin in Image J, mean CFP and YFP fluorescence intensities were measured in circular regions defined by the size of individual centromeres using Image J, and background-subtracted $CFP_{em}/FRET_{em}$ ratios were calculated.

For both static and live imaging analyses, statistical analyses were done with Prism software (GraphPad)

Protein purification and kinase assays

The plasmid encoding C-terminally His_6-tagged Aurora B was a gift from Xuebiao Yao (University of Science and Technology of China, Hefei, China). The open reading frame for Aurora B was sequenced and a non-silent point mutation was reverted (R278H) using QuikChange mutagenesis (Agilent Technologies). The pMAL

plasmid encoding INCENP$^{790-918}$ in frame with an N-terminal maltose-binding protein (MBP)-tag and a C-terminal His_6-tag was generated by Ulf Klein. Proteins were expressed in *E. coli* BL21 (DE3) and expression was induced with 0.1 mM IPTG for 4–5 h at 20°C. Aurora B-His_6 was purified under native conditions with Ni-NTA agarose beads (Qiagen) and eluted with 250 mM imidazole. MBP-INCENP$^{790-918}$-His_6 was purified under native conditions with amylose resin (New England Biolabs), eluted with 10 mM maltose, followed by a second purification step with Ni-NTA agarose beads and elution with 250 mM imidazole, according to standard procedures. Proteins were dialyzed against 20 mM Tris pH 7.4, 100 mM NaCl, 1 mM DTT, and 10% glycerol, and concentrated with Amicon Ultra centrifugal filters (Millipore). Protein concentrations were determined by infrared spectrometry using a DirectDetect system (Millipore). Full-length Ska complex comprising Ska1-His_6, untagged Ska2 and His_6-Ska3 was kindly provided by Anna Santamaria and was purified as previously described (Gaitanos et al., 2009; Chan et al., 2012). Recombinant Mps1 and Plk1 were kindly provided by Conrad von Schubert and Anna Santamaria, respectively, and were purified as previously described (Schubert et al., 2015).

For the time-course *in vitro* kinase assays shown in Figure 26A, 26C, and 26D MBP-INCENP$^{790-918}$-His_6 (0.5 μM) and Aurora B-His_6 (0.5 μM) were pre-incubated in 25 μl kinase buffer A (25 mM HEPES pH 7.4, 50 mM NaCl, 1 mM DTT, 5 mM $MgCl_2$) supplemented with EDTA-free protease inhibitor cocktail (Roche) with either recombinant Ska complex (1 μM), bovine serum albumin (BSA, 1 μM, Sigma-Aldrich) dissolved in Ska complex dialysis buffer (20 mM Tris pH 7.4, 100 mM NaCl, 1 mM DTT, and 10% glycerol) or Ska complex dialysis buffer without BSA for 30 min at

30°C. Recombinant histone H3.1 (2 μg, New England Biolabs), ATP (10 μM), and γ-^{32}P-ATP (5 μCi) were added to a final volume of 30 μl to start the kinase reactions. Reactions were stopped after 0, 20, 60, 120, and 240 s incubation time at 30°C by addition of 7.5 μl 5× Laemmli buffer and heating to 95°C. The first time point was pipetted on ice. The kinase assay shown in Figure 29 was performed as described above with the exception that anti-MBP antibodies (0.25 μM, New England Biolabs, E8032) were included during the pre-incubation step and the assay was stopped at a single time-point after 240 s. The time-course *in vitro* kinase assay shown in Figure 28C was performed essentially as described above in absence of MBP-INCENP$^{790-918}$-His_6 and recombinant histone H3.1. For the end-point autophosphorylation kinase assays shown in Figure 28A and 26E either the Ska complex, histone H3, or BSA at the indicated amounts was pre-incubated for 30 min at 30°C with Aurora B-His_6 in kinase buffer A before addition of ATP (10 μM) and γ-^{32}P-ATP (5 μCi) and reactions were stopped after 30 min at 30°C by addition of 5× Laemmli buffer and heating to 95°C. The end-point autophosphorylation kinase assays with Plk1 and Mps1 shown in 28E were performed as described above with the exception that kinase buffer B (20 mM Tris pH 7.4, 50 mM NaCl, 2 mM DTT, 10 mM $MgCl_2$) was used. For the control assay shown in Figure 26F, Histone H3 was incubated with Ska complex dialysis buffer, Ska complex (1 μM), or Ska complex and ZM447439 (1 μM and 10 μM, respectively) in kinase buffer A for 30 min at 30°C in the presence of γ-^{32}P-ATP (5 μCi). Kinase reactions were separated by SDS-PAGE, transferred to PVDF membranes or stained with Coomassie Brilliant Blue, and ^{32}P incorporation was determined by autoradiography and densitometric analysis of the bands using the gel

analyzer tool in Image J. Curve fittings and statistical analyses were done with Prism software (GraphPad).

Plk1 and Mps1 kinase assays on peptide spots were performed as previously described (Santamaria et al., 2011). Peptide arrays were synthesized on nitrocellulose membranes (Intavis) using standard Fmoc (*N*-(fluorenyl-9-methoxycarbonyl) chemistry on a MultiPep robotic spotter according to the manufacturer's instructions (Intavis).

Immunoprecipitation and *in vitro* binding assays

HeLa S3 cells were synchronized with STLC (10 μM) for 16–18 h. Mitotic cells were collected by shake-off and lysed for 20 min at 4°C in IP buffer (20 mM Tris pH 7.4, 0.5% Triton-X-100, 150 mM NaCl, 5 mM $MgCl_2$, 2 mM EGTA, 1 mM DTT, protease and phosphatase inhibitor cocktail) supplemented with 30 μg/ml DNAse and 30 μg/ml RNAse. Cell extracts were cleared at 20'000 × g for 30 min at 4°C. The supernatants (1–2 mg total protein) were incubated 2–3 h at 4°C with 3 μg of anti-Ska1 (Hanisch et al., 2006), 1.5 μg anti-Aurora B (AIM-1, BD Transductions, 611083, clone 6) or equivalent amounts of control IgG antibodies, followed by another 1 h incubation with protein G sepharose beads (GE Healthcare). Alternatively, cell extracts were incubated 3–4 h with chemically cross-linked anti-INCENP (Millipore, clone 58-217) or control IgG protein G sepharose beads. The beads were washed five times with IP buffer and boiled in 2× Laemmli buffer.

For *in vitro* binding assays, recombinant Ska complex (50 nM) was incubated for 1 h at 30°C with Aurora B-His_6 (100 nM) in binding buffer (20 mM Tris pH 7.4, 100 mM KCl, 10 mM $MgCl_2$, 1 mM DTT, 1% triton-X100 and 10% glycerol) before pull-

down with chemically cross-linked anti-Ska1 (Hanisch et al., 2006) or IgG protein G sepharose beads for 2 h at 4°C. Beads were washed five times with PBS and boiled in 2× Laemmli buffer.

Western blotting

Cells were synchronized in mitosis with STLC (10 μM) for 12–16 h and harvested by shake-off. Cells were lysed in extraction buffer (20 mM Tris pH 7.4, 0.5% Triton-X-100, 150 mM NaCl, 5 mM $MgCl_2$, 2 mM EGTA, 1 mM DTT, 30 μg/ml DNAse and 30 μg/ml RNAse, protease and phosphatase inhibitor cocktail) or boiled and sonicated in nuclear lysis buffer (20 mM Tris pH 8, 10 mM EDTA, 2% SDS). Cell lysates were resolved by SDS-PAGE and transferred to PVDF membranes. The following antibodies were used for Western blotting: mouse anti-Aurora B (1:500, AIM-1, BD Transductions, 611083, clone 6), mouse anti-His_4 (1:200, Qiagen, 34670), rabbit anti-MCAK (1:1000, generated by Zhen Dou against His-$MCAK^{588-725}$), mouse anti-MBP (1:10,000, NEB, E8032), rabbit anti-Ska1 and anti-Ska2 (1:1000) (Hanisch et al., 2006), rabbit anti-Ska3 (1:1000) (Gaitanos et al., 2009), rabbit anti-Survivin (1:1000, NB500-201, Novus Biological), and mouse anti–α-tubulin (1:3000, Sigma-Aldrich, T6199, clone DM1A).

Monoclonal antibody production

Novel monoclonal antibodies against Ska3 were generated by Anna Santamaria in conjunction with Moravian-Biotechnology (Czech Republic). The antibodies (IgG_1) were produced against His-tagged full-length human Ska complex reconstituted from *E.coli* as previously described (Gaitanos et al., 2009; Chan et al., 2012). Repeated

intraperitoneal injections of 10–50 μg of antigen into Balb/c mice were performed using Freund's adjuvants. Splenocytes where fused with SP2 myeloma cells. Supernatant screening was performed by ELISA.

Abbreviations

ACA	Anti-centromere-antibody
APC/C	Anaphase-promoting complex/cyclosome
ATP	Adenosine triphosphate
AurB	Aurora B
BSA	Bovine serum albumine
C-terminal	Carboxy-terminal
CATD	CENP-A targeting domain
CBB	Coomassie brilliant blue
CB^{DBD}	CENP-B DNA binding domain
CCAN	Constitutive centromere-associated network
CDE	Conserved DNA element
CEN	Centromere
CHR	Chromosome
CI	Confidence interval
CIN	Chromosome instability
CPC	Chromosomal passenger complex
DMEM	Dulbecco's modified eagle medium
DMSO	Dimethylsulfoxide
DNA	Deoxyribonucleic acid
DTT	Dithiothreitol
EDTA	Ethylene diamine tetraacetic acid
EGFP	Enhanced green fluorescent protein
EGTA	Ethylene glycol tetraacetic acid
EM	Electron microscopy
FCS	Fetal calf serum
FITC	Fluorescein isothiocyanate
fm	fibrous mat
FRET	Fluorescence resonance energy transfer
GFP	Green fluorescent protein
GTP	Guanosine triphosphate
H2B	Histone H2B
H3	Histone H3
H3-pS10	Histone H3 phospho-serine 10
H3-pS28	Histone H3 phospho-serine 28
H3-pT3	Histone H3 phospho-threonine 3
HEPES	4-(2-hydroxyethyl)-1-piperazineethanesulfonic acid
His	6× Histidine tag
HPF/FS	High-pressure freezing/freeze substitution
IgG	Immunoglobulin G
Int.	Intensity
IP	Immunoprecipitation
K-fiber	Kinetochore fiber
KMN	KNL-1-Mis12-Ndc80
KT	Kinetochore
KT-MT	Kinetochore-microtubule

LAP	Localization and affinity purification tag (GFP-protein S tag)
MAPs	Microtubule-associated proteins
MBP	Maltose-binding protein tag
MCC	Mitotic checkpoint complex
M_r	Relative molecular mass
mRFP	Monomeric red fluorescent protein
MT	Microtubule
MTBD	Microtubule-binding domain
NEBD	Nuclear envelope breakdown
NES	Nuclear export signal
ns	Non-significant
OA	Okadaic acid
PA	Photoactivation
PBS	Phosphate-buffered saline
PIPES	Piperazine-N,N′-bis(2-ethanesulfonic acid)
Ponc. S	Ponceau S
proTAME	Pro-tosyl-L-arginine methyl ester
PVDF	Polyvinylidene fluoride
Rel.	Relative
RNAi	Ribonucleic acid interference
RZZ	Rod-Zw10-Zwilch
SAC	Spindle assembly checkpoint
SD	Standard deviation
SDS	Sodium dodecylsulfate
SDS-PAGE	Sodium dodecylsulfate polyacrylamid gel electrophoresis
SEM	Standard error of the mean
siRNA	Small interfering ribonucleic acid
STLC	S-trityl-L-cysteine
Tris	Tris(hydroxymethyl)aminomethane
WB	Western blot
WT	Wild-type
ZM	ZM447439

References

Abad, M.A., B. Medina, A. Santamaria, J. Zou, C. Plasberg-Hill, A. Madhumalar, U. Jayachandran, P.M. Redli, J. Rappsilber, E.A. Nigg, and A.A. Jeyaprakash. 2014. Structural basis for microtubule recognition by the human kinetochore Ska complex. *Nat Comms*. 5:1–26. doi:10.1038/ncomms3964.

Akhmanova, A., and M.O. Steinmetz. 2008. Tracking the ends: a dynamic protein network controls the fate of microtubule tips. *Nat Rev Mol Cell Biol*. 9:309–322. doi:10.1038/nrm2369.

Amaro, A.C., C.P. Samora, R. Holtackers, E. Wang, I.J. Kingston, M. Alonso, M. Lampson, A.D. McAinsh, and P. Meraldi. 2010. Molecular control of kinetochore-microtubule dynamics and chromosome oscillations. *Nat Cell Biol*. 12:319–329. doi:10.1038/ncb2033.

Amor, D.J., K. Bentley, J. Ryan, J. Perry, L. Wong, H. Slater, and K.H.A. Choo. 2004. Human centromere repositioning "in progress". *Proceedings of the National Academy of Sciences*. 101:6542–6547. doi:10.1073/pnas.0308637101.

Andrews, P.D., Y. Ovechkina, N. Morrice, M. Wagenbach, K. Duncan, L. Wordeman, and J.R. Swedlow. 2004. Aurora B regulates MCAK at the mitotic centromere. *Dev. Cell*. 6:253–268.

Aravamudhan, P., A.A. Goldfarb, and A.P. Joglekar. 2015. The kinetochore encodes a mechanical switch to disrupt spindle assembly checkpoint signalling. *Nat Cell Biol*. 17:868–879. doi:10.1038/ncb3179.

Auckland, P., and A.D. McAinsh. 2015. Building an integrated model of chromosome congression. *Journal of Cell Science*. 128:3363–3374. doi:10.1242/jcs.169367.

Bakhoum, S.F., and D.A. Compton. 2012. Kinetochores and disease: keeping microtubule dynamics in check! *Current Opinion in Cell Biology*. 1–7. doi:10.1016/j.ceb.2011.11.012.

Bakhoum, S.F., G. Genovese, and D.A. Compton. 2009. Deviant Kinetochore Microtubule Dynamics Underlie Chromosomal Instability. *Current Biology*. 19:1937–1942. doi:10.1016/j.cub.2009.09.055.

Bakhoum, S.F., S.L. Thompson, A.L. Manning, and D.A. Compton. 2008. Genome stability is ensured by temporal control of kinetochore–microtubule dynamics. *Nat Cell Biol*. 11:27–35. doi:10.1038/ncb1809.

Banerjee, B., C.A. Kestner, and P.T. Stukenberg. 2014. EB1 enables spindle microtubules to regulate centromeric recruitment of Aurora B. *The Journal of Cell Biology*. 204:947–963. doi:10.1083/jcb.201307119.

Barisic, M., P. Aguiar, S. Geley, and H. Maiato. 2014. Kinetochore motors drive congression of peripheral polar chromosomes by overcoming random arm-

ejection forces. *Nature Publishing Group*. 16:1249–1256. doi:10.1038/ncb3060.

Barnhart, M.C., P.H.J.L. Kuich, M.E. Stellfox, J.A. Ward, E.A. Bassett, B.E. Black, and D.R. Foltz. 2011. HJURP is a CENP-A chromatin assembly factor sufficient to form a functional de novo kinetochore. *The Journal of Cell Biology*. 194:229–243. doi:10.1083/jcb.201012017.

Bayliss, R., T. Sardon, I. Vernos, and E. Conti. 2003. Structural Basis of Aurora-A Activation by TPX2 at the Mitotic Spindle. *Molecular Cell*. 12:851–862. doi:10.1016/S1097-2765(03)00392-7.

Bekier, M.E., T. Mazur, M.S. Rashid, and W.R. Taylor. 2015. Borealin dimerization mediates optimal CPC checkpoint function by enhancing localization to centromeres and kinetochores. *Nat Comms*. 6:6775. doi:10.1038/ncomms7775.

Black, B.E., L.E.T. Jansen, D.R. Foltz, and D.W. Cleveland. 2010. Centromere identity, function, and epigenetic propagation across cell divisions. *Cold Spring Harbor Symposia on Quantitative Biology*. 75:403–418. doi:10.1101/sqb.2010.75.038.

Black, B.E., L.E.T. Jansen, P.S. Maddox, D.R. Foltz, A.B. Desai, J.V. Shah, and D.W. Cleveland. 2007. Centromere identity maintained by nucleosomes assembled with histone H3 containing the CENP-A targeting domain. *Molecular Cell*. 25:309–322. doi:10.1016/j.molcel.2006.12.018.

Brinkley, B.R., and E. Stubblefield. 1966. The fine structure of the kinetochore of a mammalian cell in vitro. *Chromosoma*. 19:28–43.

Brouhard, G.J., and L.M. Rice. 2014. The contribution of -tubulin curvature to microtubule dynamics. *The Journal of Cell Biology*. 207:323–334. doi:10.1083/jcb.201407095.

Buster, D.W., D. Zhang, and D.J. Sharp. 2007. Poleward tubulin flux in spindles: regulation and function in mitotic cells. *Molecular Biology of the Cell*. 18:3094–3104. doi:10.1091/mbc.E06-11-0994.

Caldas, G.V., K.F. DeLuca, and J.G. DeLuca. 2013. KNL1 facilitates phosphorylation of outer kinetochore proteins by promoting Aurora B kinase activity. *The Journal of Cell Biology*. 203:957–969. doi:10.1083/jcb.201306054.

Campbell, C.S., and A. Desai. 2013. Tension sensing by Aurora B kinase is independent of survivin-based centromere localization. *Nature*. 497:118–121. doi:10.1038/nature12057.

Carmena, M., M. Wheelock, H. Funabiki, and W.C. Earnshaw. 2012. The chromosomal passenger complex (CPC): from easy rider to the godfather of mitosis. *Nat Rev Mol Cell Biol*. 13:789–803. doi:10.1038/nrm3474.

Carretero, M., M. Ruiz-Torres, M. Rodríguez-Corsino, I. Barthelemy, and A. Losada. 2013. Pds5B is required for cohesion establishment and Aurora B accumulation

at centromeres. *EMBO J*. 32:2938–2949. doi:10.1038/emboj.2013.230.

Carroll, C.W., K.J. Milks, and A.F. Straight. 2010. Dual recognition of CENP-A nucleosomes is required for centromere assembly. *The Journal of Cell Biology*. 189:1143–1155. doi:10.1083/jcb.201001013.

Cassimeris, L., C.L. Rieder, G. Rupp, and E.D. Salmon. 1990. Stability of microtubule attachment to metaphase kinetochores in PtK1 cells. *Journal of Cell Science*. 96 (Pt 1):9–15.

Chan, Y.W., A.A. Jeyaprakash, E.A. Nigg, and A. Santamaria. 2012. Aurora B controls kinetochore-microtubule attachments by inhibiting Ska complex-KMN network interaction. *The Journal of Cell Biology*. 196:563–571. doi:10.1083/jcb.201109001.

Cheeseman, I.M. 2014. The kinetochore. *Cold Spring Harbor Perspectives in Biology*. 6:a015826–a015826. doi:10.1101/cshperspect.a015826.

Cheeseman, I.M., and A. Desai. 2008. Molecular architecture of the kinetochore–microtubule interface. *Nat Rev Mol Cell Biol*. 9:33–46. doi:10.1038/nrm2310.

Cheeseman, I.M., J.S. Chappie, E.M. Wilson-Kubalek, and A. Desai. 2006. The conserved KMN network constitutes the core microtubule-binding site of the kinetochore. *Cell*. 127:983–997. doi:10.1016/j.cell.2006.09.039.

Cimini, D. 2003. Merotelic kinetochore orientation occurs frequently during early mitosis in mammalian tissue cells and error correction is achieved by two different mechanisms. *Journal of Cell Science*. 116:4213–4225. doi:10.1242/jcs.00716.

Cimini, D. 2008. Merotelic kinetochore orientation, aneuploidy, and cancer. *Biochim. Biophys. Acta*. 1786:32–40. doi:10.1016/j.bbcan.2008.05.003.

Cimini, D., B. Howell, P. Maddox, A. Khodjakov, F. Degrassi, and E.D. Salmon. 2001. Merotelic kinetochore orientation is a major mechanism of aneuploidy in mitotic mammalian tissue cells. *The Journal of Cell Biology*. 153:517–527.

Cimini, D., D. Fioravanti, E.D. Salmon, and F. Degrassi. 2002. Merotelic kinetochore orientation versus chromosome mono-orientation in the origin of lagging chromosomes in human primary cells. *Journal of Cell Science*. 115:507–515.

Cimini, D., L.A. Cameron, and E.D. Salmon. 2004. Anaphase spindle mechanics prevent mis-segregation of merotelically oriented chromosomes. *Current Biology*. 14:2149–2155. doi:10.1016/j.cub.2004.11.029.

Cimini, D., X. Wan, C.B. Hirel, and E.D. Salmon. 2006. Aurora Kinase Promotes Turnover of Kinetochore Microtubules to Reduce Chromosome Segregation Errors. *Current Biology*. 16:1711–1718. doi:10.1016/j.cub.2006.07.022.

Collin, P., O. Nashchekina, R. Walker, and J. Pines. 2013. The spindle assembly

checkpoint works like a rheostat rather than a toggle switch. *Nat Cell Biol*. 15:1378–1385. doi:10.1038/ncb2855.

Collins, K.A., S. Furuyama, and S. Biggins. 2004. Proteolysis contributes to the exclusive centromere localization of the yeast Cse4/CENP-A histone H3 variant. *Current Biology*. 14:1968–1972. doi:10.1016/j.cub.2004.10.024.

Conde e Silva, N., B.E. Black, A. Sivolob, J. Filipski, D.W. Cleveland, and A. Prunell. 2007. CENP-A-containing nucleosomes: easier disassembly versus exclusive centromeric localization. *J. Mol. Biol.* 370:555–573. doi:10.1016/j.jmb.2007.04.064.

Coudreuse, D., and P. Nurse. 2010. Driving the cell cycle with a minimal CDK control network. *Nature*. 468:1074–1079. doi:10.1038/nature09543.

Crasta, K., N.J. Ganem, R. Dagher, A.B. Lantermann, E.V. Ivanova, Y. Pan, L. Nezi, A. Protopopov, D. Chowdhury, and D. Pellman. 2012. DNA breaks and chromosome pulverization from errors in mitosis. *Nature*. 482:53–58. doi:10.1038/nature10802.

Daum, J.R., J.D. Wren, J.J. Daniel, S. Sivakumar, J.N. McAvoy, T.A. Potapova, and G.J. Gorbsky. 2009. Ska3 Is Required for Spindle Checkpoint Silencing and the Maintenance of Chromosome Cohesion in Mitosis. *Current Biology*. 19:1467–1472. doi:10.1016/j.cub.2009.07.017.

Daum, J.R., T.A. Potapova, S. Sivakumar, J.J. Daniel, J.N. Flynn, S. Rankin, and G.J. Gorbsky. 2011. Cohesion Fatigue Induces Chromatid Separation in Cells Delayed at Metaphase. *Current Biology*. 21:1018–1024. doi:10.1016/j.cub.2011.05.032.

De Antoni, A., C.G. Pearson, D. Cimini, J.C. Canman, V. Sala, L. Nezi, M. Mapelli, L. Sironi, M. Faretta, E.D. Salmon, and A. Musacchio. 2005. The Mad1/Mad2 complex as a template for Mad2 activation in the spindle assembly checkpoint. *Current Biology*. 15:214–225. doi:10.1016/j.cub.2005.01.038.

De Antoni, A., S. Maffini, S. Knapp, A. Musacchio, and S. Santaguida. 2012. A small-molecule inhibitor of Haspin alters the kinetochore functions of Aurora B. *The Journal of Cell Biology*. 199:269–284. doi:10.1083/jcb.201205119.

De Rop, V., A. Padeganeh, and P.S. Maddox. 2012. CENP-A: the key player behind centromere identity, propagation, and kinetochore assembly. *Chromosoma*. 121:527–538. doi:10.1007/s00412-012-0386-5.

DeLuca, J.G., W.E. Gall, C. Ciferri, D. Cimini, A. Musacchio, and E.D. Salmon. 2006. Kinetochore Microtubule Dynamics and Attachment Stability Are Regulated by Hec1. *Cell*. 127:969–982. doi:10.1016/j.cell.2006.09.047.

DeLuca, K.F., S.M.A. Lens, and J.G. DeLuca. 2011. Temporal changes in Hec1 phosphorylation control kinetochore-microtubule attachment stability during mitosis. *Journal of Cell Science*. 124:622–634. doi:10.1242/jcs.072629.

Dephoure, N., C. Zhou, J. Villén, S.A. Beausoleil, C.E. Bakalarski, S.J. Elledge, and S.P. Gygi. 2008. A quantitative atlas of mitotic phosphorylation. *Proc. Natl. Acad. Sci. U.S.A.* 105:10762–10767. doi:10.1073/pnas.0805139105.

Desai, A., and T.J. Mitchison. 1997. MICROTUBULE POLYMERIZATION DYNAMICS. *Annu. Rev. Cell Dev. Biol.* 13:83–117. doi:10.1146/annurev.cellbio.13.1.83.

Ditchfield, C. 2003. Aurora B couples chromosome alignment with anaphase by targeting BubR1, Mad2, and Cenp-E to kinetochores. *The Journal of Cell Biology*. 161:267–280. doi:10.1083/jcb.200208091.

Domnitz, S.B., M. Wagenbach, J. Decarreau, and L. Wordeman. 2012. MCAK activity at microtubule tips regulates spindle microtubule length to promote robust kinetochore attachment. *The Journal of Cell Biology*. 197:231–237. doi:10.1083/jcb.201108147.

Dong, Y., K.J. Vanden Beldt, X. Meng, A. Khodjakov, and B.F. McEwen. 2007. The outer plate in vertebrate kinetochores is a flexible network with multiple microtubule interactions. *Nat Cell Biol*. 9:516–522. doi:10.1038/ncb1576.

Dou, Z., C. von Schubert, R. Körner, A. Santamaria, S. Elowe, and E.A. Nigg. 2011. Quantitative mass spectrometry analysis reveals similar substrate consensus motif for human Mps1 kinase and Plk1. *PLoS ONE*. 6:e18793. doi:10.1371/journal.pone.0018793.

Elkins, J.M., S. Santaguida, A. Musacchio, and S. Knapp. 2012. Crystal Structure of Human Aurora B in Complex with INCENP and VX-680. *J. Med. Chem.* 55:7841–7848. doi:10.1021/jm3008954.

Etemad, B., T.E.F. Kuijt, and G.J.P.L. Kops. 2015. Kinetochore–microtubule attachment is sufficient to satisfy the human spindle assembly checkpoint. *Nat Comms*. 6:1–8. doi:10.1038/ncomms9987.

Evan, G.I., G.K. Lewis, G. Ramsay, and J.M. Bishop. 1985. Isolation of monoclonal antibodies specific for human c-myc proto-oncogene product. *Mol. Cell. Biol.* 5:3610–3616.

Eytan, E., K. Wang, S. Miniowitz-Shemtov, D. Sitry-Shevah, S. Kaisari, T.J. Yen, S.-T. Liu, and A. Hershko. 2014. Disassembly of mitotic checkpoint complexes by the joint action of the AAA-ATPase TRIP13 and p31(comet). *Proc. Natl. Acad. Sci. U.S.A.* 111:12019–12024. doi:10.1073/pnas.1412901111.

Flemming, W. 1882. Zellsubstanz, Kern und Zelltheilung. Verlag Vogel, Leipzig.

Foley, E.A., and T.M. Kapoor. 2013. Microtubule attachment and spindle assembly checkpoint signalling at the kinetochore. *Nat Rev Mol Cell Biol*. 14:25–37. doi:10.1038/nrm3494.

Foley, E.A., M. Maldonado, and T.M. Kapoor. 2011. Formation of stable attachments

between kinetochores and microtubules depends on the B56-PP2A phosphatase. *Nat Cell Biol*. 13:1265–1271. doi:10.1038/ncb2327.

Foltz, D.R., L.E.T. Jansen, A.O. Bailey, J.R. Yates, E.A. Bassett, S. Wood, B.E. Black, and D.W. Cleveland. 2009. Centromere-specific assembly of CENP-a nucleosomes is mediated by HJURP. *Cell*. 137:472–484. doi:10.1016/j.cell.2009.02.039.

Fu, J., M. Bian, G. Xin, Z. Deng, J. Luo, X. Guo, H. Chen, Y. Wang, Q. Jiang, and C. Zhang. 2015. TPX2 phosphorylation maintains metaphase spindle length by regulating microtubule flux. *The Journal of Cell Biology*. 210:373–383. doi:10.1083/jcb.201412109.

Fujita, Y., T. Hayashi, T. Kiyomitsu, Y. Toyoda, A. Kokubu, C. Obuse, and M. Yanagida. 2007. Priming of centromere for CENP-A recruitment by human hMis18alpha, hMis18beta, and M18BP1. *Dev. Cell*. 12:17–30. doi:10.1016/j.devcel.2006.11.002.

Fuller, B.G., M.A. Lampson, E.A. Foley, S. Rosasco-Nitcher, K.V. Le, P. Tobelmann, D.L. Brautigan, P.T. Stukenberg, and T.M. Kapoor. 2008. Midzone activation of aurora B in anaphase produces an intracellular phosphorylation gradient. *Nature*. 453:1132–1136. doi:10.1038/nature06923.

Furuyama, S., and S. Biggins. 2007. Centromere identity is specified by a single centromeric nucleosome in budding yeast. *Proceedings of the National Academy of Sciences*. 104:14706–14711. doi:10.1073/pnas.0706985104.

Gaitanos, T.N., A. Santamaria, A.A. Jeyaprakash, B. Wang, E. Conti, and E.A. Nigg. 2009. Stable kinetochore–microtubule interactions depend on the Ska complex and its new component Ska3/C13Orf3. *EMBO J*. 28:1442–1452. doi:10.1038/emboj.2009.96.

Ganem, N.J., S.A. Godinho, and D. Pellman. 2009. A mechanism linking extra centrosomes to chromosomal instability. *Nature*. 460:278–282. doi:10.1038/nature08136.

Gascoigne, K.E., and I.M. Cheeseman. 2011. Kinetochore assembly: if you build it, they will come. *Current Opinion in Cell Biology*. 23:102–108. doi:10.1016/j.ceb.2010.07.007.

Gascoigne, K.E., and I.M. Cheeseman. 2013. CDK-dependent phosphorylation and nuclear exclusion coordinately control kinetochore assembly state. *The Journal of Cell Biology*. 201:23–32. doi:10.1083/jcb.201301006.

Gascoigne, K.E., K. Takeuchi, A. Suzuki, T. Hori, T. Fukagawa, and I.M. Cheeseman. 2011. Induced Ectopic Kinetochore Assembly Bypasses the Requirement for CENP-A Nucleosomes. *Cell*. 145:410–422. doi:10.1016/j.cell.2011.03.031.

Gisselsson, D. 2008. Classification of chromosome segregation errors in cancer. *Chromosoma*. 117:511–519. doi:10.1007/s00412-008-0169-1.

Godek, K.M., L. Kabeche, and D.A. Compton. 2014. Regulation of kinetochore–microtubule attachments through homeostatic control during mitosis. *Nat Rev Mol Cell Biol*. 16:57–64. doi:10.1038/nrm3916.

Goshima, G., F. Nédélec, and R.D. Vale. 2005. Mechanisms for focusing mitotic spindle poles by minus end-directed motor proteins. *The Journal of Cell Biology*. 171:229–240. doi:10.1083/jcb.200505107.

Goto, H., Y. Yasui, E.A. Nigg, and M. Inagaki. 2002. Aurora-B phosphorylates Histone H3 at serine28 with regard to the mitotic chromosome condensation. *Genes Cells*. 7:11–17.

Hagan, R.S., M.S. Manak, H.K. Buch, M.G. Meier, P. Meraldi, J.V. Shah, and P.K. Sorger. 2011. p31(comet) acts to ensure timely spindle checkpoint silencing subsequent to kinetochore attachment. *Molecular Biology of the Cell*. 22:4236–4246. doi:10.1091/mbc.E11-03-0216.

Han, Z., G.M. Riefler, J.R. Saam, S.E. Mango, and J.M. Schumacher. 2005. The C. elegans Tousled-like Kinase Contributes to Chromosome Segregation as a Substrate and Regulator of the Aurora B Kinase. *Current Biology*. 15:894–904. doi:10.1016/j.cub.2005.04.019.

Hanisch, A., H.H.W. Silljé, and E.A. Nigg. 2006. Timely anaphase onset requires a novel spindle and kinetochore complex comprising Ska1 and Ska2. *EMBO J*. 25:5504–5515. doi:10.1038/sj.emboj.7601426.

Hardwick, K.G., R.C. Johnston, D.L. Smith, and A.W. Murray. 2000. MAD3 encodes a novel component of the spindle checkpoint which interacts with Bub3p, Cdc20p, and Mad2p. *The Journal of Cell Biology*. 148:871–882. doi:10.1083/jcb.148.5.871.

Hartwell, L.H., and M.B. Kastan. 1994. Cell cycle control and cancer. *Science*. 266:1821–1828. doi:10.1126/science.7997877.

Hauf, S., R.W. Cole, S. LaTerra, C. Zimmer, G. Schnapp, R. Walter, A. Heckel, J. van Meel, C.L. Rieder, and J.-M. Peters. 2003. The small molecule Hesperadin reveals a role for Aurora B in correcting kinetochore-microtubule attachment and in maintaining the spindle assembly checkpoint. *The Journal of Cell Biology*. 161:281–294. doi:10.1083/jcb.200208092.

Hayashi, T., Y. Fujita, O. Iwasaki, Y. Adachi, K. Takahashi, and M. Yanagida. 2004. Mis16 and Mis18 are required for CENP-A loading and histone deacetylation at centromeres. *Cell*. 118:715–729. doi:10.1016/j.cell.2004.09.002.

Heald, R., and A. Khodjakov. 2015. Thirty years of search and capture: The complex simplicity of mitotic spindle assembly. *The Journal of Cell Biology*. jcb.201510015–9. doi:10.1083/jcb.201510015.

Heun, P., S. Erhardt, M.D. Blower, S. Weiss, A.D. Skora, and G.H. Karpen. 2006. Mislocalization of the Drosophila centromere-specific histone CID promotes formation of functional ectopic kinetochores. *Dev. Cell*. 10:303–315.

doi:10.1016/j.devcel.2006.01.014.

Hewawasam, G., M. Shivaraju, M. Mattingly, S. Venkatesh, S. Martin-Brown, L. Florens, J.L. Workman, and J.L. Gerton. 2010. Psh1 is an E3 ubiquitin ligase that targets the centromeric histone variant Cse4. *Molecular Cell*. 40:444–454. doi:10.1016/j.molcel.2010.10.014.

Hiruma, Y., C. Sacristan, S.T. Pachis, A. Adamopoulos, T. Kuijt, M. Ubbink, E. von Castelmur, A. Perrakis, and G.J.P.L. Kops. 2015. CELL DIVISION CYCLE. Competition between MPS1 and microtubules at kinetochores regulates spindle checkpoint signaling. *Science*. 348:1264–1267. doi:10.1126/science.aaa4055.

Hochegger, H., S. Takeda, and T. Hunt. 2008. Cyclin-dependent kinases and cell-cycle transitions: does one fit all? *Nat Rev Mol Cell Biol*. 9:910–916. doi:10.1038/nrm2510.

Honda, R., R. Körner, and E.A. Nigg. 2003. Exploring the functional interactions between Aurora B, INCENP, and survivin in mitosis. *Molecular Biology of the Cell*. 14:3325–3341. doi:10.1091/mbc.E02-11-0769.

Hori, T., M. Amano, A. Suzuki, C.B. Backer, J.P. Welburn, Y. Dong, B.F. McEwen, W.-H. Shang, E. Suzuki, K. Okawa, I.M. Cheeseman, and T. Fukagawa. 2008. CCAN makes multiple contacts with centromeric DNA to provide distinct pathways to the outer kinetochore. *Cell*. 135:1039–1052. doi:10.1016/j.cell.2008.10.019.

Hori, T., W.-H. Shang, K. Takeuchi, and T. Fukagawa. 2013. The CCAN recruits CENP-A to the centromere and forms the structural core for kinetochore assembly. *The Journal of Cell Biology*. 200:45–60. doi:10.1083/jcb.201210106.

Hornbeck, P.V., J.M. Kornhauser, S. Tkachev, B. Zhang, E. Skrzypek, B. Murray, V. Latham, and M. Sullivan. 2012. PhosphoSitePlus: a comprehensive resource for investigating the structure and function of experimentally determined post-translational modifications in man and mouse. *Nucleic Acids Res.* 40:D261–70. doi:10.1093/nar/gkr1122.

Howell, B.J., B.F. McEwen, J.C. Canman, D.B. Hoffman, E.M. Farrar, C.L. Rieder, and E.D. Salmon. 2001. Cytoplasmic dynein/dynactin drives kinetochore protein transport to the spindle poles and has a role in mitotic spindle checkpoint inactivation. *The Journal of Cell Biology*. 155:1159–1172. doi:10.1083/jcb.200105093.

Hoyt, M.A., L. Totis, and B.T. Roberts. 1991. S. cerevisiae genes required for cell cycle arrest in response to loss of microtubule function. *Cell*. 66:507–517.

Hunter, A.W., M. Caplow, D.L. Coy, W.O. Hancock, S. Diez, L. Wordeman, and J. Howard. 2003. The Kinesin-Related Protein MCAK Is a Microtubule Depolymerase that Forms an ATP-Hydrolyzing Complex at Microtubule Ends. *Molecular Cell*. 11:445–457. doi:10.1016/S1097-2765(03)00049-2.

Hutten, S., and R.H. Kehlenbach. 2007. CRM1-mediated nuclear export: to the pore and beyond. *Trends in Cell Biology*. 17:193–201. doi:10.1016/j.tcb.2007.02.003.

Indjeian, V.B., and A.W. Murray. 2007. Budding yeast mitotic chromosomes have an intrinsic bias to biorient on the spindle. *Current Biology*. 17:1837–1846. doi:10.1016/j.cub.2007.09.056.

Izawa, D., and J. Pines. 2015. The mitotic checkpoint complex binds a second CDC20 to inhibit active APC/C. *Nature*. 517:631–634. doi:10.1038/nature13911.

Jansen, L.E.T., B.E. Black, D.R. Foltz, and D.W. Cleveland. 2007. Propagation of centromeric chromatin requires exit from mitosis. *The Journal of Cell Biology*. 176:795–805. doi:10.1083/jcb.200701066.

Janssen, A., M. van der Burg, K. Szuhai, G.J.P.L. Kops, and R.H. Medema. 2011. Chromosome segregation errors as a cause of DNA damage and structural chromosome aberrations. *Science*. 333:1895–1898. doi:10.1126/science.1210214.

Jaqaman, K., E.M. King, A.C. Amaro, J.R. Winter, J.F. Dorn, H.L. Elliott, N. McHedlishvili, S.E. McClelland, I.M. Porter, M. Posch, A. Toso, G. Danuser, A.D. McAinsh, P. Meraldi, and J.R. Swedlow. 2010. Kinetochore alignment within the metaphase plate is regulated by centromere stiffness and microtubule depolymerases. *The Journal of Cell Biology*. 188:665–679. doi:10.1083/jcb.200909005.

Jeyaprakash, A.A., A. Santamaria, U. Jayachandran, Y.W. Chan, C. Benda, E.A. Nigg, and E. Conti. 2012. Structural and Functional Organization of the Ska Complex, a Key Component of the Kinetochore-Microtubule Interface. *Molecular Cell*. 46:274–286. doi:10.1016/j.molcel.2012.03.005.

Ji, Z., H. Gao, and H. Yu. 2015. CELL DIVISION CYCLE. Kinetochore attachment sensed by competitive Mps1 and microtubule binding to Ndc80C. *Science*. 348:1260–1264. doi:10.1126/science.aaa4029.

Jokelainen, P.T. 1967. The ultrastructure and spatial organization of the metaphase kinetochore in mitotic rat cells. *J. Ultrastruct. Res.* 19:19–44.

Kalinina, I., A. Nandi, P. Delivani, M.R. Chacón, A.H. Klemm, D. Ramunno-Johnson, A. Krull, B. Lindner, N. Pavin, and I.M. Tolić-Nørrelykke. 2012. Pivoting of microtubules around the spindle pole accelerates kinetochore capture. *Nat Cell Biol*. 15:82–87. doi:10.1038/ncb2640.

Kallio, M.J., M.L. McCleland, P.T. Stukenberg, and G.J. Gorbsky. 2002. Inhibition of Aurora B Kinase Blocks Chromosome Segregation, Overrides the Spindle Checkpoint, and Perturbs Microtubule Dynamics in Mitosis. *Current Biology*. 12:900–905. doi:10.1016/S0960-9822(02)00887-4.

Kapoor, T.M., M.A. Lampson, P. Hergert, L. Cameron, D. Cimini, E.D. Salmon, B.F. McEwen, and A. Khodjakov. 2006. Chromosomes can congress to the

metaphase plate before biorientation. *Science*. 311:388–391. doi:10.1126/science.1122142.

Kapoor, T.M., T.U. Mayer, M.L. Coughlin, and T.J. Mitchison. 2000. Probing spindle assembly mechanisms with monastrol, a small molecule inhibitor of the mitotic kinesin, Eg5. *The Journal of Cell Biology*. 150:975–988.

Kelly, A.E., and H. Funabiki. 2009. Correcting aberrant kinetochore microtubule attachments: an Aurora B-centric view. *Current Opinion in Cell Biology*. 21:51–58. doi:10.1016/j.ceb.2009.01.004.

Kelly, A.E., C. Ghenoiu, J.Z. Xue, C. Zierhut, H. Kimura, and H. Funabiki. 2010. Survivin Reads Phosphorylated Histone H3 Threonine 3 to Activate the Mitotic Kinase Aurora B. *Science*. 330:235–239. doi:10.1126/science.1189505.

Kelly, A.E., S.C. Sampath, T.A. Maniar, E.M. Woo, B.T. Chait, and H. Funabiki. 2007. Chromosomal Enrichment and Activation of the Aurora B Pathway Are Coupled to Spatially Regulate Spindle Assembly. *Dev. Cell*. 12:31–43. doi:10.1016/j.devcel.2006.11.001.

Khodjakov, A., and J. Pines. 2010. Centromere tension: a divisive issue. *Nat Cell Biol*. 12:919–923. doi:10.1038/ncb1010-919.

Khodjakov, A., L. Copenagle, M.B. Gordon, D.A. Compton, and T.M. Kapoor. 2003. Minus-end capture of preformed kinetochore fibers contributes to spindle morphogenesis. *The Journal of Cell Biology*. 160:671–683. doi:10.1083/jcb.200208143.

Kim, S., and H. Yu. 2015. Multiple assembly mechanisms anchor the KMN spindle checkpoint platform at human mitotic kinetochores. *The Journal of Cell Biology*. 208:181–196. doi:10.1083/jcb.201407074.

King, J.M., and R.B. Nicklas. 2000. Tension on chromosomes increases the number of kinetochore microtubules but only within limits. *Journal of Cell Science*. 113 Pt 21:3815–3823.

Kirschner, M., and T. Mitchison. 1986. Beyond self-assembly: from microtubules to morphogenesis. *Cell*. 45:329–342.

Kiyomitsu, T., C. Obuse, and M. Yanagida. 2007. Human Blinkin/AF15q14 is required for chromosome alignment and the mitotic checkpoint through direct interaction with Bub1 and BubR1. *Dev. Cell*. 13:663–676. doi:10.1016/j.devcel.2007.09.005.

Klein, U.R., E.A. Nigg, and U. Gruneberg. 2006. Centromere targeting of the chromosomal passenger complex requires a ternary subcomplex of Borealin, Survivin, and the N-terminal domain of INCENP. *Molecular Biology of the Cell*. 17:2547–2558. doi:10.1091/mbc.E05-12-1133.

Kline-Smith, S.L. 2003. Depletion of Centromeric MCAK Leads to Chromosome Congression and Segregation Defects Due to Improper Kinetochore Attachments.

Molecular Biology of the Cell. 15:1146–1159. doi:10.1091/mbc.E03-08-0581.

Kline-Smith, S.L., and C.E. Walczak. 2004. Mitotic Spindle Assembly and Chromosome Segregation. *Molecular Cell*. 15:317–327. doi:10.1016/j.molcel.2004.07.012.

Kops, G.J.P.L., A.T. Saurin, and P. Meraldi. 2010. Finding the middle ground: how kinetochores power chromosome congression. *Cell. Mol. Life Sci.* 67:2145–2161. doi:10.1007/s00018-010-0321-y.

Krenn, V., and A. Musacchio. 2015. The Aurora B Kinase in Chromosome Bi-Orientation and Spindle Checkpoint Signaling. *Front. Oncol.* 5:473–18. doi:10.3389/fonc.2015.00225.

Kudo, N., N. Matsumori, H. Taoka, D. Fujiwara, E.P. Schreiner, B. Wolff, M. Yoshida, and S. Horinouchi. 1999. Leptomycin B inactivates CRM1/exportin 1 by covalent modification at a cysteine residue in the central conserved region. *Proceedings of the National Academy of Sciences*. 96:9112–9117.

Kufer, T.A. 2002. Human TPX2 is required for targeting Aurora-A kinase to the spindle. *The Journal of Cell Biology*. 158:617–623. doi:10.1083/jcb.200204155.

Lampson, M.A., K. Renduchitala, A. Khodjakov, and T.M. Kapoor. 2004. Correcting improper chromosome–spindle attachments during cell division. *Nat Cell Biol*. 6:6–237. doi:10.1038/ncb1102.

Lan, W., X. Zhang, S.L. Kline-Smith, S.E. Rosasco, G.A. Barrett-Wilt, J. Shabanowitz, D.F. Hunt, C.E. Walczak, and P.T. Stukenberg. 2004. Aurora B Phosphorylates Centromeric MCAK and Regulates Its Localization and Microtubule Depolymerization Activity. *Current Biology*. 14:273–286. doi:10.1016/j.cub.2004.01.055.

Lara-Gonzalez, P., and S.S. Taylor. 2012. Cohesion Fatigue Explains Why Pharmacological Inhibition of the APC/C Induces a Spindle Checkpoint-Dependent Mitotic Arrest. *PLoS ONE*. 7:e49041–14. doi:10.1371/journal.pone.0049041.

Li, R., and A.W. Murray. 1991. Feedback control of mitosis in budding yeast. *Cell*. 66:519–531.

Liu, D., G. Vader, M.J.M. Vromans, M.A. Lampson, and S.M.A. Lens. 2009. Sensing chromosome bi-orientation by spatial separation of aurora B kinase from kinetochore substrates. *Science*. 323:1350–1353. doi:10.1126/science.1167000.

Liu, D., M. Vleugel, C.B. Backer, T. Hori, T. Fukagawa, I.M. Cheeseman, and M.A. Lampson. 2010. Regulated targeting of protein phosphatase 1 to the outer kinetochore by KNL1 opposes Aurora B kinase. *The Journal of Cell Biology*. 188:809–820. doi:10.1083/jcb.201001006.

Liu, D., O. Davydenko, and M.A. Lampson. 2012. Polo-like kinase-1 regulates

kinetochore-microtubule dynamics and spindle checkpoint silencing. *The Journal of Cell Biology*. 198:491–499. doi:10.1083/jcb.201205090.

Liu, S.-T., J.B. Rattner, S.A. Jablonski, and T.J. Yen. 2006. Mapping the assembly pathways that specify formation of the trilaminar kinetochore plates in human cells. *The Journal of Cell Biology*. 175:41–53. doi:10.1083/jcb.200606020.

Lončarek, J., O. Kisurina-Evgenieva, T. Vinogradova, P. Hergert, S. La Terra, T.M. Kapoor, and A. Khodjakov. 2007. The centromere geometry essential for keeping mitosis error free is controlled by spindle forces. *Nature*. 450:745–749. doi:10.1038/nature06344.

Luo, X., and H. Yu. 2008. Protein metamorphosis: the two-state behavior of Mad2. *Structure*. 16:1616–1625. doi:10.1016/j.str.2008.10.002.

Maddox, P.S., F. Hyndman, J. Monen, K. Oegema, and A. Desai. 2007. Functional genomics identifies a Myb domain-containing protein family required for assembly of CENP-A chromatin. *The Journal of Cell Biology*. 176:757–763. doi:10.1083/jcb.200701065.

Maffini, S., A.R.R. Maia, A.L. Manning, Z. Maliga, A.L. Pereira, M. Junqueira, A. Shevchenko, A. Hyman, J.R. Yates III, N. Galjart, D.A. Compton, and H. Maiato. 2009. Motor-Independent Targeting of CLASPs to Kinetochores by CENP-E Promotes Microtubule Turnover and Poleward Flux. *Current Biology*. 19:1566–1572. doi:10.1016/j.cub.2009.07.059.

Magidson, V., C.B. O'Connell, J. Lončarek, R. Paul, A. Mogilner, and A. Khodjakov. 2011. The spatial arrangement of chromosomes during prometaphase facilitates spindle assembly. *Cell*. 146:555–567. doi:10.1016/j.cell.2011.07.012.

Magidson, V., R. Paul, N. Yang, J.G. Ault, C.B. O'Connell, I. Tikhonenko, B.F. McEwen, A. Mogilner, and A. Khodjakov. 2015. Adaptive changes in the kinetochore architecture facilitate proper spindle assembly. *Nat Cell Biol*. 1–21. doi:10.1038/ncb3223.

Maiato, H. 2004. The dynamic kinetochore-microtubule interface. *Journal of Cell Science*. 117:5461–5477. doi:10.1242/jcs.01536.

Maiato, H., C.L. Rieder, and A. Khodjakov. 2004a. Kinetochore-driven formation of kinetochore fibers contributes to spindle assembly during animal mitosis. *The Journal of Cell Biology*. 167:831–840. doi:10.1083/jcb.200407090.

Maiato, H., P. Sampaio, and C.E. Sunkel. 2004b. Microtubule-Associated Proteins and their Essential Roles During Mitosis. *Int. Rev. Cytol.* 1–123.

Maiato, H., P.J. Hergert, S. Moutinho-Pereira, Y. Dong, K.J. VandenBeldt, C.L. Rieder, and B.F. McEwen. 2006. The ultrastructure of the kinetochore and kinetochore fiber in Drosophila somatic cells. *Chromosoma*. 115:469–480. doi:10.1007/s00412-006-0076-2.

Malumbres, M., and M. Barbacid. 2005. Mammalian cyclin-dependent kinases. *Trends Biochem. Sci.* 30:630–641. doi:10.1016/j.tibs.2005.09.005.

Malumbres, M., and M. Barbacid. 2009. Cell cycle, CDKs and cancer: a changing paradigm. *Nat Rev Cancer*. 9:153–166. doi:10.1038/nrc2602.

Mao, Y., A. Abrieu, and D.W. Cleveland. 2003. Activating and Silencing the Mitotic Checkpoint through CENP-E-Dependent Activation/Inactivation of BubR1. *Cell*. 114:87–98.

Mapelli, M., and A. Musacchio. 2007. MAD contortions: conformational dimerization boosts spindle checkpoint signaling. *Curr. Opin. Struct. Biol.* 17:716–725. doi:10.1016/j.sbi.2007.08.011.

Mapelli, M., F.V. Filipp, G. Rancati, L. Massimiliano, L. Nezi, G. Stier, R.S. Hagan, S. Confalonieri, S. Piatti, M. Sattler, and A. Musacchio. 2006. Determinants of conformational dimerization of Mad2 and its inhibition by p31comet. *EMBO J*. 25:1273–1284. doi:10.1038/sj.emboj.7601033.

Mapelli, M., L. Massimiliano, S. Santaguida, and A. Musacchio. 2007. The Mad2 conformational dimer: structure and implications for the spindle assembly checkpoint. *Cell*. 131:730–743. doi:10.1016/j.cell.2007.08.049.

Maresca, T.J., and E.D. Salmon. 2009. Intrakinetochore stretch is associated with changes in kinetochore phosphorylation and spindle assembly checkpoint activity. *The Journal of Cell Biology*. 184:373–381. doi:10.1083/jcb.200808130.

Margolis, R.L., and L. Wilson. 1978. Opposite end assembly and disassembly of microtubules at steady state in vitro. *Cell*. 13:1–8. doi:10.1016/0092-8674(78)90132-0.

Martin-Lluesma, S., V.M. Stucke, and E.A. Nigg. 2002. Role of Hec1 in spindle checkpoint signaling and kinetochore recruitment of Mad1/Mad2. *Science*. 297:2267–2270. doi:10.1126/science.1075596.

Masumoto, H., H. Masukata, Y. Muro, N. Nozaki, and T. Okazaki. 1989. A human centromere antigen (CENP-B) interacts with a short specific sequence in alphoid DNA, a human centromeric satellite. *The Journal of Cell Biology*. 109:1963–1973.

McEwen, B.F., A.B. Heagle, G.O. Cassels, K.F. Buttle, and C.L. Rieder. 1997. Kinetochore fiber maturation in PtK1 cells and its implications for the mechanisms of chromosome congression and anaphase onset. *The Journal of Cell Biology*. 137:1567–1580.

McEwen, B.F., and Y. Dong. 2010. Contrasting models for kinetochore microtubule attachment in mammalian cells. *Cell. Mol. Life Sci.* 67:2163–2172. doi:10.1007/s00018-010-0322-x.

McEwen, B.F., C.E. Hsieh, A.L. Mattheyses, and C.L. Rieder. 1998. A new look at kinetochore structure in vertebrate somatic cells using high-pressure freezing and

freeze substitution. *Chromosoma*. 107:366–375.

McEwen, B.F., G.K. Chan, B. Zubrowski, M.S. Savoian, M.T. Sauer, and T.J. Yen. 2001. CENP-E is essential for reliable bioriented spindle attachment, but chromosome alignment can be achieved via redundant mechanisms in mammalian cells. *Molecular Biology of the Cell*. 12:2776–2789.

McHedlishvili, N., S. Wieser, R. Holtackers, J. Mouysset, M. Belwal, A.C. Amaro, and P. Meraldi. 2012. Kinetochores accelerate centrosome separation to ensure faithful chromosome segregation. *Journal of Cell Science*. 125:906–918. doi:10.1242/jcs.091967.

McIntosh, J.R., E. O'Toole, K. Zhudenkov, M. Morphew, C. Schwartz, F.I. Ataullakhanov, and E.L. Grishchuk. 2013. Conserved and divergent features of kinetochores and spindle microtubule ends from five species. *The Journal of Cell Biology*. 200:459–474. doi:10.1083/jcb.201209154.

McIntosh, J.R., E.L. Grishchuk, M.K. Morphew, A.K. Efremov, K. Zhudenkov, V.A. Volkov, I.M. Cheeseman, A. Desai, D.N. Mastronarde, and F.I. Ataullakhanov. 2008. Fibrils connect microtubule tips with kinetochores: a mechanism to couple tubulin dynamics to chromosome motion. *Cell*. 135:322–333. doi:10.1016/j.cell.2008.08.038.

McKinley, K.L., and I.M. Cheeseman. 2014. Polo-like kinase 1 licenses CENP-A deposition at centromeres. *Cell*. 158:397–411. doi:10.1016/j.cell.2014.06.016.

McKinley, K.L., and I.M. Cheeseman. 2015. The molecular basis for centromere identity and function. *Nature Publishing Group*. 1–14. doi:10.1038/nrm.2015.5.

Melters, D.P., L.V. Paliulis, I.F. Korf, and S.W.L. Chan. 2012. Holocentric chromosomes: convergent evolution, meiotic adaptations, and genomic analysis. *Chromosome Res.* 20:579–593. doi:10.1007/s10577-012-9292-1.

Mendiburo, M.J., J. Padeken, S. Fülöp, A. Schepers, and P. Heun. 2011. Drosophila CENH3 is sufficient for centromere formation. *Science*. 334:686–690. doi:10.1126/science.1206880.

Meunier, S., and I. Vernos. 2015. Acentrosomal Microtubule Assembly in Mitosis: The Where, When, and How. *Trends in Cell Biology*. 1–8. doi:10.1016/j.tcb.2015.09.001.

Mitchison, T., and M. Kirschner. 1984. Dynamic instability of microtubule growth. *Nature*.

Mitchison, T.J. 1989. Polewards microtubule flux in the mitotic spindle: evidence from photoactivation of fluorescence. *The Journal of Cell Biology*. 109:637–652.

Morgan, D.O. 2007. The cell cycle: principles of control.

Muñoz-Barrera, M., and F. Monje-Casas. 2014. Increased Aurora B activity causes

continuous disruption of kinetochore-microtubule attachments and spindle instability. *Proc. Natl. Acad. Sci. U.S.A.* 111:E3996–4005. doi:10.1073/pnas.1408017111.

Murata-Hori, M., and Y.-L. Wang. 2002. The Kinase Activity of Aurora B Is Required for Kinetochore-Microtubule Interactions during Mitosis. *Current Biology*. 12:894–899. doi:10.1016/S0960-9822(02)00848-5.

Musacchio, A. 2015. The Molecular Biology of Spindle Assembly Checkpoint Signaling Dynamics. *Current Biology*. 25:R1002–R1018. doi:10.1016/j.cub.2015.08.051.

Musacchio, A., and E.D. Salmon. 2007. The spindle-assembly checkpoint in space and time. *Nat Rev Mol Cell Biol*. 8:379–393. doi:10.1038/nrm2163.

Nicklas, R.B. 1997. How cells get the right chromosomes. *Science*. 275:632–637. doi:10.1126/science.275.5300.632.

Nicklas, R.B., and S.C. Ward. 1994. Elements of error correction in mitosis: microtubule capture, release, and tension. *The Journal of Cell Biology*. 126:1241–1253.

Nishino, T., K. Takeuchi, K.E. Gascoigne, A. Suzuki, T. Hori, T. Oyama, K. Morikawa, I.M. Cheeseman, and T. Fukagawa. 2012. CENP-T-W-S-X forms a unique centromeric chromatin structure with a histone-like fold. *Cell*. 148:487–501. doi:10.1016/j.cell.2011.11.061.

Nixon, F.M., C. Gutiérrez-Caballero, F.E. Hood, D.G. Booth, I.A. Prior, and S.J. Royle. 2015. The mesh is a network of microtubule connectors that stabilizes individual kinetochore fibers of the mitotic spindle. *eLife*. 4:1937. doi:10.7554/eLife.07635.

Nousiainen, M., H.H.W. Silljé, G. Sauer, E.A. Nigg, and R. Körner. 2006. Phosphoproteome analysis of the human mitotic spindle. *Proceedings of the National Academy of Sciences*. 103:5391–5396. doi:10.1073/pnas.0507066103.

O'Connell, C.B., A. Khodjakov, and B.F. McEwen. 2012. Kinetochore flexibility: creating a dynamic chromosome–spindle interface. *Current Opinion in Cell Biology*. 24:40–47. doi:10.1016/j.ceb.2011.12.008.

Oegema, K., and A.A. Hyman. 2006. Cell division. *WormBook*. 1–40. doi:10.1895/wormbook.1.72.1.

Ohta, S., J.-C. Bukowski-Wills, L. Sanchez-Pulido, F. de L. Alves, L. Wood, Z.A. Chen, M. Platani, L. Fischer, D.F. Hudson, C.P. Ponting, T. Fukagawa, W.C. Earnshaw, and J. Rappsilber. 2010. The Protein Composition of Mitotic Chromosomes Determined Using Multiclassifier Combinatorial Proteomics. *Cell*. 142:810–821. doi:10.1016/j.cell.2010.07.047.

Ohzeki, J.-I., M. Nakano, T. Okada, and H. Masumoto. 2002. CENP-B box is required for de novo centromere chromatin assembly on human alphoid DNA. *The Journal*

of Cell Biology. 159:765–775. doi:10.1083/jcb.200207112.

Pankiv, S., T.H. Clausen, T. Lamark, A. Brech, J.-A. Bruun, H. Outzen, A. Øvervatn, G. Bjørkøy, and T. Johansen. 2007. p62/SQSTM1 binds directly to Atg8/LC3 to facilitate degradation of ubiquitinated protein aggregates by autophagy. *J. Biol. Chem.* 282:24131–24145. doi:10.1074/jbc.M702824200.

Papini, D., L. Langemeyer, M.A. Abad, A. Kerr, I. Samejima, P.A. Eyers, A.A. Jeyaprakash, J.M.G. Higgins, F.A. Barr, and W.C. Earnshaw. 2015. TD-60 links RalA GTPase function to the CPC in mitosis. *Nat Comms*. 6:7678. doi:10.1038/ncomms8678.

Paul, R., R. Wollman, W.T. Silkworth, I.K. Nardi, D. Cimini, and A. Mogilner. 2009. Computer simulations predict that chromosome movements and rotations accelerate mitotic spindle assembly without compromising accuracy. *Proc. Natl. Acad. Sci. U.S.A.* 106:15708–15713. doi:10.1073/pnas.0908261106.

Paweletz, N. 2001. Walther Flemming: pioneer of mitosis research. *Nat Rev Mol Cell Biol*. 2:72–75. doi:10.1038/35048077.

Perpelescu, M., and T. Fukagawa. 2011. The ABCs of CENPs. *Chromosoma*. 120:425–446. doi:10.1007/s00412-011-0330-0.

Petrovic, A., S. Pasqualato, P. Dube, V. Krenn, S. Santaguida, D. Cittaro, S. Monzani, L. Massimiliano, J. Keller, A. Tarricone, A. Maiolica, H. Stark, and A. Musacchio. 2010. The MIS12 complex is a protein interaction hub for outer kinetochore assembly. *The Journal of Cell Biology*. 190:835–852. doi:10.1083/jcb.201002070.

Petsalaki, E., T. Akoumianaki, E.J. Black, D.A.F. Gillespie, and G. Zachos. 2011. Phosphorylation at serine 331 is required for Aurora B activation. *The Journal of Cell Biology*. 195:449–466. doi:10.1083/jcb.201104023.

Posch, M., G.A. Khoudoli, S. Swift, E.M. King, J.G. DeLuca, and J.R. Swedlow. 2010. Sds22 regulates aurora B activity and microtubule-kinetochore interactions at mitosis. *The Journal of Cell Biology*. 191:61–74. doi:10.1083/jcb.200912046.

Raaijmakers, J.A., M.E. Tanenbaum, A.F. Maia, and R.H. Medema. 2009. RAMA1 is a novel kinetochore protein involved in kinetochore-microtubule attachment. *Journal of Cell Science*. 122:2436–2445. doi:10.1242/jcs.051912.

Rago, F., K.E. Gascoigne, and I.M. Cheeseman. 2015. Distinct organization and regulation of the outer kinetochore KMN network downstream of CENP-C and CENP-T. *Curr. Biol.* 25:671–677. doi:10.1016/j.cub.2015.01.059.

Ranjitkar, P., M.O. Press, X. Yi, R. Baker, M.J. MacCoss, and S. Biggins. 2010. An E3 ubiquitin ligase prevents ectopic localization of the centromeric histone H3 variant via the centromere targeting domain. *Molecular Cell*. 40:455–464. doi:10.1016/j.molcel.2010.09.025.

Régnier, V., P. Vagnarelli, T. Fukagawa, T. Zerjal, E. Burns, D. Trouche, W.

Earnshaw, and W. Brown. 2005. CENP-A is required for accurate chromosome segregation and sustained kinetochore association of BubR1. *Mol. Cell. Biol.* 25:3967–3981. doi:10.1128/MCB.25.10.3967-3981.2005.

Rieder, C.L., and A. Khodjakov. 2003. Mitosis through the microscope: advances in seeing inside live dividing cells. *Science*. 300:91–96. doi:10.1126/science.1082177.

Rieder, C.L., and E.D. Salmon. 1998. The vertebrate cell kinetochore and its roles during mitosis. *Trends in Cell Biology*. 8:310–318. doi:10.1016/S0962-8924(98)01299-9.

Rieder, C.L., R.W. Cole, A. Khodjakov, and G. Sluder. 1995. The checkpoint delaying anaphase in response to chromosome monoorientation is mediated by an inhibitory signal produced by unattached kinetochores. *The Journal of Cell Biology*. 130:941–948.

Rogers, G.C. 2005. Spindle microtubules in flux. *Journal of Cell Science*. 118:1105–1116. doi:10.1242/jcs.02284.

Roos, U.P. 1973. Light and electron microscopy of rat kangaroo cells in mitosis. II. Kinetochore structure and function. *Chromosoma*. 41:195–220.

Rosasco-Nitcher, S.E., W. Lan, S. Khorasanizadeh, and P.T. Stukenberg. 2008. Centromeric Aurora-B Activation Requires TD-60, Microtubules, and Substrate Priming Phosphorylation. *Science*. 319:469–472. doi:10.1126/science.1148980.

Salimian, K.J., E.R. Ballister, E.M. Smoak, S. Wood, T. Panchenko, M.A. Lampson, and B.E. Black. 2011. Feedback Control in Sensing Chromosome Biorientation by the Aurora B Kinase. *Current Biology*. 21:1158–1165. doi:10.1016/j.cub.2011.06.015.

Salmon, E.D., D. Cimini, L.A. Cameron, and J.G. DeLuca. 2005. Merotelic kinetochores in mammalian tissue cells. *Philosophical Transactions of the Royal Society B: Biological Sciences*. 360:553–568. doi:10.1098/rstb.2004.1610.

Santaguida, S., and A. Musacchio. 2009. The life and miracles of kinetochores. *EMBO J.* 28:2511–2531. doi:10.1038/emboj.2009.173.

Santamaria, A., B. Wang, S. Elowe, R. Malik, F. Zhang, M. Bauer, A. Schmidt, H.H.W. Silljé, R. Körner, and E.A. Nigg. 2011. The Plk1-dependent phosphoproteome of the early mitotic spindle. *Mol. Cell Proteomics*. 10:M110.004457–M110.004457. doi:10.1074/mcp.M110.004457.

Santamaria, A., R. Neef, U. Eberspächer, K. Eis, M. Husemann, D. Mumberg, S. Prechtl, V. Schulze, G. Siemeister, L. Wortmann, F.A. Barr, and E.A. Nigg. 2007. Use of the novel Plk1 inhibitor ZK-thiazolidinone to elucidate functions of Plk1 in early and late stages of mitosis. *Molecular Biology of the Cell*. 18:4024–4036. doi:10.1091/mbc.E07-05-0517.

Sarangapani, K.K., and C.L. Asbury. 2014. Catch and release: how do kinetochores hook the right microtubules during mitosis? *Trends in Genetics*. 30:150–159. doi:10.1016/j.tig.2014.02.004.

Sarangapani, K.K., B. Akiyoshi, N.M. Duggan, S. Biggins, and C.L. Asbury. 2013. Phosphoregulation promotes release of kinetochores from dynamic microtubules via multiple mechanisms. *Proc. Natl. Acad. Sci. U.S.A.* 110:7282–7287. doi:10.1073/pnas.1220700110.

Schmidt, J.C., H. Arthanari, A. Boeszoermenyi, N.M. Dashkevich, E.M. Wilson-Kubalek, N. Monnier, M. Markus, M. Oberer, R.A. Milligan, M. Bathe, G. Wagner, E.L. Grishchuk, and I.M. Cheeseman. 2012. The Kinetochore-Bound Ska1 Complex Tracks Depolymerizing Microtubules and Binds to Curved Protofilaments. *Dev. Cell*. 23:968–980. doi:10.1016/j.devcel.2012.09.012.

Schnerch, D., and E.A. Nigg. 2015. Structural centrosome aberrations favor proliferation by abrogating microtubule-dependent tissue integrity of breast epithelial mammospheres. *Oncogene*. doi:10.1038/onc.2015.332.

Schubert, von, C., F. Cubizolles, J.M. Bracher, T. Sliedrecht, G.J.P.L. Kops, and E.A. Nigg. 2015. Plk1 and Mps1 Cooperatively Regulate the Spindle Assembly Checkpoint in Human Cells. *CellReports*. 1–34. doi:10.1016/j.celrep.2015.06.007.

Screpanti, E., A. De Antoni, G.M. Alushin, A. Petrovic, T. Melis, E. Nogales, and A. Musacchio. 2011. Direct Binding of Cenp-C to the Mis12 Complex Joins the Inner and Outer Kinetochore. *Current Biology*. 21:391–398. doi:10.1016/j.cub.2010.12.039.

Sessa, F., M. Mapelli, C. Ciferri, C. Tarricone, L.B. Areces, T.R. Schneider, P.T. Stukenberg, and A. Musacchio. 2005. Mechanism of Aurora B Activation by INCENP and Inhibition by Hesperadin. *Molecular Cell*. 18:379–391. doi:10.1016/j.molcel.2005.03.031.

Shrestha, R.L., and V.M. Draviam. 2013. Lateral to End-on Conversion of Chromosome-Microtubule Attachment Requires Kinesins CENP-E and MCAK. *Current Biology*. 23:1514–1526. doi:10.1016/j.cub.2013.06.040.

Silkworth, W.T., I.K. Nardi, R. Paul, A. Mogilner, and D. Cimini. 2012. Timing of centrosome separation is important for accurate chromosome segregation. *Molecular Biology of the Cell*. 23:401–411. doi:10.1091/mbc.E11-02-0095.

Silljé, H.H.W., S. Nagel, R. Körner, and E.A. Nigg. 2006. HURP Is a Ran-Importin β-Regulated Protein that Stabilizes Kinetochore Microtubules in the Vicinity of Chromosomes. *Current Biology*. 16:731–742. doi:10.1016/j.cub.2006.02.070.

Silva, M.C.C., D.L. Bodor, M.E. Stellfox, N.M.C. Martins, H. Hochegger, D.R. Foltz, and L.E.T. Jansen. 2012. Cdk activity couples epigenetic centromere inheritance to cell cycle progression. *Dev. Cell*. 22:52–63. doi:10.1016/j.devcel.2011.10.014.

Sivakumar, S., J.R. Daum, A.R. Tipton, S. Rankin, and G.J. Gorbsky. 2014. The

spindle and kinetochore-associated (Ska) complex enhances binding of the anaphase-promoting complex/cyclosome (APC/C) to chromosomes and promotes mitotic exit. *Molecular Biology of the Cell*. 25:594–605. doi:10.1091/mbc.E13-07-0421.

Steigemann, P., C. Wurzenberger, M.H.A. Schmitz, M. Held, J. Guizetti, S. Maar, and D.W. Gerlich. 2009. Aurora B-Mediated Abscission Checkpoint Protects against Tetraploidization. *Cell*. 136:473–484. doi:10.1016/j.cell.2008.12.020.

Stern, B., and P. Nurse. 1996. A quantitative model for the cdc2 control of S phase and mitosis in fission yeast. *Trends in Genetics*. 12:345–350.

Stukenberg, P.T., and D.J. Burke. 2015. Connecting the microtubule attachment status of each kinetochore to cell cycle arrest through the spindle assembly checkpoint. *Chromosoma*. 1–18. doi:10.1007/s00412-015-0515-z.

Sudakin, V., G.K. Chan, and T.J. Yen. 2001. Checkpoint inhibition of the APC/C in HeLa cells is mediated by a complex of BUBR1, BUB3, CDC20, and MAD2. *The Journal of Cell Biology*. 154:925–936. doi:10.1083/jcb.200102093.

Sugimoto, K., H. Yata, Y. Muro, and M. Himeno. 1994. Human centromere protein C (CENP-C) is a DNA-binding protein which possesses a novel DNA-binding motif. *J. Biochem.* 116:877–881.

Sugiyama, K., K. Sugiura, T. Hara, K. Sugimoto, and H. Shima. 2002a. Aurora-B associated protein phosphatases as negative regulators of kinase activation. *Oncogene*.

Sugiyama, K., K. Sugiura, T. Hara, K. Sugimoto, H. Shima, K. Honda, K. Furukawa, S. Yamashita, and T. Urano. 2002b. Aurora-B associated protein phosphatases as negative regulators of kinase activation. *Oncogene*. 21:3103–3111. doi:10.1038/sj.onc.1205432.

Suzuki, A., B.L. Badger, X. Wan, J.G. DeLuca, and E.D. Salmon. 2014. The Architecture of CCAN Proteins Creates a Structural Integrity to Resist Spindle Forces and Achieve Proper Intrakinetochore Stretch. *Dev. Cell*. 30:717–730. doi:10.1016/j.devcel.2014.08.003.

Tanno, Y., H. Susumu, M. Kawamura, H. Sugimura, T. Honda, and Y. Watanabe. 2015. The inner centromere-shugoshin network prevents chromosomal instability. *Science*. 349:1237–1240. doi:10.1126/science.aaa2655.

Tanno, Y., T.S. Kitajima, T. Honda, Y. Ando, K.-I. Ishiguro, and Y. Watanabe. 2010. Phosphorylation of mammalian Sgo2 by Aurora B recruits PP2A and MCAK to centromeres. *Genes & Development*. 24:2169–2179. doi:10.1101/gad.1945310.

Tauchman, E.C., F.J. Boehm, and J.G. DeLuca. 2015. Stable kinetochore–microtubule attachment is sufficient to silence the spindle assembly checkpoint in human cells. *Nat Comms*. 6:1–9. doi:10.1038/ncomms10036.

Thompson, S.L., and D.A. Compton. 2008. Examining the link between chromosomal instability and aneuploidy in human cells. *The Journal of Cell Biology*. 180:665–672. doi:10.1083/jcb.200712029.

Tseng, B.S., L. Tan, T.M. Kapoor, and H. Funabiki. 2010. Dual Detection of Chromosomes and Microtubules by the Chromosomal Passenger Complex Drives Spindle Assembly. *Dev. Cell*. 18:903–912. doi:10.1016/j.devcel.2010.05.018.

Umbreit, N.T., D.R. Gestaut, J.F. Tien, B.S. Vollmar, T. Gonen, C.L. Asbury, and T.N. Davis. 2012. The Ndc80 kinetochore complex directly modulates microtubule dynamics. *Proc. Natl. Acad. Sci. U.S.A.* 109:16113–16118. doi:10.1073/pnas.1209615109.

van der Waal, M.S., A.T. Saurin, M.J.M. Vromans, M. Vleugel, C. Wurzenberger, D.W. Gerlich, R.H. Medema, G.J.P.L. Kops, and S.M.A. Lens. 2012. Mps1 promotes rapid centromere accumulation of Aurora B. *EMBO rep*. 13:847–854. doi:10.1038/embor.2012.93.

Van Hooser, A.A., I.I. Ouspenski, H.C. Gregson, D.A. Starr, T.J. Yen, M.L. Goldberg, K. Yokomori, W.C. Earnshaw, K.F. Sullivan, and B.R. Brinkley. 2001. Specification of kinetochore-forming chromatin by the histone H3 variant CENP-A. *Journal of Cell Science*. 114:3529–3542.

Varma, D., and E.D. Salmon. 2012. The KMN protein network--chief conductors of the kinetochore orchestra. *Journal of Cell Science*. 125:5927–5936. doi:10.1242/jcs.093724.

Varma, D., X. Wan, D. Cheerambathur, R. Gassmann, A. Suzuki, J. Lawrimore, A. Desai, and E.D. Salmon. 2013. Spindle assembly checkpoint proteins are positioned close to core microtubule attachment sites at kinetochores. *The Journal of Cell Biology*. 202:735–746. doi:10.1083/jcb.201304197.

Verdaasdonk, J.S., and K. Bloom. 2011. Centromeres: unique chromatin structures that drive chromosome segregation. *Nature Publishing Group*. 12:320–332. doi:10.1038/nrm3107.

Walczak, C.E., S. Cai, and A. Khodjakov. 2010. Mechanisms of chromosome behaviour during mitosis. *Nat Rev Mol Cell Biol*. 11:91–102. doi:10.1038/nrm2832.

Wan, X., R.P. O'Quinn, H.L. Pierce, A.P. Joglekar, W.E. Gall, J.G. DeLuca, C.W. Carroll, S.-T. Liu, T.J. Yen, B.F. McEwen, P.T. Stukenberg, A. Desai, and E.D. Salmon. 2009. Protein Architecture of the Human Kinetochore Microtubule Attachment Site. *Cell*. 137:672–684. doi:10.1016/j.cell.2009.03.035.

Wang, E., E.R. Ballister, and M.A. Lampson. 2011a. Aurora B dynamics at centromeres create a diffusion-based phosphorylation gradient. *The Journal of Cell Biology*. 194:539–549. doi:10.1083/jcb.201103044.

Wang, F., J. Dai, J.R. Daum, E. Niedzialkowska, B. Banerjee, P.T. Stukenberg, G.J. Gorbsky, and J.M.G. Higgins. 2010. Histone H3 Thr-3 Phosphorylation by Haspin Positions Aurora B at Centromeres in Mitosis. *Science*. 330:231–235. doi:10.1126/science.1189435.

Wang, F., N.P. Ulyanova, J.R. Daum, D. Patnaik, A.V. Kateneva, G.J. Gorbsky, and J.M.G. Higgins. 2012. Haspin inhibitors reveal centromeric functions of Aurora B in chromosome segregation. *The Journal of Cell Biology*. 199:251–268. doi:10.1083/jcb.201205106.

Wang, F., N.P. Ulyanova, M.S. van der Waal, D. Patnaik, S.M.A. Lens, and J.M.G. Higgins. 2011b. A Positive Feedback Loop Involving Haspin and Aurora B Promotes CPC Accumulation at Centromeres in Mitosis. *Current Biology*. 21:1061–1069. doi:10.1016/j.cub.2011.05.016.

Wang, H.-W., and E. Nogales. 2005. Nucleotide-dependent bending flexibility of tubulin regulates microtubule assembly. *Nature*. 435:911–915. doi:10.1038/nature03606.

Weaver, L.N., and C.E. Walczak. 2015. Spatial gradients controlling spindle assembly. *Biochm. Soc. Trans.* 43:7–12. doi:10.1042/BST20140243.

Weiss, E., and M. Winey. 1996. The Saccharomyces cerevisiae spindle pole body duplication gene MPS1 is part of a mitotic checkpoint. *The Journal of Cell Biology*. 132:111–123.

Welburn, J.P.I., and I.M. Cheeseman. 2008. Toward a Molecular Structure of the Eukaryotic Kinetochore. *Dev. Cell*. 15:645–655. doi:10.1016/j.devcel.2008.10.011.

Welburn, J.P.I., E.L. Grishchuk, C.B. Backer, E.M. Wilson-Kubalek, J.R. Yates III, and I.M. Cheeseman. 2009. The Human Kinetochore Ska1 Complex Facilitates Microtubule Depolymerization-Coupled Motility. *Dev. Cell*. 16:374–385. doi:10.1016/j.devcel.2009.01.011.

Welburn, J.P.I., M. Vleugel, D. Liu, J.R. Yates III, M.A. Lampson, T. Fukagawa, and I.M. Cheeseman. 2010. Aurora B Phosphorylates Spatially Distinct Targets to Differentially Regulate the Kinetochore-Microtubule Interface. *Molecular Cell*. 38:383–392. doi:10.1016/j.molcel.2010.02.034.

Westhorpe, F.G., A. Tighe, P. Lara-Gonzalez, and S.S. Taylor. 2011. p31comet-mediated extraction of Mad2 from the MCC promotes efficient mitotic exit. *Journal of Cell Science*. 124:3905–3916. doi:10.1242/jcs.093286.

Wollman, R., E.N. Cytrynbaum, J.T. Jones, T. Meyer, J.M. Scholey, and A. Mogilner. 2005. Efficient Chromosome Capture Requires a Bias in the “Search-and-Capture” Process during Mitotic-Spindle Assembly. *Current Biology*. 15:828–832. doi:10.1016/j.cub.2005.03.019.

Wordeman, L., M. Wagenbach, and G. von Dassow. 2007. MCAK facilitates chromosome movement by promoting kinetochore microtubule turnover. *The*

Journal of Cell Biology. 179:869–879. doi:10.1083/jcb.200707120.

Yamagishi, Y., C.-H. Yang, Y. Tanno, and Y. Watanabe. 2012. MPS1/Mph1 phosphorylates the kinetochore protein KNL1/Spc7 to recruit SAC components. *Nat Cell Biol*. 14:746–752. doi:10.1038/ncb2515.

Yamagishi, Y., T. Honda, Y. Tanno, and Y. Watanabe. 2010. Two Histone Marks Establish the Inner Centromere and Chromosome Bi-Orientation. *Science*. 330:239–243. doi:10.1126/science.1194498.

Yamagishi, Y., T. Sakuno, Y. Goto, and Y. Watanabe. 2014. Kinetochore composition and its function: lessons from yeasts. *FEMS Microbiol Rev*. 38:185–200. doi:10.1111/1574-6976.12049.

Yasui, Y., T. Urano, A. Kawajiri, K.-I. Nagata, M. Tatsuka, H. Saya, K. Furukawa, T. Takahashi, I. Izawa, and M. Inagaki. 2004. Autophosphorylation of a newly identified site of Aurora-B is indispensable for cytokinesis. *J. Biol. Chem.* 279:12997–13003. doi:10.1074/jbc.M311128200.

Yue, Z., A. Carvalho, Z. Xu, X. Yuan, S. Cardinale, S. Ribeiro, F. Lai, H. Ogawa, E. Gudmundsdottir, R. Gassmann, C.G. Morrison, S. Ruchaud, and W.C. Earnshaw. 2008. Deconstructing Survivin: comprehensive genetic analysis of Survivin function by conditional knockout in a vertebrate cell line. *The Journal of Cell Biology*. 183:279–296. doi:10.1083/jcb.200806118.

Zaytsev, A.V., and E.L. Grishchuk. 2015. Basic mechanism for biorientation of mitotic chromosomes is provided by the kinetochore geometry and indiscriminate turnover of kinetochore microtubules. *Molecular Biology of the Cell*. 26:3985–3998. doi:10.1091/mbc.E15-06-0384.

Zhai, Y., P.J. Kronebusch, and G.G. Borisy. 1995. Kinetochore microtubule dynamics and the metaphase-anaphase transition. *The Journal of Cell Biology*. 131:721–734.

Publications

Parts of this thesis have been published in:

Abad MA, Medina B, Santamaria A, Zou J, Plasberg-Hill C, Madhumalar A, Jayachandran U, **Redli PM**, Rappsilber J, Nigg EA, Jeyaprakash AA. Structural basis for microtubule recognition by the human kinetochore Ska complex. 2014. *Nature Communications*. 5: 2964.

Redli PM, Gasic I, Meraldi P, Nigg EA, Santamaria A. The human Ska complex promotes Aurora B activity to ensure chromosome biorientation and faithful chromosome segregation. 2016. (Under review in *Journal of Cell Biology*).

Acknowledgements

First of all, I would like to thank Erich Nigg for providing me the opportunity to pursue my doctoral studies in his lab. I highly appreciate his mentoring and his valuable scientific input, as well as the intellectual freedom and independence he granted me during this project.

I further would like to thank Anna Santamaria, who has supervised this work. I am grateful for Anna's continuous interest in and support of my scientific progress (also after her move to Spain as an independent group leader), for being always open for fruitful discussions, and her encouragement during both successful and "dry" periods. Moreover, I thank her for corrections and comments on this thesis.

Patrick Meraldi and Clemens Cabernard are thanked for their helpful feedback and advise during my thesis advisory committee meetings. Patrick Meraldi I would also like to thank for reviewing this thesis and his participation as a co-examiner in my defense committee.

For experimental and technical support, special thanks go to Ivana Gasic in P. Meraldi's lab (for her help with the photodissipation and KT tracking assays), Anna Santamaria (for sharing the load on the photodissipation/flux measurements), and Conrad von Schubert (for initial help with FRET sensor imaging and help with the peptide spotting). Additionally, I appreciate that I could trade on reagents generated by present and past members of the Nigg lab, namely, by Anna Santamaria, Ying Wai Chan, Conrad von Schubert, Anja Hanisch, Thomas Gaitanos, Ulf Klein, and Zhen Dou. For sharing cell lines and reagents, I also thank T. Brummer, I.M. Cheeseman, D.W. Gerlich, A.A. Jeyaprakash and M.A. Abad, T. Johanson, M. Lampson, P. Scheiffele, and X. Yao.

For excellent lab organization and management, I owe thank to Elena Nigg and Fabien Cubizolles.

Furthermore, I am grateful to my current and former workmates and friends in the Nigg lab for valuable scientific exchange, their contribution to an enjoyable working atmosphere, and most importantly for sharing many great and funny moments both inside and outside of the lab. So, my warm thanks to Christian Arquint, Conrad von Schubert, Jasmine Bracher, Lukas Cajanek, Anna-Maria Gabryjonczyk, Anna Santamaria, Fabien Cubizolles, Manuel Bauer, Anna Baron, Ana Amaro Meyer, Dominik Schnerch, Christina Vigano, Olivier Ganier, and Agathe Morand.

Finally, I am indebted to my family and all my friends for continuously supporting me throughout my quest as a PhD student. Thank you!